POLITECNICO DI TORINO

Corso di Laurea Magistrale in Ingegneria Biomedica

Master Thesis

Characterization of vibration-induced artefacts in EMG signals

Advisors:

Eng. Alberto Botter

Eng. Giacinto Luigi Cerone

Eng. Matteo Aventaggiato

Candidate:

Daria Di Miceli

Anno Accademico 2018/2019

To Daniela,
my guardian angel.

"We must be willing be to let go of the life we planned so as to have the life that is waiting for us."

Joseph Campbell

Summary

Hand amputation due to traumatic events or diseases causes relevant impairments on the capabilities of a person. The use of hand prostheses has the potential to radically improve the quality of life of hand amputees. Active hand prostheses are usually controlled by myoelectric signals collected by means of surface electrodes placed on the residual stump muscles. These signals are used to identify movement intention and control hand fingers.

Vibrotactile stimuli have been proposed to provide the user with a feedback aimed at improving the usability of the prostheses. Usually, vibrator and bipolar electrodes are placed in close proximity for practical and constructive reasons. However, in this configuration, vibrations could cause a movement artifact on the sEMG signals used to control the hand movement.

This study focused on the characterization of the vibration artifact on sEMG signal. Three potential sources of the motion artifact were analyzed: changes of the impedance unbalance between the exploring electrodes; variations of the half-cell potential; design characteristic of the analog front-end amplifier. The effects of these factors were studied in three steps: theoretically; using custom-made circuits (bench experiments) and experimentally.

Initially, a bipolar EMG detection system was built on an electronic board. The circuit included a standard front-end electronics (INA333) and the electrical models of the

electrode-skin contact made with discrete components; RC parallels for the impedances (Z_e) and batteries for the half-cell potentials (E_{hc}). In the bench experiments variations of the Z_e and E_{hc} were obtained through switches.
With this approach, we obtained a model-based characterization of the movement artifact that was compared with the theoretical analysis of the considered circuits. In the second step, the tests of the first phase were repeated by replacing the circuital model of the electrode-skin contact with actual electrodes on the subject. Movement-induced changes in the properties of electrode-skin contact were simulated by changing the size of the exploring and reference electrodes. In the third step, we applied a motor-driven vibrator at different distances from the exploring and the reference electrodes to induce motion artifacts in bipolar EMG recording in the conditions previously simulated. Tests were repeated for different values of the input capacitance of the analog front-end.

The theoretical considerations and signal recorded in bench experiments showed that the common-mode variations of the half-cell potential cause the appearance of spike-like artifacts due to both the electrode-skin impedance unbalance and the input capacitance of the front-end amplifier. As expected, the differential mode changes of the half-cell potential induce shifts of the baseline of the signal, and the impedance unbalance causes the modulation of the powerline interference that implies the appearance of spike-like artefact with sudden changes. The experimental analysis (third step) showed that vibrations of the exploring and reference electrodes cause spike-like artefacts, whose amplitude was comparable with the amplitude of the sEMG signal.
These results demonstrate the importance of: i) the proper skin preparation to achieve stable properties of the electrode-skin interface (Z_e and E_{hc}); ii) proper positioning of the reference and exploring electrodes with respect to the vibro-tactile feedback source; iii) the design of the analog front-end amplifier.
The artefact observed by the vibrations of the reference electrode resulted lower than that caused by the vibrations of the exploring electrodes. Therefore, this observation suggests positioning the reference electrode and the vibrator distant with respect to exploring electrodes in order to reduce the vibration-induced artefacts on the sEMG

signal. Despite the lower amplitude of the vibration-artefact caused by the reference electrode, the results suggest the potential usefulness of the two-electrodes biopotential amplifiers in case of applications where high robustness to vibration artefacts is required, removing one source of motion artefact.

Tables of Contents

Chapter 1

Introduction

This thesis concerns the study of vibration-induced artefacts in EMG signals. This analysis was motivated by recent development in the hand-prosthesis devices which integrates a vibro-tactile system to provide the user with a feedback aimed at improving the usability of the prostheses. In myoelectric controlled prosthesis vibrator and bipolar electrodes are placed in close proximity for practical and constructive reasons. In this configuration the vibration may causes a movement artifact on the sEMG signals used to control the hand movement.
This chapter provides: a brief overview of myoelectric prosthetic devices (research and commercial), a description of sEMG signal detection and conditioning, and of vibro-tactile feedback in hand prosthesis.

1.1 Myoelectric robotic prostheses

It is estimated that, in 2005, 41,000 people were living without the upper limb or part of it. Hand amputation due to traumatic events or diseases causes relevant impairments on the capabilities of a person. Recent advances in man-machine interfaces suggest that clever, naturally controlled, and proportionate robotic prostheses could be reality in the future of a disabled person. However, several steps are required to obtain naturally controlled prostheses [1]. There are three methods to control hand prostheses through biological signals: interfacing directly the brain through EEG [2], peripheral nerves [3]

or muscles [4]. The last method uses muscles signals (sEMG, surface electromyography) to control the robotic system. This kind of prosthesis is referred is referred to as myoelectric prosthesis [1].

Myoelectric robotic prostheses generally contain two main parts: a prosthetic hand and a control system. The hand prostheses include cosmetic prosthesis (mechanical support), kinematic prosthesis (functional capabilities, like the opening and the closing of gripper hand through the motion of the shoulder) and myoelectric prosthesis (patient can control a battery-powered prosthesis with the electrical signal produced by remainder muscles). Many prosthetic hands are commercially available, but most of these reproduce only few movements [1].

The detection system consists of two or three sEMG electrodes mounted in correspondence to specific muscles on the forearm (Figure 1). The signal detected from these muscles is used for controlling the prosthetic hand. The number of available movements depends on the number of control strategies employed [1].

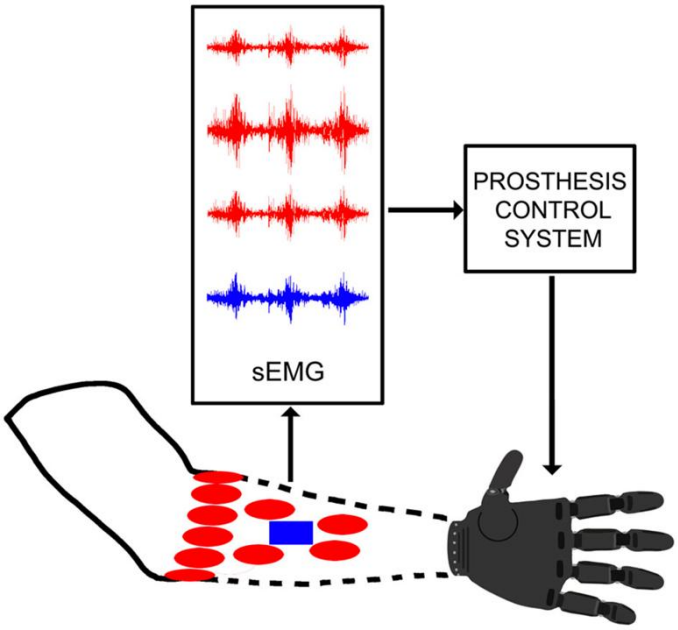

Figure 1:Scheme of a generic myoelectric control system. The blue rectangle is relative to commercial prosthesis without pattern recognition instead, red ellipses to research with pattern recognition in the control system [1].

1.1.1 State of the art in scientific research and commercial hand prostheses

Patter recognition or proportional control approaches are the most common control procedures, which can be applied to sEMG and multimodal signals. Algorithms of pattern recognition are necessary to categorize the movement. These approaches in different cases have shown classification accuracy over 90 – 95% on less than 10 classes [5] but usually under 80 – 90% [6].

The Proportional control of some degrees of freedom of prosthesis can afford to have more natural control with an unsupervised or supervised method [7],[8]. The first methods are based on signal factorization, requiring initial calibration. These are independent of the number and the placement of the electrodes. The second, instead, are drawn on regression technique (e.g. Lineal Regression, LR, Artificial Neural Network, ANN, Support Vector Machines, SVM) [1].

The market shows the existence of a very advanced prosthetic hands and control system. Among the commercial devices the prostheses have important mechanical and control differences. Firstly, for example, the number of actuators is two for Otto Bock Michelangelo, five for Steeper Bebionic 3, and six for Touch Bionics i-limb Quantum and Vincent Evolution 2. Secondly, the number of finger position encoders ranges between zero for Touch Bionics i-limb Quantum and Vincent Evolution 2, two for Otto Bock Michelangelo and five for Steeper Bebionic 3 [1].

Research prostheses are usually developed for the study of novel design and innovative control methods. Since they are not made for trade, they are designed to leave out some aspects that are more important for commercial prostheses, such as robustness, weight, ease of mass production and costs [9].
Through the successes and failures of commercial hands and the durability of research hands, it is understood that there must be compromises between the complexity of the hands (for example, the number of degrees of freedom) and the robustness/durability of these. Consequently, the research hands are usually less robust and more complex than commercial hands [9].
Being the EMG signal the source of information the control of robotic device, a high-quality detection of this signal is of paramount importance. In the following section, a description of the issues related to EMG signal detection and conditioning and the possible sources of noise and artefacts are reported.

1.2 Electromyographic signal detection and conditioning

1.2.1 The half-cell potential

The electrodes are metal surfaces placed on the skin that convert this ionic current into an electronic current carried by the electrons [10].
Generally, the electrodes for the biopotential recording are made of metallic materials or covered by metallic salts [11]. When an electrode is immersed in an electrolytic

solution, at the metal-electrolyte interface oxidative and reductive chemical reactions arise (Figure 2), by forming a double-layer charge at this interface (Figure 3).

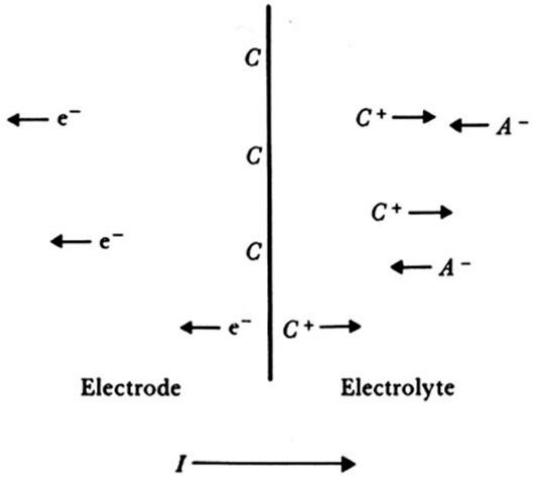

Figure 2: Electrode – electrolyte interface. The current cross it from left to right. The electrode consists of metallic atoms C. the electrolyte in an aqueous solution containing cation of the electrode metal C_+ and anions A_- [12].

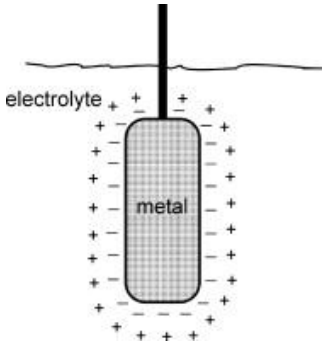

Figure 3: Double - layer of charge at the metal – electrolyte interface.

The double-layer charge could be seen as a capacitor localized on the metal surface of the electrode. This phenomenon causes the polarization of the electrode compared to the solution, and the metal is at a different potential than that of the solution [12], [13]. The potential is called half-cell potential and depends on different parameters, such as the metal used, the concentration and composition of the electrolytic solution, and the affinity of the ions in solution with the surface of the metal [13]. Experimentally, the absolute half-cell potential is impossible to measure, because of a second electrode in contact with the solution is necessary. The Standard Hydrogen Electrode (SHE) has

been chosen like a specific reference electrode and its potential is conventionally set at zero for all temperatures [11]. The standard potential E^0(V) of one chemical reaction compared to the SHE potential is shown in Table 1. These values are related to the temperature of 25°C, the concentration of 1mol, the partial gas pressure of 1atm (101,325kPa), and the single activity [11].

Table 1: Potential of several metals material compared to the SHE potential [11].

Metal and redox reaction	E^0(V)
$Al^{3+} + 3e^- \rightarrow Al$	-1,663
$Zn^{2+} + 2e^- \rightarrow Zn$	-0,762
$Cr^{3+} + 3e^- \rightarrow Cr$	-0,744
$Fe^{2+} + 2e^- \rightarrow Fe$	-0,409
$Cd^{2+} + 2e^- \rightarrow Cd$	-0,402
$Ni^{2+} + 2e^- \rightarrow Ni$	-0,240
$Pb^{2+} + 2e^- \rightarrow Pb$	-0,127
$Fe^{3+} + 3e^- \rightarrow Fe$	-0,024
$2H^+ + 2e^- \rightarrow H_2$	0,0
$AgCl + e^- \rightarrow Ag + Cl^-$	0,223
$Hg_2Cl_2 + 2e^- \rightarrow 2Hg + 2Cl^-$	0,268
$Cu^{2+} + 2e^- \rightarrow Cu$	0,339
$Cu^+ + e^- \rightarrow Cu$	0,520
$Ag^+ + e^- \rightarrow Ag$	0,799
$Pt^{2+} + 2e^- \rightarrow Pt$	1,188
$Au^{3+} + 3e^- \rightarrow Au$	1,520
$Au^+ + e^- \rightarrow Au$	1,830

If the measurement conditions are different from those of the standard potential, the half-cell potential can be obtained by the Nernst equation. If the half-cell equation is of the kind [11]:

$$\alpha A + \beta B + ne^- \leftrightarrow \gamma C + \delta D \quad (1)$$

the half-cell potential is:

$$E = E^0 - \frac{RT}{nF} \ln\left(\frac{a_C^\gamma a_D^\delta}{a_A^\alpha a_B^\beta}\right) \quad (2)$$

where:

E^0 is the standard potential of the electrode;

R is the molar gas constant (8,314462 J mol^{-1} K^{-1});

T is the absolute temperature (K);

F is the Faraday constant (96,485 kJ mol^{-1});

is the activity of the C element.

1.2.2 Electrode – skin interface

When the electrode is placed on the skin two contacts are formed: the electrode-electrolyte (i.e. body tissues, bodily fluid or gel for electrode) interface and the electrolyte-skin interface. Also, the electrode is connected with the input of an amplifier circuit, so it is good to be able to have an electrical model of these interfaces.

The equivalent model of the electrode-electrolyte contact, shown in Figure 4, is made by an RC parallel (C_d and R_d) that is the impedance of the interface, one series resistor R_S, thus the electrolyte resistance, and one series battery that represent the half-cell potential (E_{hc}).

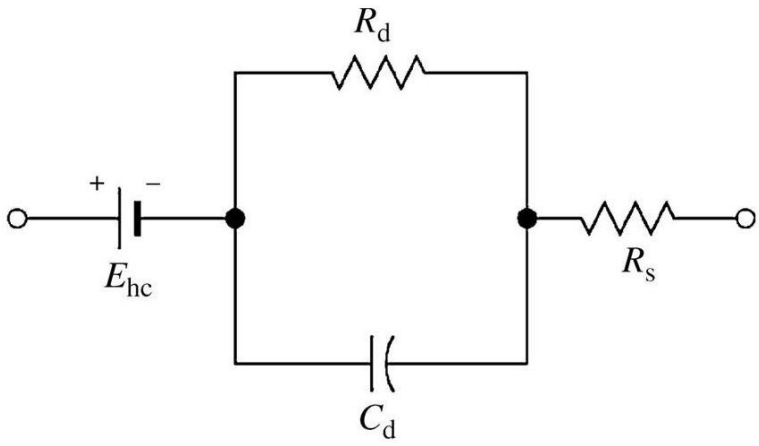

Figure 4: Equivalent circuit for a biopotential electrode in contact with an electrolyte. E_{hc} is the half-cell potential, R_d e C_d make up the impedance associated with the electrode-electrolyte interface and polarization effects, and R_s is the series resistance associated with interface effects and due to resistance in the electrolyte [12].

The electrolyte-skin interface has the same electrical model[12]. So, Figure 5 shows the total electrical equivalent circuit obtained when the electrode is placed against the skin, by including the two contact described above [12].

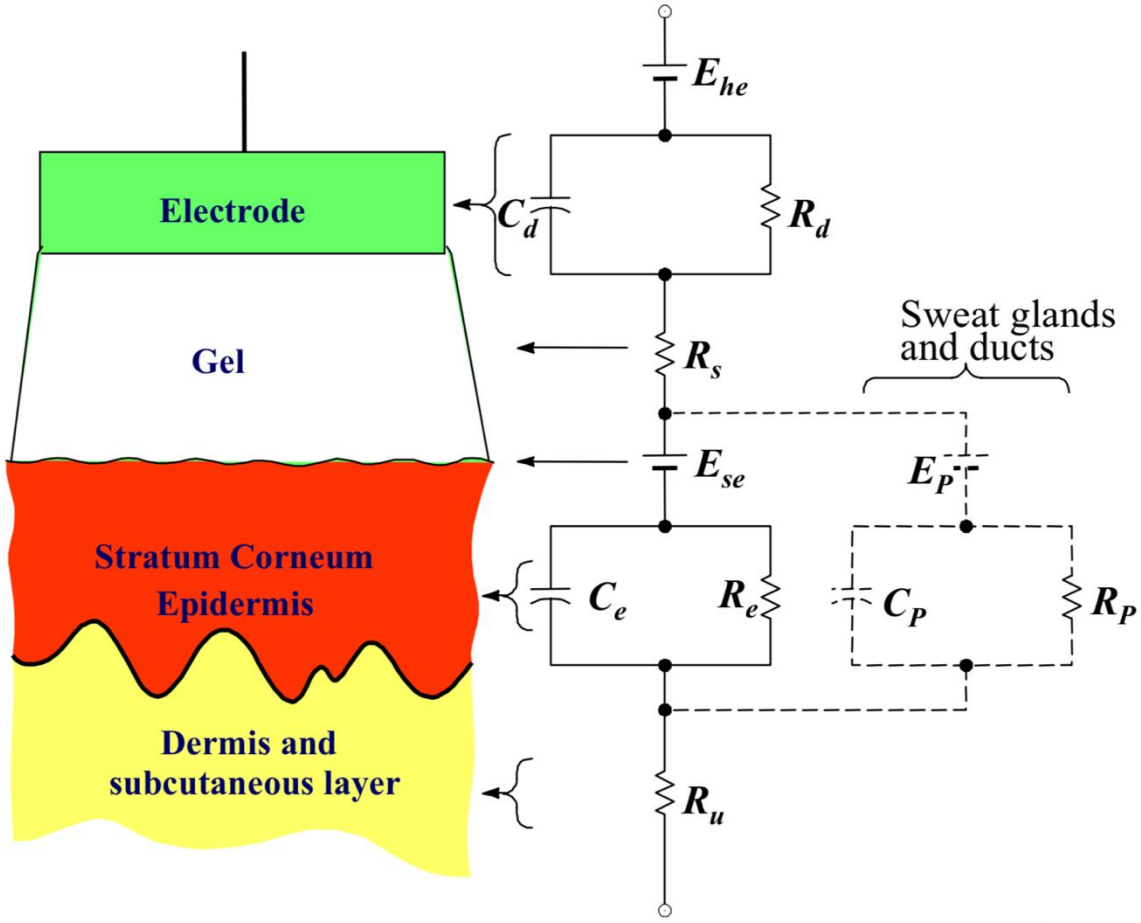

Figure 5: Total electrical equivalent circuit obtained when the electrode is placed against the skin. Each circuit element on the right represents the corresponding physical process showed in the left-hand diagram [12],[14].

1.2.3 Types of electrodes

There are two commonly used types of electrodes:

- Dry electrodes in direct contact with the skin,
- Gelled electrodes using an electrolytic gel as a chemical interface between the skin and the metallic part of the electrode.

Dry electrodes are usually bar and array electrodes and are considerably heavier (typically >20g) than gelled electrodes (<1g). So, maintaining electrode fixation for dry

electrodes is difficult compared to gelled electrodes, because of their higher inertial mass [15].

Gelled electrodes use an electrolytic gel as a chemical interface between the skin and the metallic part of the electrode. Ag-AgCl is the most common composite for the metallic part of gelled electrodes. The chemical reactions take place at the metal-electrolyte interface, where the AgCl layer allows the current of the muscle a simpler passage through the metal-electrolyte interface [16].

1.2.4 Impedance, dc voltage and noise of the electrodes

The stability of impedance taking place between the electrode and the skin during the recording EMG time and its balance between electrode sites have a significant effect on the signal to noise ratio [17]. The improving and the stabilization of the contact are commonly achieved by shaving, cleaning and rubbing the skin with a slightly abrasive cloth soaked in water or in a solvent, and by applying Ag or AgCl electrodes with a conductive gel. The electrode-skin impedance of this type electrodes is an almost resistive impedance in the EMG frequency range [18]. Electrodes made with others metal, instead, presents capacitive components that introduce an additional filtering [22]. This impedance depends on the skin preparation, and decreases with the increasing of the electrode surface [18].

The skin is a moderately conductive tissue (made of cells whose material consist of electrolyte solutions) in which current carried by ions. The metal of the electrode is a highly conducting material where current is carried by electrons. Positioning the electrodes on the skin the resulting interface is intrinsically noisy. It generates the most important source of noise in EMG recording, so it limits the possibility to detect the small potential [18].

A DC voltage generated at the metal-electrolyte interface is referred to as the “battery” effect [18],[19],[20]. Two equal electrodes are generally used in a differential configuration and the impedance at each side will not be the same, however it should be relatively similar [15], [18]. The dc or slowly changing voltage may be present between

the two electrodes [18], [19]. The differential amplifier only cancels common signal components so dc and slowly changing voltage could remain in the signal after the subtraction [21]. The residual of the dc component, when amplified, can caused the instability, inaccuracy and saturation of the amplifier. In general, balanced impedance between the electrode sides ensures a lower interference and as a result a higher signal to noise ratio [15]. The impedance should be constant during the recording time, because the signal to noise ratio could change if the impedance drift during the measurement session [15]. Concluding, slight skin abrasion or "peeling" with adhesive tape reduce electrode – skin impedance, noise, dc voltage and also the motion artefact [18], [22].

1.3 Vibro-tactile feedback in hand prostheses

1.3.1 Sensory communication in Rehabilitation engineering

Beside the control modalities, also the sensory feedback (i.e. the transfer of the information from the hand prosthesis to the brain) is very important to improve the subject ability to control the prosthesis. For this reason, sensory feedback in prosthetic devices becoming a common development trend both in research and in the commercia context.

Several techniques used the tactile sense as an input channel, because the skin responds to thermal, chemical, electrical and mechanical stimuli. The last two are the only types of stimuli used for sensory feedback. In the past, Szeto e Saunders [23] studied electrocutaneous and vibratory stimulation channels. The electrocutaneous stimulators, compared to mechanical vibrators, have no moving component and the contact of the recording electrodes with the skin is more constant. Moreover, they have a low power consumption, are easy to manufacture and able to produce a stimulation whose frequency and intensity can be easily controlled. Considering these advantages one sensory feedback, electrocutaneous stimulation has been employed by several researchers (Figure 6).

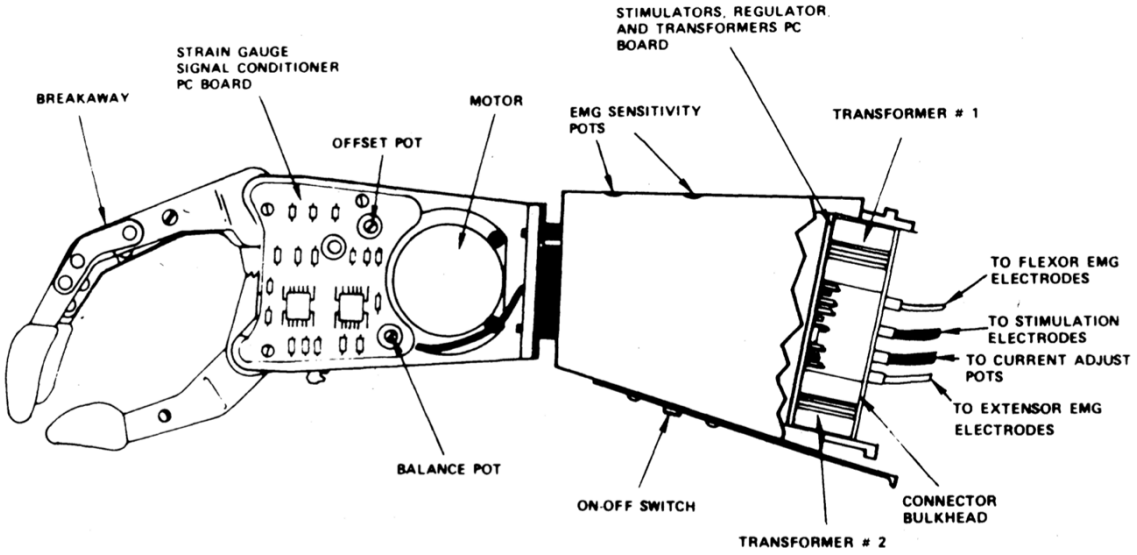

Figure 6: Myoelectric hand prostheses with the connections of supplemental sensory feedback in the right of the figure[24].

Sensory feedback using mechanical vibrators placed near the skin is another emerging technique. The skin is deformed by either compression or extension, and the EMG detection electrodes in proximity of the vibrator may move with respect to the skin. Variations of the electrical properties of the skin and of the electrode-skin interface may therefore occur, thus causing motion artefacts (vibration artefacts) on the sEMG signal. This is a relevant issue, considering that EMGs are used to control the prosthetic device. It is therefore very important to identify the experimental and circuital conditions under which the vibration artefact is minimized.

1.3.2 The possible causes of motion artefact

In general, the possible causes of motion artefact on biopotentials detected from the skin surface are [25], [26], [27]:

1. Cables motion, that generates triboelectric noise by friction and deformation of cables insulation [28],[29],[30]. Cables motion causes the change of the input capacity of the preamplifier, generating parametric fluctuations in the input network [25].

2. Movement of the metal-electrolyte interface. When the electrolyte is agitated compared to the metal, the half-cell potential changes, because the metallic ion gradient at the interface is altered [26], [31].
3. Stretching and compression of the skin. Pressing or pulling down the electrode deforms the underlying skin and the skin potential E_{se} (Figure 5) changes by causing motion artefact [25], [26], [27]. The sEMG recorded shows a rapid change in the baseline, until it returns to the initial condition[26].

1.3.3 Minimizing of motion artefact

The motion artefact, caused by cables motion, can be minimized by locating the preamplifier on the electrodes [28],[29],[30]. Nevertheless, the motion artefact caused by cables motion will not be covered by this study because this effect is irrelevant for the hand prostheses. Usually, the myoelectric prostheses use embedded electrodes.
Movements at the metal – electrolyte interface are another cause of motion artefact [12]. According to Gatzke [32], the movement of pure silver electrode in the electrolyte caused 15mV of artefact. Coating the Ag with AgCl reduced this artefact by a factor of 10. The non-polarizable metal-metal/halide electrode with an electrolytic gel, containing the same ion, ensure a more constant concentration at the electrode-electrolyte interface [26]. The Figure 7 shows that the offset potential is the sum of all biopotential sources, thus the skin potential and the electrode potential and the biopotential.

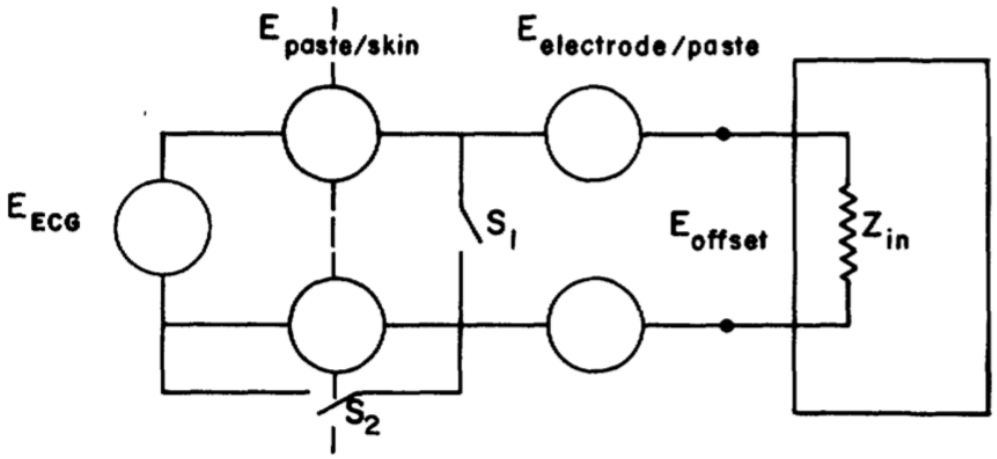

Figure 7: Simplified skin model showing the biopotential, the skin potential, the electrode potential, and the resultant sum, called Eoffset [26].

Tam and Weber [26] measured the offset potential with a pair of electrodes filled with paste, placed face to face, without involving the skin. Figure 8 shows the offset potential of a few commercial products for 29 minutes after contact was made. During the first 5 minutes the potential quickly changed, but then the offset potential stabilized. Disturbing the electrode-paste interface by squeezing the electrodes Figure 9a, no significant change in the offset could be measured. Then moving the electrodes (Figure 9b), the offset potential remained about constant until paste was connecting the two electrodes.

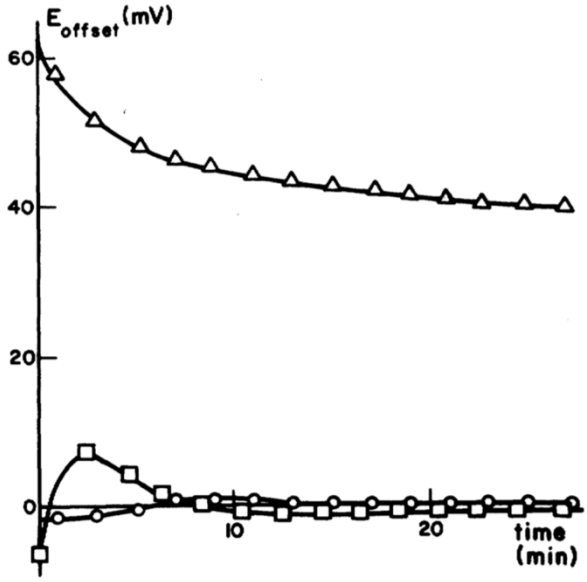

Figure 8: Offset potential of two Becton-Dickinson 7901 disposable electrodes placed face to face versus time after application. Δ = Ferris Red Dot Gel Type 600 (Ferris Medical Corp.); □ = NASA ECG Paste [33]*; ° = EKG Crème 204(Cardiac Electronics, Inc.).* [26]

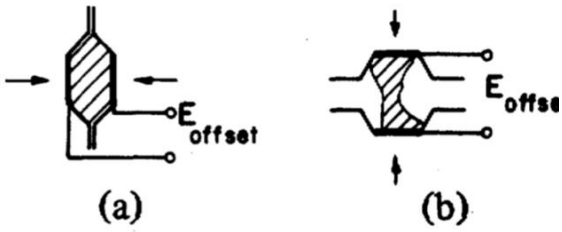

Figure 9: Two electrodes placed face to face with paste between. (a) Force on electrodes causes little artefact; (b) Separation causes little artefact as long as there is a paste bridge. [26]

Analysis of this artefact signal showed that this artefact is minimized with Ag-AgCl electrodes [26].

Finally, the stretch of the skin is a source of motion artefact. However, Tam and Webster [25], [26] showed that this artefact reduces to a negligible value with 20 strokes of very fine sandpaper. The barrier layer is scratched and the potential E_{se} of the skin is short-circuited. They measured the skin potential on the chest using NASA paste for different degree of skin abrasion with fine sandpaper [26]. In Figure 10 one sees that the most significant drop in the skin potential occurred after twenty sandpaper strokes. After this treatment, the skin potential remained stable with time compared to that of unabraded skin. Moreover, when pressing the electrode on the abraded skin, the variation of skin potential did not exceed 0.1mV. The amplitude of the skin potential

depends on the degree of abrasion, but when it is too vigorous could cause skin irritation, depending on the paste and the adhesive of the electrode [26].

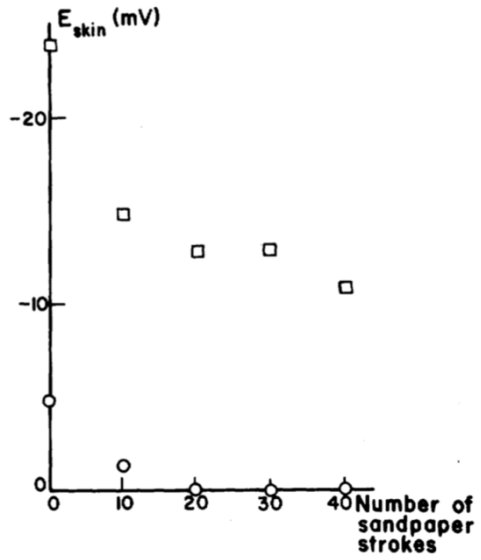

Figure 10: Skin abrasion reduces both skin potential and motion artefact. □= skin potential; ∘= change in skin potential when the electrode is pressed. [26]

Tam and Webster [25], [26] indeed tested fifteen commercial gels and found only five are mild to avoid irritation. The level of irritation depends on NaCl concentration. For these five mild pastes the irritations remained acceptable for a 24h period of the test, like is showed in Figure 11. The last three pastes, on the right of the figure, are a reference isotonic paste, prepared by them [26].

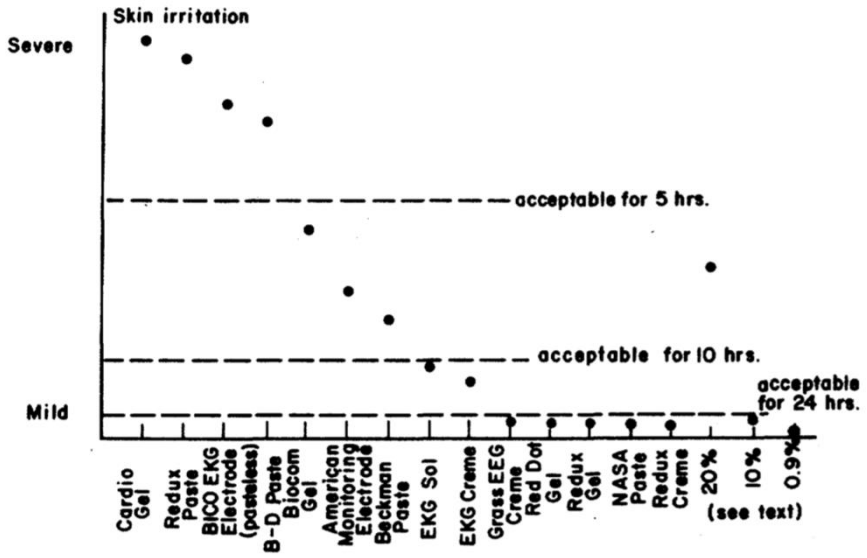

Figure 11: Skin irritation level when several commercial pastes are used on skin abraded twenty times [26].

They also found that, with mild gel (0.9 percent NaCl), the skin regrows in 24h and then the artefact returned. Instead, with high concentration paste (NASA, 9 percent NaCl) the skin remained injured and the artefact did not return [25], [26]. So, the electrode paste and the sites should be changed daily [26]. Another technique was developed by Burbank and Webster and that is the puncture technique. A blood lancet protruding 0.5mm from X-Acto knife blade chuck punctured the skin 20 times [25]. In Figure 12 one sees the improvements obtained with this technique in the signal recorded, highlighting the decrease of the artefact.

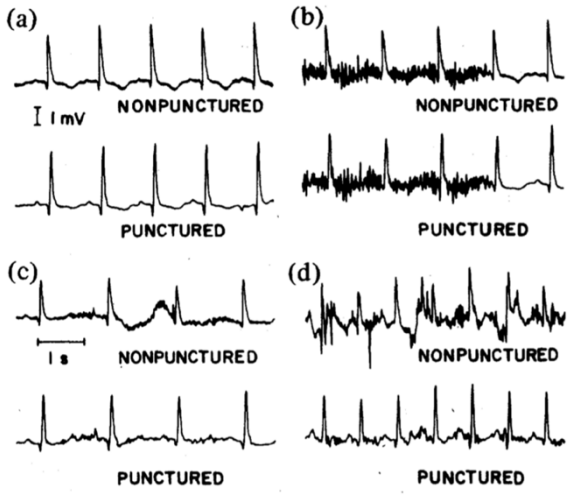

Figure 12: Comparison of ECG simultaneously taken from punctured (ten 0.5mm punctures) and non-punctured electrodes sites. (a)subject standing at rest, (b) isometric contraction of the pectorals, (c) rolling over in bed, and (d) running on a treadmill.[25]

1.4 Current issues and the aim of the thesis

Myoelectric-controlled hand prostheses record the surface EMG of the residual stump muscles to identify the movement intention and control hand fingers. Therefore, the quality of the EMG detection is important to obtain clean control signal with high signal to noise ratio.

In prosthesis equipped with vibrotactile feedback system, the issue of signal quality is particularly relevant because, beside the classical problems affecting the quality of EMG signals, also vibration induced motion artefacts may reduce the quality of the detected signal. Usually, vibrator and EMG electrodes are placed in close proximity for practical and constructive reasons. In this configuration, the vibrator causes mechanical stress of the skin, and also variations of the electrode-skin interface. These could cause a motion artifact on the sEMG signals used to control the hand movement, and therefore a worsening of the prosthesis performance.

The present study was carried-out in collaboration with BionIT Labs (Lecce, Italy), active in the field of myoelectric prosthesis design and commercialization. The aim of this study is to characterize the vibration artefact on sEMG signal, caused by the

vibrotactile stimuli and to identify strategies to minimize it (i.e. the reciprocal placement of the electrodes and the vibrator, the characteristics of the front-end used to record the sEMG signals, and the preparation of the skin of the stump). Three potential sources of the motion artifact will be analyzed: the changes of the impedance unbalance, the common-mode and the differential-mode variations of the half-cell potential.

The effects of these factors on the quality of detected EMG signals will be studied in three steps: theoretically; using custom-made circuits and experimentally.

The expected results are the appearance of a superimposed signal on the sEMG, because its frequency could be on the bandwidth of the signal of interest. This undesired signal could be spikes-like artefacts, high powerline interference and shifts of the baseline of the signals.

Chapter 2

Identification and Modelling of motion artefact sources

2.1 Sources of motion artefact

2.1.1 Introduction

Sources of motion artefact are: cable motion; electrode-skin contact movements; pressuring and stretching of the skin.

- Deformations of the cable generate triboelectric noise. The input capacity of the preamplifier changes, generating parametric fluctuations in the input network [25]., this cause will not be covered by this study because this effect is irrelevant for the hand prosthesis. Usually, the myoelectric prostheses use embedded electrodes.
- Electrode-skin contact movements and pressure or stretching of the skin generate changes of its electrical properties. The half-cell potential changes because the double-layer of charge at the electrode-electrolyte interface E_{hc} and the skin potential E_{se} are altered (Figure 5). The impedance Z_e of the electrode-

skin contact changes, by causing variations of the impedance unbalance between the exploring electrodes.

Motion artefact caused by electrode-skin contact movement or pressuring and stretching of the skin was analyzed in this study. Three effects were identified:

- change of the impedance unbalance ΔZe,
- common-mode variation of the half-cell potential E_{hc},
- differential-mode variation of the half-cell potential E_{hc}.

Three different circuits have been made to simulate the variation of these sources.

2.1.2 Changes of the impedance unbalance

The sEMG signal is usually recorded by means of a differential front-end connected to two exploring electrodes placed on the skin. If the electrodes impedances of the two electrodes are unbalanced the common-mode input signal generates a differential component that is amplified by the front-end. Movements of the electrodes with respect to the skin may cause changes of the impedance unbalance ΔZe at the input of the front-end.

The circuit, showed in Figure 13, generates variations of the amplifier output with induced-changes of the impedance unbalance, while the half-cell potential is kept constant. It is not used to record biopotentials, but explain the influence of the impedance unbalance in case of sEMG recording. The circuit consists of:

- C_{E1} and R_{E1}: the capacitive and the resistive components of the exploring electrodes;
- C_1 and R_1: the capacitive and the resistive components of the reference electrode;
- E_{hc1}: the half-cell potential of the reference electrode;
- C_2, R_2, and R_3: the capacitive and the resistive components of the impedance unbalance ΔZ_e between the two terminals of the front-end;
- S_1 (a switch). If it is open the impedance unbalance ΔZ_e corresponds to the parallel of C_2, R_2, while if it is closed Z_e becomes the parallel of C_2, R_2, and R_3;
- Z_{I1} and Z_{I2}, that are the input impedances of the front-end.

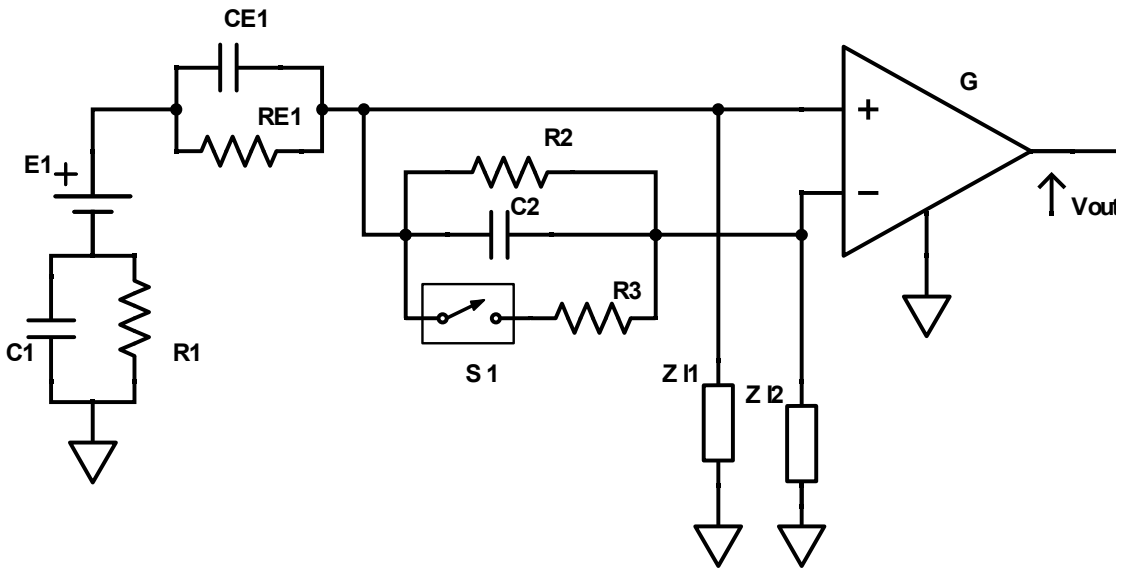

Figure 13: The circuit generates variations of amplifier output corresponding to induced- variations of the impedance unbalance ΔZe, while the half-cell potential is kept constant. C_{E1} and R_{E1}: the capacitive and the resistive components of the exploring electrode. C_1 and R_1: the capacitive and the resistive components of the reference electrode; E_{hc1}: the half-cell potential of the reference electrode; C_2 R_2 and R_3: the capacitive and the resistive components of the impedance unbalance between the two terminals of the front-end; S_1 (a switch). If it is open the impedance unbalance consists of C_2, R_2, while if it is closed Z_e becomes the parallel of C_2, R_2, and R_3; Z_{I1} and Z_{I2}: the input impedances of the front-end and finally.

The exploring electrodes was represented by one split-electrode R_{E1} C_{E1}. An impedance unbalance is 'seen' at the input of the front-end. It is made by parallel of the capacitance C_2, the resistor R_2, and the switch S_1 series-connected with the resistor R_3. S_1 is used to variate this impedance:

- If S_1 is open at the input of amplifier there is an impedance made by the parallel R_2 and C_2;

- If S_1 is close, C_2 and R_2 are paralleled with the resistance R_3. If the value of R_3 is lower than the resultant impedance of the parallel between R_2 and C_2, the impedance unbalance decreases.

When S_1 is open the capacitance charges, while when the switch is closed it discharges. The output voltage of the front-end is affected by the charge and the discharge of the capacitor C_2. It depends on the value of the common-mode voltage, of the impedance unbalance and the amplitude of the ΔZ_echanges. The output signal will display shifts of the baseline and the increase of the powerline interference corresponding to the quick variation of the impedance unbalance, by causing an artefact outgoing.

2.1.3 Common-mode variations of the half-cell potential

The input DC voltage (Ehc) of the front-end could change, because the exploring electrodes are pressed or the underlying skin is stretched. In particular, identical electrodes with the same condition of the underlying skin will produce the same change of half-cell potential, if both undergo to the same mechanical stress. In this case, the common-mode half-cell potential changes. It also changes when the reference electrode is excited, while the exploring electrodes are on rest. The common-mode potential may become differential, because of the impedance unbalance at the input of the amplifier. Figure 14 shows the reference circuit that produces variations of the amplifier output with common-mode induced-changes of the half-cell potential and constant impedance unbalance. The components of the circuit are the following:

- two series-connected batteries V_1 and V_2 were used to generate the input common-mode half-cell potential of the differential front-end;
- one switch S_1 in parallel with one battery V_1, so the common-mode signal could range with its opening and closing;
- a constant impedance unbalance ΔZe at the input of the front-end, made by the parallel of one resistance R_1 and one condenser C_1;
- Z_{I1} and $Z_{I2,}$ that are the input impedances of the front-end.

The surface of the reference electrode is considered larger than the exploring electrodes. The resistive component is inversely proportional to the surface, so $R_r << R_e$ and the reference electrodes is considered short-circuited.

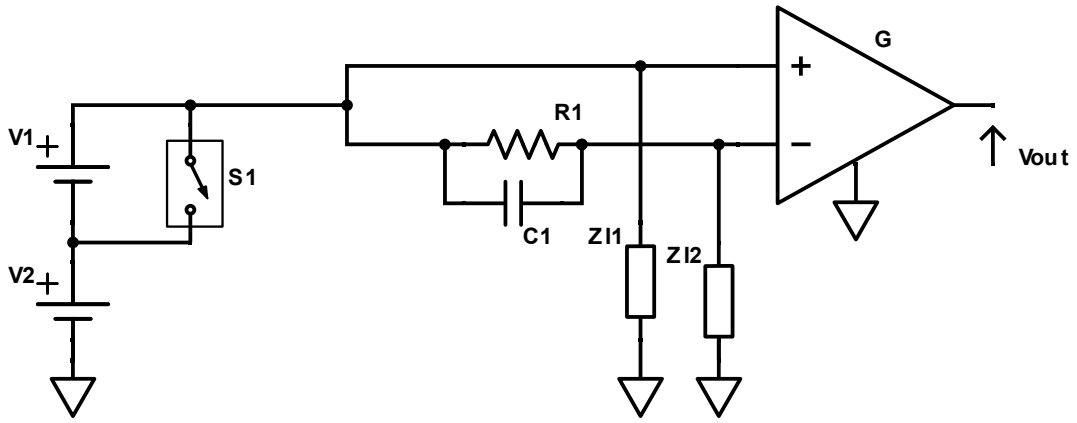

Figure 14: The circuit produces changes of the amplifier output with common-mode induced-changes of the half-cell potential and constant impedance unbalance ΔZe. It includes: two series batteries V_1 and V_2 were used to generate the input common-mode half-cell potential of the differential front-end; one switch S_1 in parallel with one battery V_1, so the common-mode signal can range with its opening and closing; a constant impedance unbalance at the input of the differential front-end, made by the parallel of one resistance R_1 and one capacitance C_1; Z_{I1} and Z_{I2}, are the input impedances of the front-end.

Variations of input common-mode potential is obtained with the two batteries V_1 and $V_{2,}$ and the switch S1. The DC common-mode voltage became an AC voltage by opening and closing the switch S_1. This potential becomes a differential signal because of the impedance unbalance at the input of the front-end. So, the resulting AC differential signal is amplified possibly creating artefact on the signal.

2.1.4 Differential-mode alteration of the half-cell potential

The input DC voltage (Ehc) of the front-end could change, because the exploring electrodes are pressed or the underlying skin is stretched. The half-cell potential E_{hc} at the electrode-skin interface changes and also the skin potential E_{se}. Usually, this deviation is not equal for both electrodes, so a differential-mode potential born and adds up to the sEMG signal. Figure 15 shows the circuit that reproduces quick differential-mode alterations of the half-cell potential. The circuit consists of:

- two batteries V_1 and V_2 used to create the differential mode half-cell potential at the input of the front-end;
- one switch S_1 placed in parallel with one battery. When S_1 is open or closed the potential of positive terminal varies compared to the negative terminal that remains constant. Consequently, the whole differential signal changes;
- Z_1 and Z_2 represent the impedance of the exploring electrodes;
- Z_{I1} and Z_{I2} are the input impedances of the front-end;

The surface of the reference electrode is considered larger than the exploring electrodes. The resistive component is inversely proportional to the surface, so $R_r << R_e$ and the reference electrode is considered short-circuited.

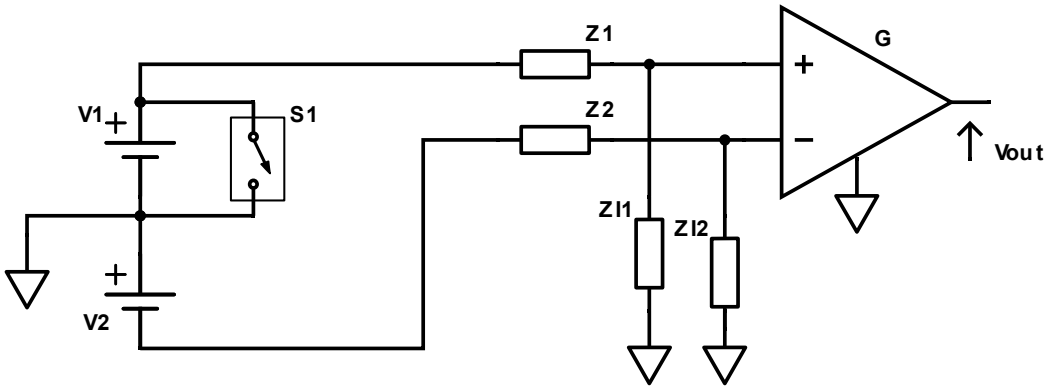

Figure 15: The circuit reproduces quick differential-mode alterations of the half-cell potential. It consists of: two batteries V_1 and V_2 used to create the differential mode

half-cell potential at the input of the front-end; one switch S_1 placed in parallel with one battery. When S_1 is open or closed the potential of positive terminal varies while the potential of negative terminal remains constant. Consequently, the whole differential signal changes; Z_1 and Z_2, represent the impedance of the exploring electrodes; Z_{I1} and $Z_{I2,}$ are the input impedances of the front-end.

The impedance of the exploring electrodes Z_1 and Z_2 are the identical and the impedance unbalance is considered null. Variations of the differential input half-cell potential is obtained by the two batteries and the switch S_1. Differential variations of the input voltage are always amplified and showed at the output voltage. It causes baseline shifts of the output signals or spike-like signals with quick variations, by causing motion artefact. This could be filtered only if its frequency is out of band compared to the bandwidth of sEMG signal.

2.2 Effect of the amplifier input capacitance on the motion artefact rejection

2.2.1 Introduction

In the theoretical analysis the coupling between the electrode-amplifier system and the input signals was made considering two input signals:

- the common mode input at the front-end;
- the differential-mode input at the front-end.

This analysis was made to study the effect of:

- the capacitive component Ce of the exploring electrodes impedance, and
- the reactive component of the input impedance Z_i of the front-end.

In this analysis the surface of the reference electrode is assumed larger than the exploring electrodes. Since the resistive component of the impedance is inversely proportional to the surface of the electrode, R_r is considered negligible with respect to R_e.

2.2.2 Common-mode input excitation

The common-mode input signal V_c generates signal components at the output of the front-end, because of:

1. The presence of the impedance unbalance ΔZe between the exploring electrodes, which create Vd at the input of the front-end;
2. The finite CMRR of the instrumentation amplifier
3. The presence of impedance unbalance of the input impedance of the amplifier;

The impedance unbalance inside the front-end is constant and its value is very small, so it may be excluded.

The CMRR of the instrumentation amplifier must be as high as possible for rejecting the common-mode signal. It is important to note that CMRR varies with the frequency. Specifically, it decreases with the increasing of the frequency. However, in narrow bandwidths, such as that of the sEMG signal, CMRR variability with frequency is not relevant.

The influence of the impedance unbalance ΔZe on the input signal depends on the value of the input impedance Z_i of the instrumentation amplifier. This has a reactive component C_i that changes with the frequency, reduces the rejection of the common-mode and how the impedance unbalance affects the output signal.

The impedance Z_i is the parallel of a resistor R_i and the capacitor C_i. The common-mode input signal associated with the half-cell potential may change because of pressing on the electrodes or stretching of the underlying skin. If the mechanical stress is quick the frequency of the voltage variations is high and the reactive component of the input impedance Z_i drops. The impedance Z_i will be small because at high frequency it is dominated by the capacitor. These considerations support the hypothesis that front-end with very low input capacitance may improve the rejection of movement artefacts associated with rapid variations of common mode half-cell potentials.

The transfer function between the electrodes and the amplifier has been calculated to understand the influence of C_i on the amplitude of movement artefact. Also, the capacitance C_e of the exploring electrodes-skin contact could change rapidly during a

motion artefact by causing changes of the electrode-amplifier coupling. Therefore, the analysis included as variable parameter also the value of Ce.

The equivalent common-mode circuit showing the coupling between a common-mode signal and an electrode-amplifier system is shown in Figure 16. As mentioned above, the surface of the reference electrode is considered larger than the exploring electrodes, so R_r is considered negligible with respect to R_e.

The differential signal at the input of the amplifier, caused by the common-mode signal, is:

$$V_d = V_+ - V_- \tag{6}$$

Therefore, the input-referred transfer function between the electrodes and the amplifier results:

$$H^*(s) = \frac{V_+ - V_-}{V_c} \tag{7}$$

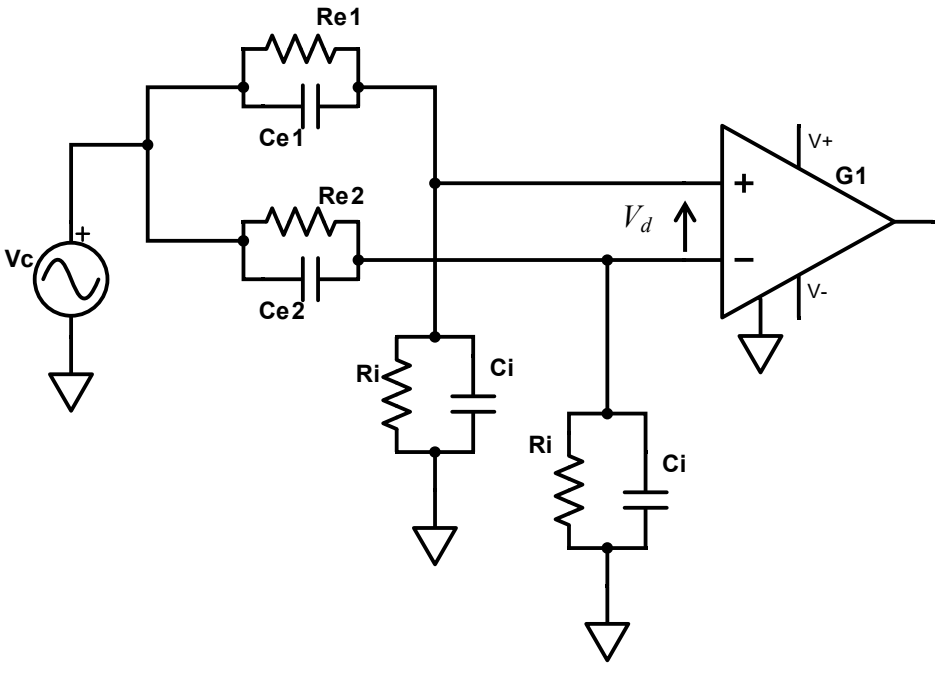

Figure 16: Schematic circuit of biopotential sampling made in a differential configuration with common-mode excitation.

V_+ and V_- are the potential respectively of the positive and negative terminal, and they change with the frequency.

$$V_+ = \frac{R_i * (1 + sC_{e1}R_{e1})}{R_i + sC_{e1}R_{e1}R_i + R_{e1} + sC_iR_{e1}R_i} \quad (6.1)$$

$$V_- = \frac{R_i * (1 + sC_{e2}R_{e2})}{R_i + sC_{e2}R_{e2}R_i + R_{e2} + sC_iR_{e2}R_i} \quad (6.2)$$

Finally, the transfer function H(s) results:

$$H(s) = \frac{R_i\Delta R_e(1 + sC_iR_i)\left(1 + s\left(\frac{R_{e1}^2}{\Delta R_e} + R_{e1}\right)\Delta C_e\right)}{(R_i + R_{e1})(R_i + R_{e2})[1 + s(R_i \oplus R_{e1})(C_{e1} + C_i)][1 + (R_i \oplus R_{e2})(C_{e2} + C_i)]} \quad (7.1)$$

This transfer function has been analyzed in MATLAB varying:

- R_i and C_i;
- The percentage of impedance unbalance ΔZe;
- R_e and several values C_e.

The Bode diagrams of different transfer functions, showed in Figure 17, was obtained choosing:

- The capacitive component C_e of the electrodes of 0, 10pF, 100pF, 1nF, and 10nF;
- The resistive component R_e of the electrodes of 100kΩ;
- The impedance unbalance between the exploring electrodes of 10%;
- The resistive R_i and the capacitive C_i component of the input impedance of the front-end of 100GΩ and 3pF, specifications of the instrumentation amplifier (INA 333)

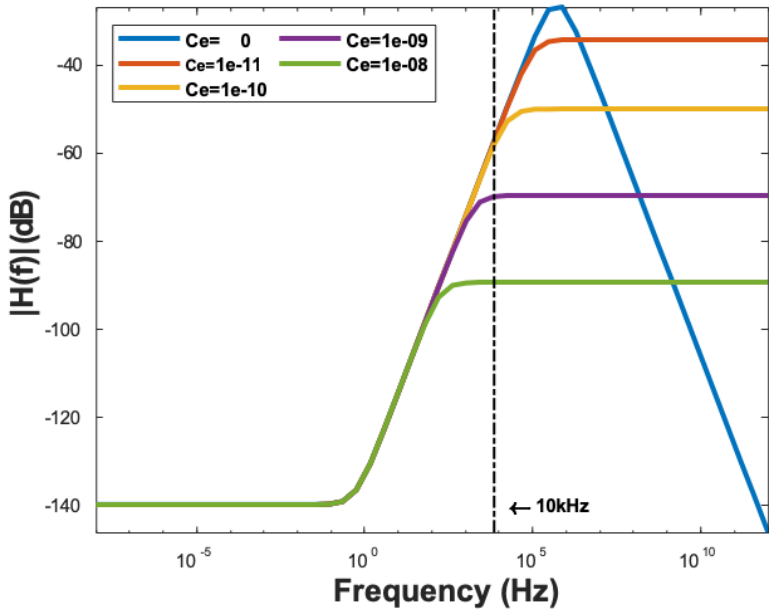

Figure 17: Bode diagram of the electrode-amplifier coupling transfer functions with common-mode input. The impedance unbalance ΔZe is set to 10%, while the capacitance of the exploring electrodes is set to the values showed in the legend of the figure. The dashed line highlights the value of the attenuation for all transfer function at the frequency of 10kHz. The input capacitance Ci is 3pF of the INA333 and of the impedance of the exploring electrodes Re is 100kΩ.

The Table 2 show the module of each transfer functions for different values of Ce. The attenuation at high frequencies varies with the value of Ce.

Table 2: Gain of the transfer functions in Figure 17 at the frequency of 10kHz corresponding to each value of Ce.

Frequency / Input capacitance	f= 10kHz
Ce= 10nF	-90dB (30000V/V)
Ce=1nF	-70dB (3000V/V)
Ce=100pF	-50dB (300V/V)
Ce=10pF	-50dB (300V/V)

With small electrodes (Ce=10pF-100pF) the input signal will be attenuated less than with large electrodes (Ce=1nF-10nF). This may be one of the reasons which make electrode-amplifier systems with large electrodes less affected by motion artefacts.

The contact surface of the electrodes could decrease during the motion artefact, reducing the value of the C_e. The influence of the input reactive component is of particular interest when the capacitance of the electrode Ce became small. The transfer function was analyzed in MATLAB obtaining the Bode diagram of the transfer function variable with each value of C_i, shown in Figure 18. There were chosen:

- The capacitive component C_i of the input impedance of the front-end of 3pF (specification of the INA333), 30pF, 300pF,
- The resistive component of the input impedance of the front-end of 100G (specification of the INA333).
- The resistive R_e and capacitive component C_e of the input-impedance of the front-end of 10M and 100pF (small electrodes),
- The impedance unbalance between the exploring electrodes of 10%.

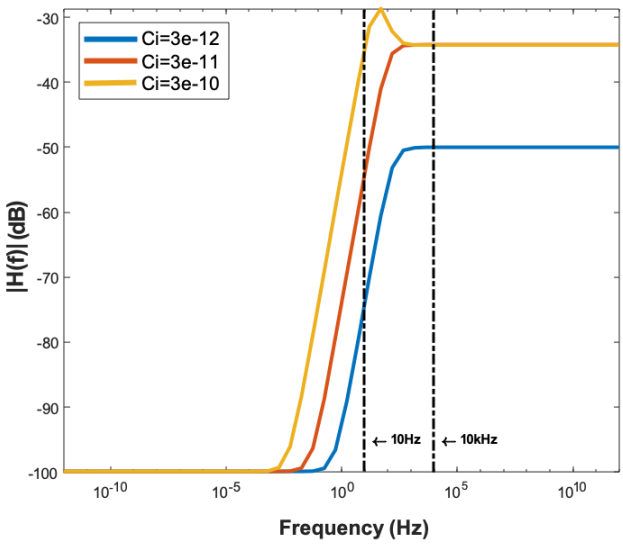

Figure 18: Bode diagram of the electrode-amplifier coupling transfer functions with common-mode excitation. The impedance unbalance ΔZe is set to 10%, while the

capacitance of the input impedance is set to the values showed in the legend of the figure. The two dashed lines highlights the value of the attenuation for all transfer function at the frequency of 10Hz and 10kHz. The value of Ce is 100pF and of Re is 10kΩ.

The attenuation particularly depends on the excitation frequency and the value of the reactive component C_i. Table 3 shows the value of the gain for two frequency and for each value of Ci.

Table 3: Gain of the transfer functions in Figure 18 corresponding to each value of input capacitance Ci and two values of frequency.

Frequency / Input capacitance	f= 10Hz	f= 10kHz
Ci= 3pF	-75dB (5623V/V)	-50dB (316V/V)
Ci=30pF	-55dB (562.3V/V)	-34dB (50V/V)
Ci=300pF	-35dB (56.23V/V)	-34dB (50V/V)

The attenuation at high frequency is lower than the low frequency for each transfer function in Figure 18. The reactive component of the input impedance decreases with the increase of the frequency. The influence of the impedance unbalance increases compared to the input impedance Zi. So, the amplitude of the common-mode component that becomes differential increases, and the attenuation results lower than the low frequency.

In conclusion, the behavior of the electrode-amplifier coupling with a common-mode excitation depends on:

- the value of capacitance C_e of the electrode-skin also with a low input capacitance Ci of the front-end. Electrodes with large contact surfaces are

preferred compared to the small electrodes because the corresponding transfer function shows a higher attenuation at each frequency;

- the value of the reactive component of the input impedance Z_i of the front-end. It decreases with the increase of the frequency and the weight of the impedance unbalance at the input of the front-end increases. Front-end with lowest input capacitance are preferred against the motion artefact.
- the excitation frequency. Low excitation frequency is preferred compared to the high excitation frequency, because the corresponding attenuation is lower. Motion artefacts at low frequency are more attenuated than at high frequency.

2.2.3 Differential-mode input excitation

The transfer function of the electrode-amplifier system with differential-mode excitation was analyzed. Differential-mode variations of the half-cell potential are amplified with the differential gain of the differential amplifier. Also in this case the reactive component of input impedance Z_i could influence the recording of the signals. The scheme of the reference circuit is shown in Figure 19, where R_i and C_i is the resistance and the capacitance of the differential input impedance of the front-end, R_{e1} and R_{e2} is the impedances of the exploring electrodes (supposed purely resistive). The input differential voltage was made by a Wheatstone bridge, described in section 3.1.3. It was simplified by its Thevenin equivalent circuit made by a voltage generator V_1 series-connected with a resistor R_w. V1 and Rw are the voltage and the impedance 'seen' by the pins A and B of Figure 26 and Figure 19.

The surface of the reference electrode is considered larger than the exploring electrodes, so R_r is considered negligible with respect to R_e.

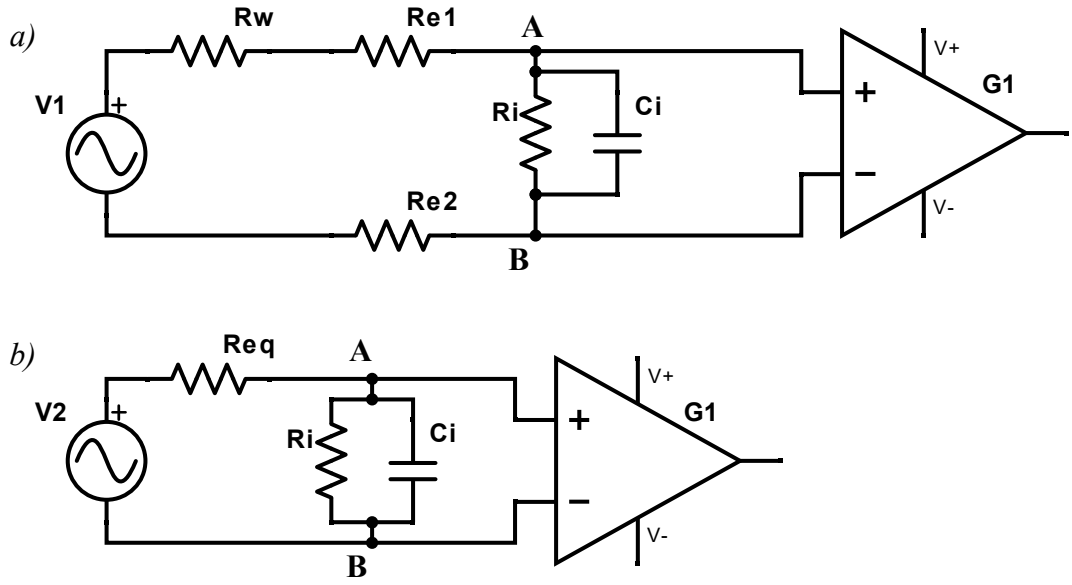

Figure 19: a) Schematic circuit of biopotential sampling made in a differential configuration with differential-mode excitation; b) Equivalent circuit

The value of R_i and C_i were 100G and 3pF, because of the specifics of the instrumentation amplifier datasheet (INA 333), R_{e1} and R_{e2} were 10kΩ, and R_w resulted 158,1kΩ. R_w, R_{e1}, and R_{e2} were three series resistors and the equivalent resistance results:

$$R_{eq} = (R_w + R_{e1} + R_{e2}) = 178{,}1k\Omega \tag{8}$$

The transfer function of the electrode-amplifier coupling is:

$$H(s) = \frac{R_i}{R_i + R_e} \cdot \frac{1}{1 + sC_i(R_{eq} \oplus R_i)} \tag{9}$$

and the resulting Bode diagram is shown in Figure 20. It is a low pass filter where the cutoff frequency is the pole frequency.

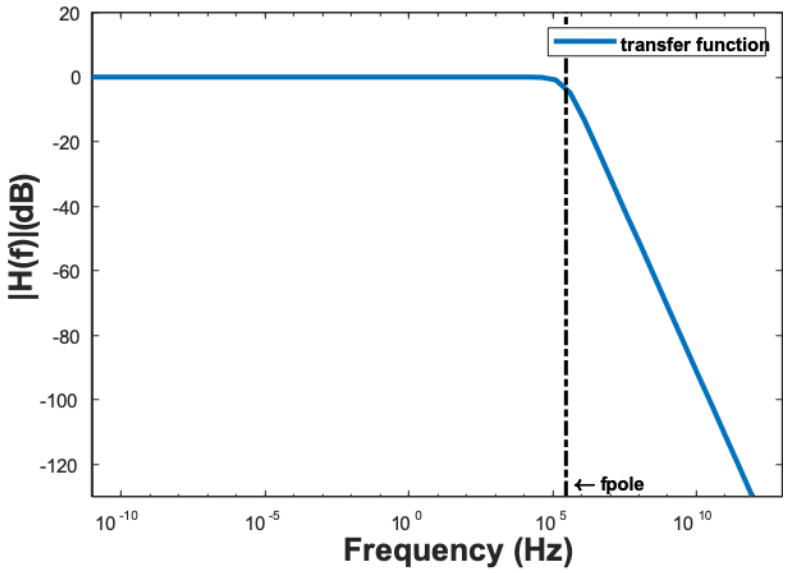

Figure 20: Bode diagram of the electrode-amplifier coupling transfer functions with differential-mode excitation. The dashed line highlights the value of the attenuation for all transfer function at the frequency of the pole (298kHz).

$$f_p = \frac{1}{2\pi C_i (R_{eq} \oplus R_i)} = 298kHz \tag{10}$$

$$|H(0)| = \frac{R_i}{R_i + R_e} \cong 1V/V \ \rightarrow 0dB \tag{11}$$

The pole frequency is very high, over the bandwidth of the sEMG signal (10-500Hz) and gain of the bandwidth is 0dB, i.e. 1V/V.

Concluding, the reactive component of the differential input impedance does not affect the electrode-amplifier coupling with differential excitation. The reactive component of the differential-mode input impedance does not cause distortion or attenuation of the differential input voltage. The differential input is normally amplified by the front-end and it overlaps the sEMG signal if its frequency is within the bandwidth of interest.

As a consequence, it would be desirable move left the pole, by decreasing the fp. The value of Ri and Ci are specifications of the amplifier, so the value of R_{eq} should be increased. The resistive component of the electrode impedance increases with the decrease of the surface. This specific analysis with differential-mode excitation suggests

the reducing of the electrodes surface. However, considering the global context with also the common-mode excitation (analyzed in the previous paragraph 2.2.2) the increasing of the electrode impedance could be a problem.

Chapter 3

Design and Test of circuit simulating motion-artefact generation

3.1 Design of circuit

3.1.1 Introduction

The experiments were performed using a custom-made circuit, a bipolar EMG detection system built on an electronic board. The circuit included the front-end and the electrical models of the electrode-skin contact made with discrete components; RC parallels for the impedances (Ze) and batteries for the half cell potentials (Ehc). Variations of the Ze and Ehc simulating the three hypothesized causes of motion artifact were obtained through switches.

3.1.2 Power supply and Front-end

An analog front-end was used to record the sEMG signal. It was made in two stages:

- The Instrumentation Amplifier INA333;
- The low-pass filter with cutoff frequency at 482Hz.

Both stages are supplied between 0V and 5V of voltage. The supply voltage was obtained by a 9V battery and a voltage regulator L7805. Three capacitors (C_1= 10μF, C_2= 47μF, and C_3= 47μF) were added to avoid voltage fluctuations, with C_2 and C_3 electrolytic capacitors. Figure 21 shows the electronic circuit. S1 is the on/off switch.

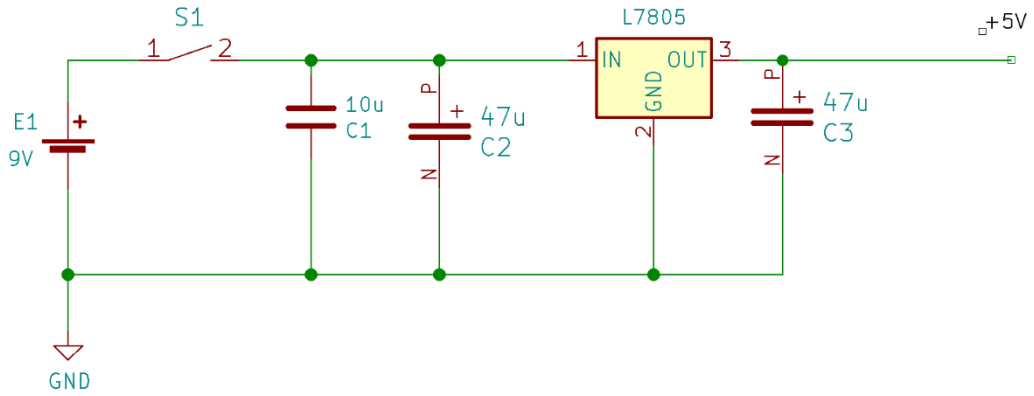

Figure 21: Electronic circuit of the power supply. E_1 is the battery; S_1 is the switch to remove the power supply; L7805 is a voltage regulator from 9V to 5V; C_1, C_2, and C_3 are the capacitor to avoid voltage fluctuations, of which C_2 and a C_3 are electrolytes.

The first stage of the front-end was the Instrumentation Amplifier INA333 that was characterized by these features [34]:

- Common-mode rejection ratio CMRR= 115dB (>100dB);
- Input impedance |Zi|= 1.1G at 50Hz, minimizing the common-mode to differential-mode conversion caused by the impedance unbalance between the exploring electrodes;
- Low bias current 1pA;
- Low noise level within the bandwidth of sEMG signal (10-500Hz), 50nV/Hz.

The simplified schematic of the Instrumentation Amplifier INA333 is displayed in Figure 22. The transfer function is [34]:

$$H'(s) = 1 + \frac{R'}{Z_G} \tag{3}$$

Where R'=100kΩ is a specific of the datasheet and is cannot be modified, while Z_G is the impedance 'seen' by the pins 1 and 8. R' and Z_G define the gain G_1 of the amplifier:

$$G_1 = 1 + \frac{100k\Omega}{R_G} \tag{4}$$

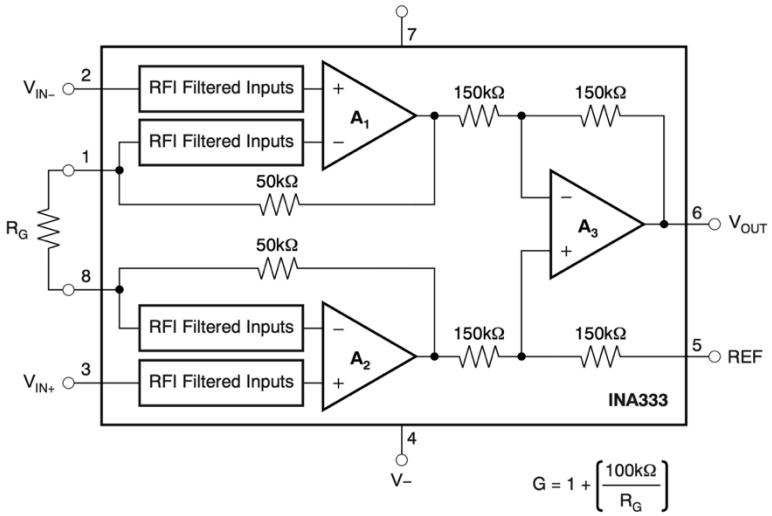

Figure 22: Simplified Schematic of the Instrumentation Amplifier INA333; G_1 is the gain of the amplifier.[34]

An R_G= 1kΩ was selected to obtain a differential amplification of 101(V/V), meaning 40dB within the bandwidth of the transfer function.

Typical characteristic shown in Figure 23 is a low pass filter with the cutoff frequency of 3,5kHz at T_A=25°C, V_S=5V, R_L=10kΩ, and V_{REF} equal to mid-supply [34].

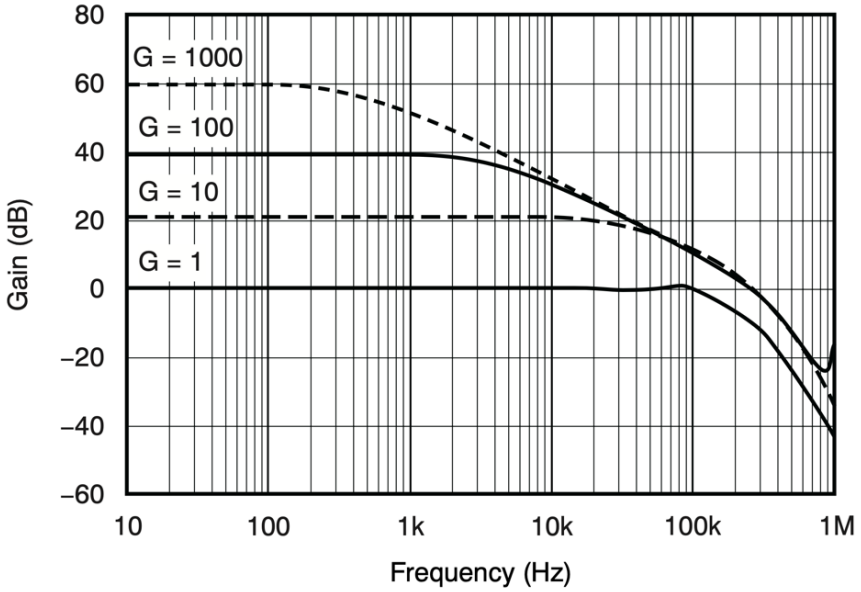

Figure 23: Typical characteristic, Gain vs Frequency. The trend corresponding to G_1=100 is of interest [34].

The DC component is not filtered by the INA333, so the amplifier could saturate if the half-cell potential at the electrode-skin interface had higher values than 50mV.
The second stage of the front-end was the active low-pass filter of Sallen-Key, which has this transfer function:

$$H(s) = \frac{v_o}{v_i} = \frac{\frac{A}{R_1 R_2 R_3 R_4}}{s^2 + s\left(\frac{1}{R_1 C_1} + \frac{1}{R_2 C_1} + \frac{1-A}{R_2 C_2}\right) + \frac{1}{R_1 R_2 C_1 C_2}} \quad (5)$$

The electronic circuit of this filter is shown in Figure 24, where R_3 and R_4 (both 33kΩ) define the amplification (2V/V). C_1 and C_2 were two capacitors of 10nF.

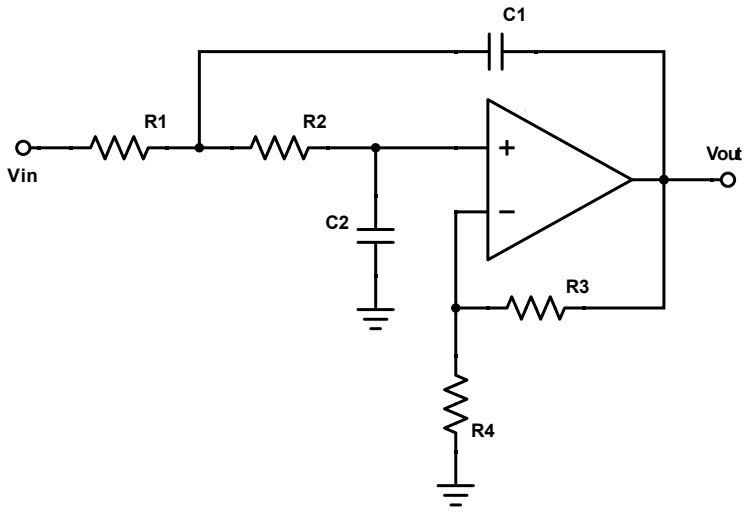

Figure 24: Schematic of active low-pass filter Sallen-Key.

This study focused on the characterization of the vibration artifact on sEMG signal. The DC component is of particular interest because its changes are one of the possible causes of motion artefact. Therefore, the cutoff frequency of the active low-pass filter was 482Hz, including the sEMG signal frequency band and the DC component.

The resulting amplification of the front-end was $G = G_1 \cdot G_2 = 202(V/V)$, i.e. 46dB. Thus, in order to avoid the saturation of the front-end the peak input voltage should be lower than $\frac{5V}{202} = 24{,}7mV$. The amplitude of the sEMG signal is normally lower 5-6mV, but the DC voltage of the half-cell potential (20-500mV) was not filtered and could be a problem for the saturation of the front-end.

The second stage of the front-end includes a voltage follower (Figure 25), which has at the input a resistive divider made by two equal resistors of 33kΩ to obtain the reference voltage of the front-end, that was the mid-supply (2,5V).

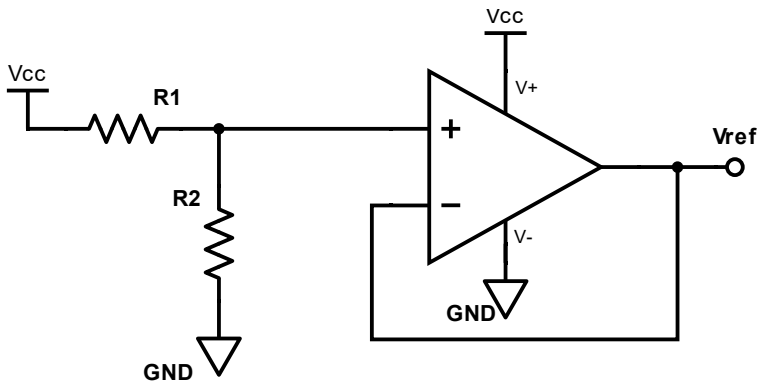

Figure 25: Voltage follower used to define the reference voltage at mid-supply 2,5V/V.

3.1.3 Design of circuit simulating the input excitations

The circuit of Figure 26 was made to simulate the three possible variations of the electrode-skin properties (mentioned in section 2.1) that could cause motion artefacts. It was mounted on an electronic board and in Figure 26 four areas can be identified:

- the upper part is the power supply (paragraph 3.1.2);
- the central part replicates the variations of the impedance unbalance ΔZe between the two input terminals of the front-end or the common-mode changes of the half-cell potential (paragraphs 2.1.2 and 2.1.3);
- the lower part simulates the differential-mode variations of the half-cell potential (paragraph 2.1.4);
- the right-hand includes a double switcher to select the input excitation of the front-end.

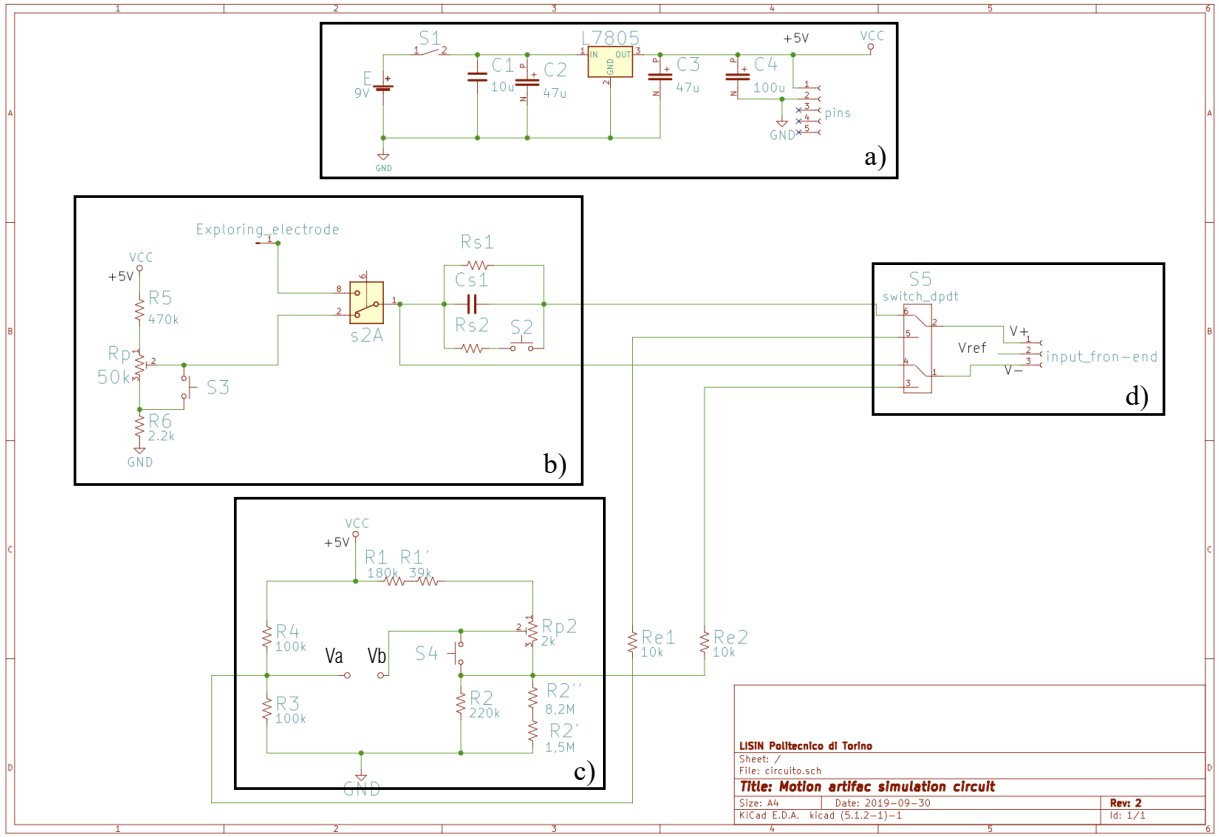

Figure 26: Overall electronic circuit of motion artefact simulation. a) The upper part is the power supply; b) the central part replicates the variations of the impedance unbalance ΔZe at the input of the front-end or common-mode changes of the half-cell potential; c) the lower part simulates differentia-mode variations of the half-cell potential and finally; d) the right-hand of the circuit includes a double switcher to select the input excitation.

In Figure 27 three sections corresponding to the simulation of three input excitations (defined in paragraph 2.1) are outlined:

- changes of the impedance unbalance ΔZe at the input of the front-end;
- common-mode fluctuations of the half-cell potential;
- Differential-mode variations of the half-cell potential.

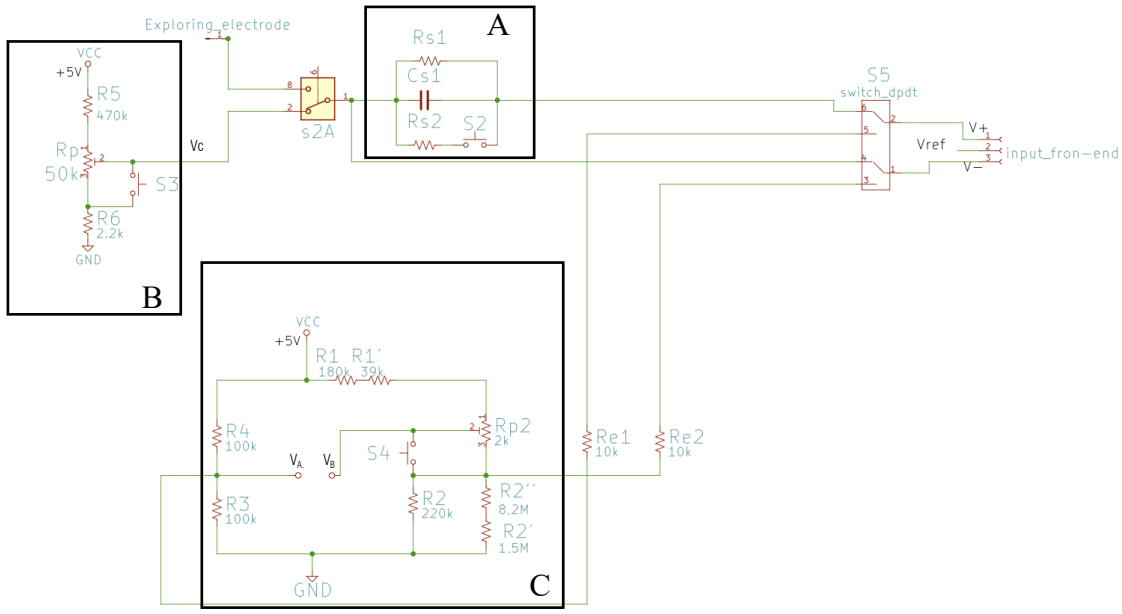

Figure 27: A) R_{s1}, C_{s2}, R_{s2}, and S_2 formed a variable impedance unbalance; variations of this component were obtained by opening and closing S_2, while the half-cell potential is kept constant selecting with S_{2A} the pin 8. The values of R_{s1}, C_{s1} and R_{s2} were chosen at each test then performed. B) Common-mode variations of the half-cell potential were made by S_3, R_5, R_p, and R_6 that built a variable passive divider of the power supply, in which R_p was a trimmer. Quick variations of this potential were generated by opening and closing S_3 with the selector S_{2A} on pin 1 and S_2 open. Their amplitude was chosen varying the value of R_p. In cases A and B these variations were at the input of the front-end if the selector S_5 was on the pins 4 and 6. C) Differential-mode changes of the half-cell potential were obtained with a Wheatstone bridge composed by R_4, R_3, R_1, R_1', R_{p2} (trimmer), R_2, R_2', R_2'', and the push button S_4. R_{e1} and R_{e2} represented the impedance of the exploring electrodes (purely resistive and balanced to each other). Variations of the differential voltage V_a-V_b were generated by opening and closing the push button S_4, and their amplitude was chosen varying the value of R_{p2}. In this case the push button S_5 should be on pins 3 and 5.

The circuits described above were used to define three experiments (describes below) aimed at model-based characterization the motion artefact on the sEMG signal. Three potential sources of the motion artefact were analyzed: the changes of the impedance unbalance ΔZ_e with a DC common-mode half-cell potential; the common-mode variations of the half-cell potential with a constant impedance unbalance ΔZ_e at the input of the front-end; and the differential-mode variations of the half-cell potential E_{hc}.

EXPERIMENT 1: Variation of the impedance unbalance ΔZe at the input of the front-end. A variable impedance, showed in Figure 27A, built by the parallel of Rs1, Cs1 and R_{s2} series-connected with the push button S_2.

Positioning:

- S_{2A} on pin 8, and
- S_5 on pins 4 and 6

the half-cell potential remained constant.

The impedance unbalance ΔZe 'seen' at the input of the front-end changed though S_1:

- S_1 open: is the parallel of R_{s1} and C_{s1};
- S_1 closed: is the parallel of R_{s1} and C_{s1} and R_{s2}.

The amplitude of the variations depends on the value of the capacitive C_{s2} and resistive component R_{s1}, R_{s2}, that were chosen at each test then performed

EXPERIMENT 2 Common-mode variation of the half-cell potential E_{hc} with constant impedance unbalance ΔZe at the input of the front-end. A variable voltage divider of power supply, showed in Figure 27B, was made to generate variations in the simulated half-cell potential. Considering that the amplitude of the half-cell potential ranges from 20mV to 500mV the variable voltage divider was built with R_5=470kΩ, R_p that was a multi-turn trimmer of 50kΩ, and R_6=2.2kΩ obtaining the desired range of voltage. Also, the push button S_3 was added in parallel to the trimmer to achieve quick changes of the voltage. The push button S_2 remained open keeping the impedance unbalance constant.

By positioning:

- the selector S_{2A} on the pin 2, and
- S_5 on the pins 4 and 6

It was possible to obtain changes of the simulated half-cell potential by pressing S_3 as follows:

- S_3 open: common-mode voltage V_c is the potential on the resistor R_p and R_6;
- S_3 closed: common-mode voltage Vc is the potential on the resistor R_6, because R_p is short-circuited.

The amplitude of the induced common mode voltage changes could be varied by acting on the trimmer R_p. The impedance unbalance was the $R_{s1}C_{s1}$ parallel and converted the common-mode variations into differential-mode at the input of the front-end.

EXPERIMENT 3 Differential-mode variations of the half-cell potential at the input of the front-end. These variations were obtained by the Wheatstone bridge of Figure 27C. Considering that the amplification G=202V/V of the front- end and the magnitude order of the half-cell of tens mV, the Wheatstone bridge was designed to obtain a differential variable output voltage on the scale of mV. It was built with R_3=R_4, R_1=180kΩ, R_1'=39kΩ, R_{p2} that was a multi-turn trimmer of 2kΩ, R_2=220kΩ, R_2' =8,2MΩ, R_2'' =1,5MΩ. The differential input voltage V_a-V_b ranged between $\pm 6mV$, thus the resultant output voltage ranged between $\pm 1.01V$ and the front-end (powered between) cannot saturate. R_{e1}=10kΩ and Re2=10kΩ represented the impedances of the exploring electrodes (purely resistive and balanced to each other). The push button S_4 was added in parallel with the trimmer to achieve quick variations of this voltage. By positioning:

- the double switch S_5 on the pins 3 and 5

the differential input voltage V_a-V_b quick changed through S_4 because the voltage V_b is altered.

- S_4 open: the resistance of the trimmer is equal to R_{p2};
- S_4 closed: the resistance of the trimmer is short-circuited.

The amplitude of this rapid variations was chosen varying the value of the trimmer R_{p2} that changed the value of the voltage V_b.

3.2 Bench test

3.2.1 Introduction

Three Bench Test were implemented to simulate the three hypothesized sources of motion artefact trough custom-made circuit (described in paragraph 3.1.3). The electrical models of the electrode-skin contact were made by discrete components: RC parallels for the impedances (Ze), and batteries for the half cell potentials (Ehc).

The experimental setup showed in Figure 28, is the same for all the Bench Test. It includes the experimental circuit (paragraph 3.1.3), the front-end (paragraph 3.1.2), and a digital oscilloscope connected to a Personal Computer (PC) through USB.

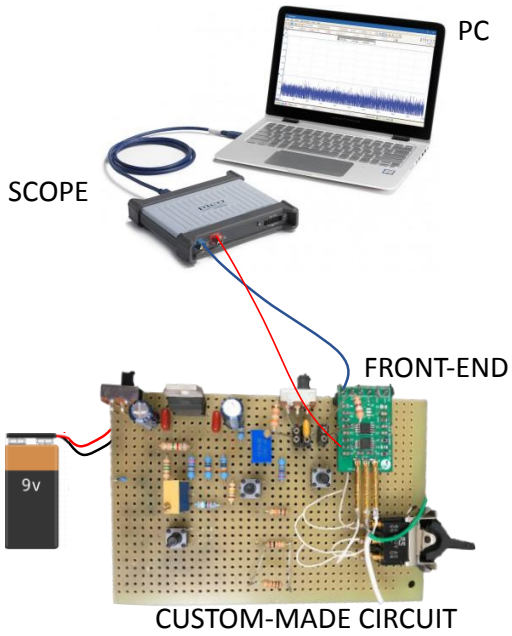

Figure 28: Experimental setup of the Bench Test. It includes the custom-made circuit (paragraph 3.1.3), the front-end (paragraph 3.1.2), and a digital oscilloscope ((PicoScope 3203D) connected to the Personal Computer (PC) through USB.

3.2.2 EXPERIMENT 1: Changes of the impedance unbalance

Variations of the contact surface between the electrode and the skin cause changes of the impedance Z_e and of the half-cell potential E_{hc} at the interface. Considering the exploring electrodes, changes of their contact-surface create variations of the impedance

unbalance at the input of the front-end and differential-mode variations of the half-cell potential. The two effects were analyzed separately by means of custom-made circuit, described in paragraph 3.1.3. In this experiment the only changes of the impedance unbalance at the input of the front-end with a DC common-mode input voltage were analyzed. The DC common-mode voltage becomes differential because of the impedance unbalance ΔZ_e. If the ΔZ_e changes the DC differential-mode voltage becomes an AC voltage at the input of the front-end. This signal is amplified by the front-end by causing artefacts on the recorded output signals.

This experiment was implemented by means of the experimental circuit (Figure 27A) in which the electrical model of the impedance unbalance was made with discrete components. The exploring electrode is placed face-to-face with the reference electrode obtaining the DC common-mode input voltage (the half-cell potential at this interface).

The reference circuit is showed in Figure 29:

- C_{E1} and R_{E1} represent the capacitive and the resistive components of the impedance of the exploring electrodes;
- C_1 and R_1 constitute the capacitive and the resistive components of the impedance of the reference electrode;
- E_{hc1} describes the half-cell potential at the interface between the exploring and reference electrodes; they are two identical electrodes placed face to face, so the half-cell potential at this interface will be low and constant.
- C_2, R_2, and R_3 represent the capacitive and the resistive components of the impedance unbalance ΔZ_e between the two terminals of the front-end;
- S_1 is a normally open push button, and if it is open the impedance unbalance ΔZ_e consists of C_2, R_2, while if it is closed ΔZ_e becomes the parallel of C_2, R_2, and R_3;
- Z_{I1} and Z_{I2} are the input impedances of the first stage of the front-end (INA333);
- G_1 is the gain instrumentation amplifier INA333;
- G_2 is the gain Sallen-Key low-pass filter.

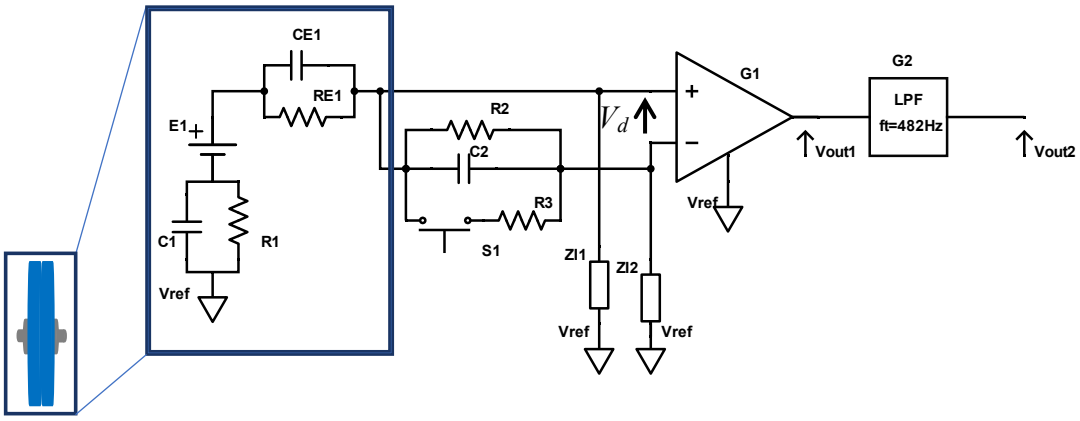

Figure 29: This Electronic circuit allows to record the amplifier output with variations impedance unbalance ΔZe. The exploring and reference electrode are identical and placed face to face and the half-cell potential at the interface results low and constant. C_{E1} and R_{E1} represent the capacitive and the resistive components of the impedance of the exploring electrodes. C_1 and R_1 constitute the capacitive and the resistive components of the impedance of the reference electrode. E_1 describes the half-cell potential of the interface between the exploring and the reference electrodes. C_2, R_2, and R_3 represent the capacitive and the resistive components of the impedance unbalance ΔZ_e between the two input-terminals of the front-end. S_1 is a normally open push button, and if it is open the impedance unbalance ΔZ_e is the parallel of C_2 and R_2, while if it is closed ΔZ_e becomes the parallel of C_2, R_2 and R_3. Z_{I1} and Z_{I2}, are the input impedances of the first stage of the front-end (INA333). G_1 is the gain instrumentation amplifier INA333. G_2 is the gain Sallen-Key low-pass filter.

The impedance unbalance 'seen' between the two input of the front-end changes by opening and closing the push button S_1.

- S_1 open: ΔZe is the resultant impedance of the parallel between the resistance R_2 and the capacitance C_2.
- S_1 open: ΔZe is the resultant impedance of the parallel between the resistances R_2, R_3, and the capacitance C_2.

The signal is recorded at the output of the two stages of the front-end: the unfiltered signal $Vout_1$ and the low-pass filtered signals $Vout_2$.

During the motion artefact, the contact surface between the electrode and the skin can decrease. The capacitive component at the interface decreases and the resistive component increases compared to the case of good electrode-skin contact. Considering

tens of Hertz as frequency of the ΔZe input variations, the values of the electronic components were chosen to obtain amplitude of the ΔZe changes in the order of kΩ and MΩ.

TEST 1 The value of the impedance unbalance ΔZe at the input of the front-end changes by opening and closing the push button S_1 of the circuit (Figure 29). The chosen values of the capacitive and resistive components are: R_2=3,9MΩ, R_3= 390MΩ, and C_2= 1μF. The value of the ΔZe changed between:

- 10kΩ (i.e. at 15Hz) with S1 open; and
- 300Ω (i.e. at 15Hz) with S1 closed.

So, the impedance unbalance ΔZe decreased by a factor 10^2 closing S_1.

The Figure 30 shows the input-referred signal obtained by closing and opening the push button S1. It is the filtered signal at the output of the front-end.

Initially S_1 was open so the ΔZe was in the order of tens kΩ. The input-referred signal shows a DC component at -155μV due to the common-mode half-cell potential became differential because of ΔZe and it was amplified by the front-end. The absolute value of the half-cell potential for actual electrode in contact with the skin normally is around 20-500mV, but in this case two equal electrodes are placed face to face. As expected, the half-cell potential of their interface is rightly low (-155μV). Then the S_1 was closed and the impedance unbalance ΔZe became in the order of hundreds Ω. The impedance unbalance ΔZe decreases by a factor 10^2 and the voltage rapidly became zero. Finally, the S_1 was reopened and the signal returns to -155 μV with a load time of 10s.

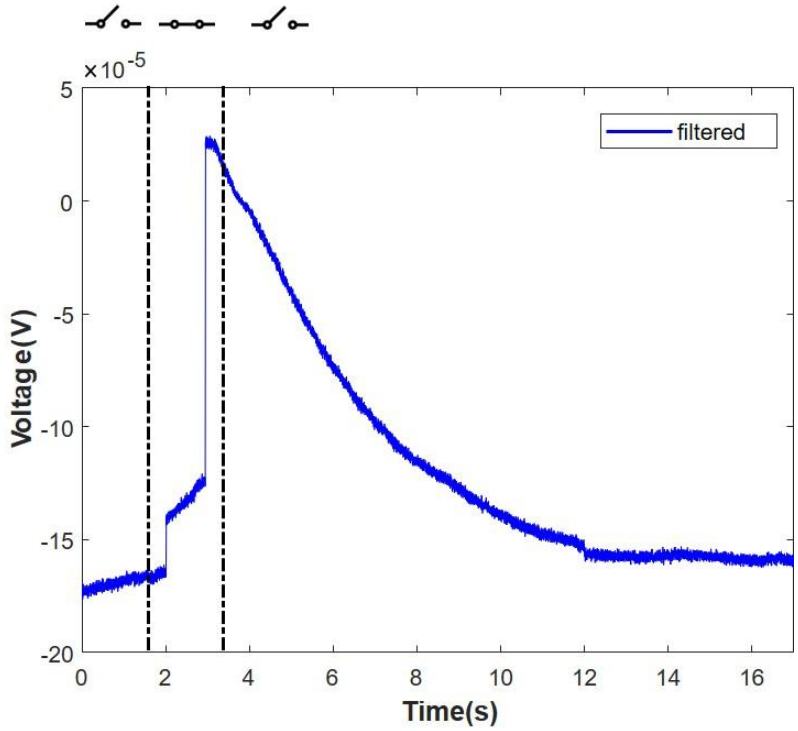

Figure 30: Output signal of the experiment 1, test 1 corresponding to the closing and the opening of the push button S_1. It is the low-pass filtered output signal referred to the input of the front-end. Initially S_1 is open, the ΔZe is about 10kΩ (i.e. at 15Hz) and the signal is about -155 μV. Then the S_1 is closed, the impedance unbalance ΔZe becomes above 300Ω (i.e. at 15Hz) and the signal rapidly (decay time) becomes zero. Finally, S_1 is open and the signal slowly return to the initial DC voltage (load time 10s).

The DC common-mode input voltage becomes AC differential-mode voltage at the input of the front-end due to the change of the impedance unbalance. As expected, the baseline of the signal shifts because of the variation of the impedance unbalance ΔZe. By closing and opening the push button S_1 the capacitance C_2 rapidly discharged and slowly charged (depending on the chosen value of C_2, R_2, R_3). The value of the capacitive component C_2 of the ΔZe is of 1μF, so the decay time (rising edge) is lower than the load time (10s). The amplitude of the shift of 155 μV revealed comparable with the amplitude of the EMG signal (μV to mV). The recorded signal may result within the bandwidth of the EMG front-end appearing as an artefact.

TEST 2 During the motion artefact also the capacitive and the resistive component of the impedance Z_e at the electrode-skin interface can assume different values, changing

both the capacitive and the resistive components of the impedance unbalance. The same setup described in TEST 1 was repeated, by changing the value of the capacitance C_2. The values of the electronic components were: R_2=3,9MΩ, R_3= 390MΩ, and C_2=220nF. The value of the ΔZe changes by opening and closing the push button S_1, between:

- 50kΩ (i.e. at 15Hz) with S1 open; and
- 300Ω (i.e. at 15Hz) with S1 closed.

The impedance unbalance ΔZe decreases by a factor 10^2 closing S_1 as the previous test. However, in this experiment the value of the capacitance C_2 was decreased. Figure 31 presents the output signals obtained by closing and opening the push button S_1. This is the filtered signal at the output of the front-end, and it is referred to the input.

Initially the push button S_1 was open and the ΔZe was about tens kΩ. The common-mode half-cell potential became differential and it was amplified by the front-end showing a DC output voltage of -120μV. Then S_1 was closed and the impedance unbalance ΔZe became above hundreds Ω. The impedance unbalance ΔZe decreased by a factor 10^2 and the DC component quickly became 20μV. Finally, S_1 was reopen returning to the initial DC voltage.

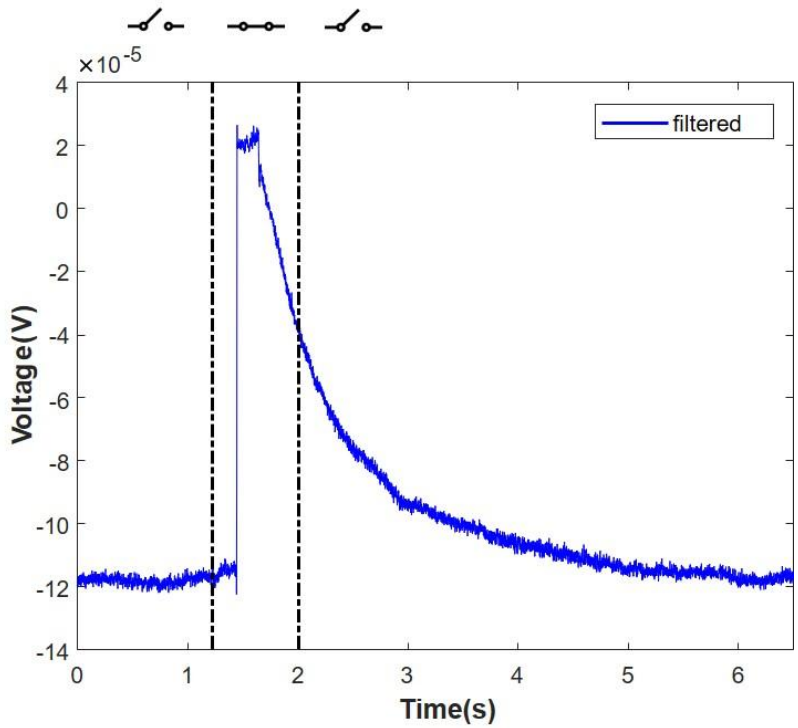

Figure 31: Output signal of the experiment 1, test 2 corresponding to the closing and the opening of the push button S_1. It is the low-pass filtered output signal of the front-

end referred to the input. Initially S_1 is open so the ΔZe is about 50kΩ (i.e. at 15Hz) and the voltage is about -120μV. Then the S_1 is closed, the impedance unbalance ΔZe became above 300Ω (i.e. at 15Hz) and the signal rapidly becomes 20μV. Finally, S_1 was open and the signal returns to the initial DC voltage (load time 5s).

As expected, the trend of the signals is about the same of the test 1, but being C_2 smaller than before the load time (5s) becomes lower. The DC component remained the same because the resistive component of the impedance unbalance was not changed between the two tests. The signal arising from the baseline-shifts may fall within the bandwidth of the EMG front-end appearing as an artefact, because of the value of the impedance unbalance ΔZe.

TEST 3 Usually, the impedance unbalance between two dry exploring electrodes (R_e=100kΩ) is about 10kΩ. Changes of the contact surface between these electrodes and the skin cause an increase of impedance unbalance ΔZe, varying its resistive and capacitive components. During the motion artefact the impedance unbalance can change in the order of MΩ. To simulate this situation, the same setup described in TEST 2 was repeated, by changing the value of the electronic components: R_2=8,2MΩ, R_3= 10kΩ, and C_2=1nF. The ΔZe changes by opening and closing the push button S_1, between:

- 10MΩ (i.e. at 15Hz) with S1 open; and
- 10kΩ (i.e. at 15Hz) with S1 closed.

The impedance unbalance ΔZe changes by a factor 10^3, higher than the previous two tests.

The value of the capacitance C_2 is lower than the previous test 1 and 2.

Figure 32 shows the output signal obtained by closing and opening the push button S1. It is the filtered signal at the output of the front-end, and it is referred to the input.

Initially, the signal is about zero because S_1 was closed and ΔZe was above tens kΩ. Then the signal shifts and the powerline interference increase because S_1 was open and ΔZe was about tens MΩ. The common-mode input voltage became differential through the high impedance unbalance at the input of the front-end. The output signal shows the appearance of the powerline interference shifted at about 500μV.

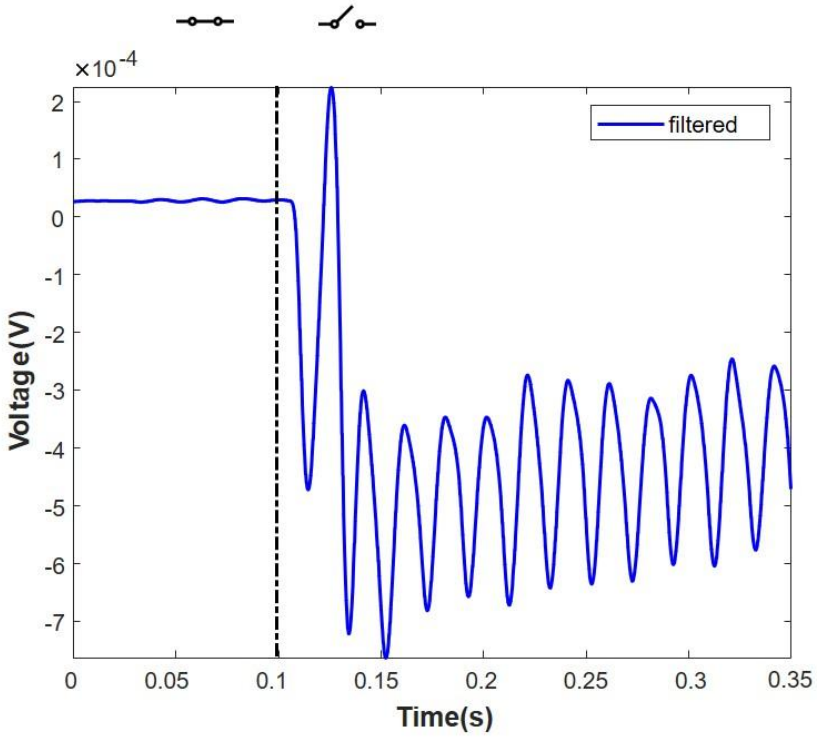

Figure 32: Output signal of the experiment 1, test 3 corresponding to the opening of the push button S_1. It is the low-pass filtered input-referred signal. Initially S_1 is closed so the ΔZe was about 10kΩ (i.e. at 15Hz). Then S_1 is open and the impedance unbalance ΔZe becomes above 1MΩ (i.e. at 15Hz). The amplitude of the shift is of 500μV, but the amplitude of the powerline interference results greater than the previous tests. The impedance unbalance when S_1 is open is of MΩ, so the powerline interference appears at the input of the front-end as differential signal and it is amplified by the front-end.

The amplitude of the baseline-shift of 500μV (comparable with the amplitude of the sEMG signal of $\mu V - mV$) is higher than the previous tests because of the higher impedance unbalance. In this case also the amplitude of the powerline interference became high and its effect is greater than the effect of the baseline shift. The capacitance C2 charges by opening S_1, but in this case the charged is modulated by the powerline interference. If the variation of the impedance unbalance is very quick the appearance of the powerline interference became a spike-like artefact on the output signal and the baseline-shift will not be substantial.

CONCLUSIONS Sudden changes of the impedance unbalance between the exploring electrodes causes motion artefact. The tests demonstrate that two types of motion artefact can be observed:

- Slow shifts of the signal baseline;
- Spike-like artefact, because of the modulation of the powerline interference.

These changes of the output signal caused by the impulsive variations of the impedance unbalance depends on the value of:

- the common-mode voltage;
- the impedance unbalance (the load and delay times of the capacitance C_2).

The common-mode voltage together with the impedance unbalance define the amplitude of the DC voltage and of the powerline interference at the output of the front-end. The value of the resistive and capacitive components of the impedance unbalance define the load and the decay time of the capacitance C_2. These values depend on the value of the impedance of the exploring electrodes Ze, which changes during the motion artefact due to variations of contact surface and thickness with the skin.

Concluding these tests showed that also without differences of E_{hc} between the exploring electrodes changes of the impedance unbalance at the input of the front-end cause artefact on the output signal. Usually, the input signals are high-pass filtered to remove the DC component and the low-frequency components. However, considering the baseline-shift (tests 1 and 2), the rising edge of the signals remains after the high-pass filter and becomes a spike-like artefact. This can be the case of movements of the electrodes with respect to the skin. Considering the modulation of the powerline interference (test 3) it appears as a spike-like artefact if the variations of the impedance unbalance at the input of the front-end is very quick. These can be the case of a rapid decrease of the contact-surface between the electrode and the skin.

3.2.3 EXPERIMENT 2: Common-mode variations of the half-cell potential

Common variations of the half-cell potential at the input of the front-end are one of the possible sources of motion artefact explained in paragraph 2.1.3. Pressure on reference electrode or movement of the underlying skin causes variations of the half-cell potential of the reference electrode causing a common-mode voltage variation at the input of the front-end. The common-mode AC signal became differential when the exploring

electrodes are unbalanced to each other. The custom-made circuit described in section 3.1.3 was used to create variations of the common-mode input voltage with an impedance unbalance 'seen' by the input of the front-end.

The experimental circuit is showed in Figure 33. It consists of:

- R4, R2 (trimmer), and R3: built the voltage divider described in paragraph 3.1.3. It simulates a common-mode half-cell potential at the input of the front-end;
- one push button S_1 in parallel with the trimmer used to rapidly changes the common-mode voltage;
- R_1=39kΩ parallel-connected with C_1= 1nF: create an impedance unbalance at the input of the front-end. This converts the common-mode voltage V_c into differential-mode V_d.
- Z_{I1} and Z_{I2}: the input impedances of the front-end;
- G_1: the gain instrumentation amplifier INA333;
- G_2: the gain Sallen-Key low pass filter.

The signals were recorded at the output of the instrumentation amplifier Vout1 and after the low-pass filter Vout2.

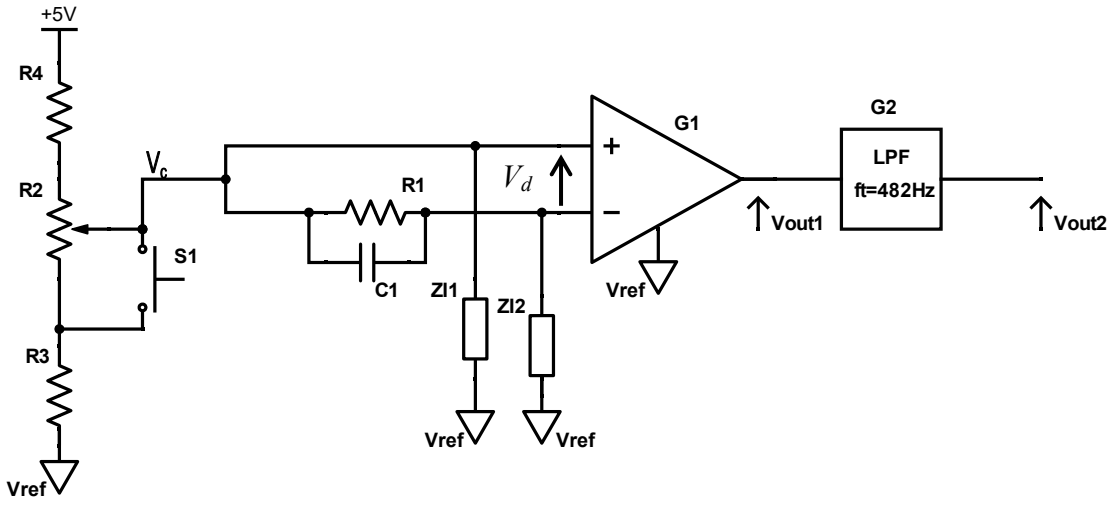

Figure 33: This Electronic circuit allows to create variations of the common-mode voltage V_c with an impedance unbalance 'seen' by the input of the front-end. R4, R2(trimmer), and R3 built the voltage divider described in paragraph 3.1.3. It creates the common-mode at the input of the front-end simulating the half-cell potential of the electrode-skin interface. The push button S_1 in parallel with the trimmer rapidly

changes the common-mode voltage. The parallel of R_1=39kΩ and C_1= 1nF defines the impedance unbalance ΔZ_e at the input of the front-end. Z_{I1} and $Z_{I2,}$ are the input impedances of the front-end. G_1 is the gain of the instrumentation amplifier INA333. G_2 is the gain of the Sallen-Key low pass filter.

TEST 1 The common input voltage V_c changes by means of the push button S_1. Usually, the common-mode signal is rejected by the front-end with a low common-mode gain compared to the differential-mode gain (high Common Mode Rejection Ratio, CMRR). However, the appearance of impedance unbalance between the two inputs of the front-end converts the common-mode voltage into differential-mode, thus it is amplified by the front-end. Variations of the common-mode voltage become differential-mode AC voltage at the input of the front-end, causing changes of the output signal.

In this test the amplitude of the common-mode voltage variation obtained through the push button S_1 was of 0,9mV. The trend of the output signals is showed in Figure 34. They are characterized by the presence of positive Figure 34, and negative Figure 34b spikes, corresponding to the closing and opening of the push button S_1 (decrease and increase of the common-mode voltage).

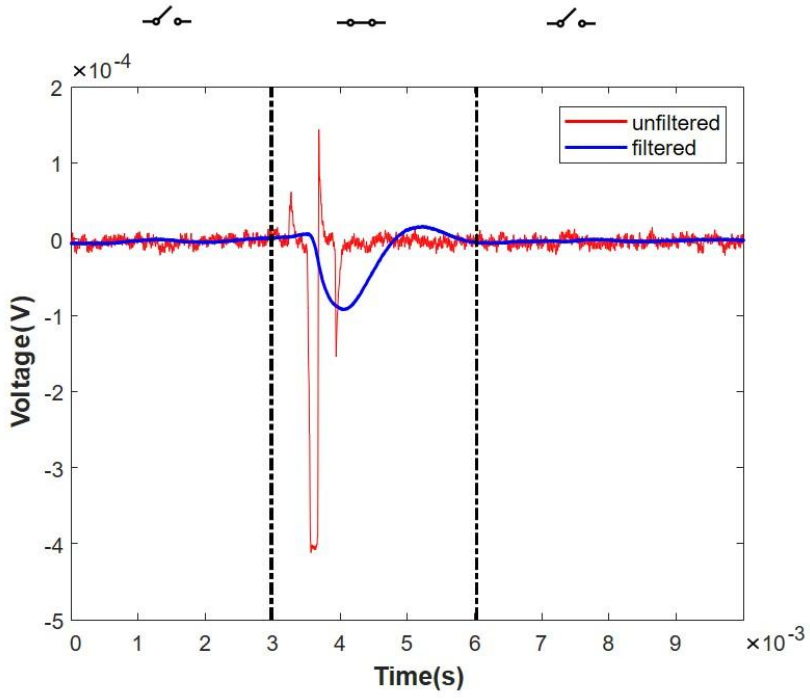

a)

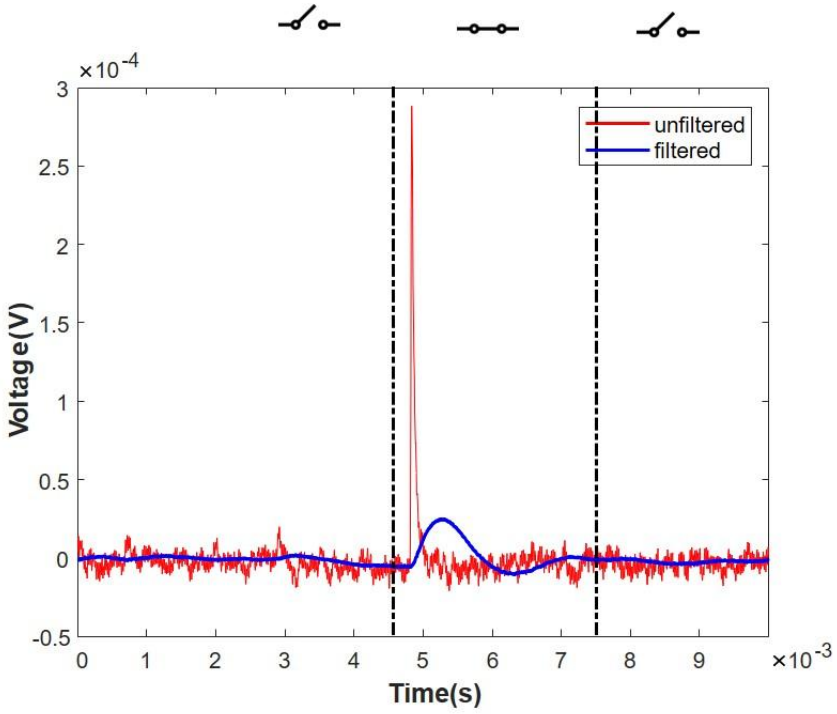

b)

Figure 34: Output signals of the experiment 2 referred to the input of the front-end. The red line is the unfiltered output signal, instead the blue line is the low-pass filtered output signal. Considering the filtered signal, the amplitude of the negative spike (figure a) results 108μV, while of the positive spike (figure b) is 34,7μV. The time period is 3ms for both spikes corresponding to a frequency of 333Hz.

The signals are referred to the input of the front-end. The red line is the unfiltered output signal, while the blue line is the low-pass filtered output signal. The filtered signal, in term of amplitude, is characterized by a negative spike of 108μV and a positive spike of 34,7μV. The time period is 3ms and the corresponding first harmonic is of 333Hz. The frequency of the artefact may be within the bandwidth of the sEMG signal and their amplitudes may be comparable to the amplitude of the sEMG signal (from μV to mV). Consequently, these spikes may overlap the useful signals becoming spike-like artefacts.

CONCLUSIONS Variations of the common-mode input voltage may cause the appearance of spikes on the output signal. Also small input voltage variations are transformed into AC differential voltage because of the impedance unbalance at the

input of the front-end. The frequency components of the spikes resulted within the bandwidth of the sEMG signal and their amplitudes were comparable to the amplitude of the sEMG signal (from μV to mV). The time period of the artefact had the same order of magnitude of an action potential (ms).

Concluding, the test shows that common-mode variations of the half-cell potential (i.e. caused by changes in properties of the electrode-skin interface of the reference electrodes) with an impedance unbalance ΔZ_e and finite Z_i between the exploring electrodes may cause spike-like motion artefacts, which appear action potentials. In order to avoid this type of artefacts having low value of the impedance unbalance at the input of the front-end and electrodes and a low half-cell potential becomes important, because the AC differential-mode voltage at the input of the front-end would be lower.

3.2.4 EXPERIMENT 3: Differential-mode alteration of the half-cell potential

Differential-mode alterations of the half-cell potential E_{hc} is one of the hypothesized sources of motion artefact. Pressure on the exploring electrodes or movement of the underlying skin cause variations in properties of electrode-skin contacts (Z_e and E_{hc}). Different changes between the two exploring electrodes produce an AC differential-mode half-cell potential at the input of the front-end. The custom-made circuit described in paragraph 3.1.3., was used to analyze the amplifier output with a variation of the differential-mode input voltage.

The circuit of this experiment is shown in Figure 35:

- R_1, R_2(trimmer), R_3, R_4 and R_5 are the resistors of the Wheatstone bridge described in paragraph 3.1.3. It creates a controlled differential-mode voltage V_a-V_b at the input of the front-end, by simulating differential variations of the half-cell potential;
- The push button S_1 (normally open) is used to rapidly change the differential input voltage V_a-V_b;
- Z_1 and Z_2 represent the impedance of the exploring electrodes;
- Z_{I1} and Z_{I2} are the input impedances of the instrumentation amplifier (INA333);
- G_1 is the gain of the instrumentation amplifier INA333;
- G_2 is the gain of the Sallen-Key low pass filter.

The output signals were recorded through the oscilloscope both after the instrumentation amplifier (V_{out1}) and after the low-pass filter at f_t= 482Hz (V_{out2}).

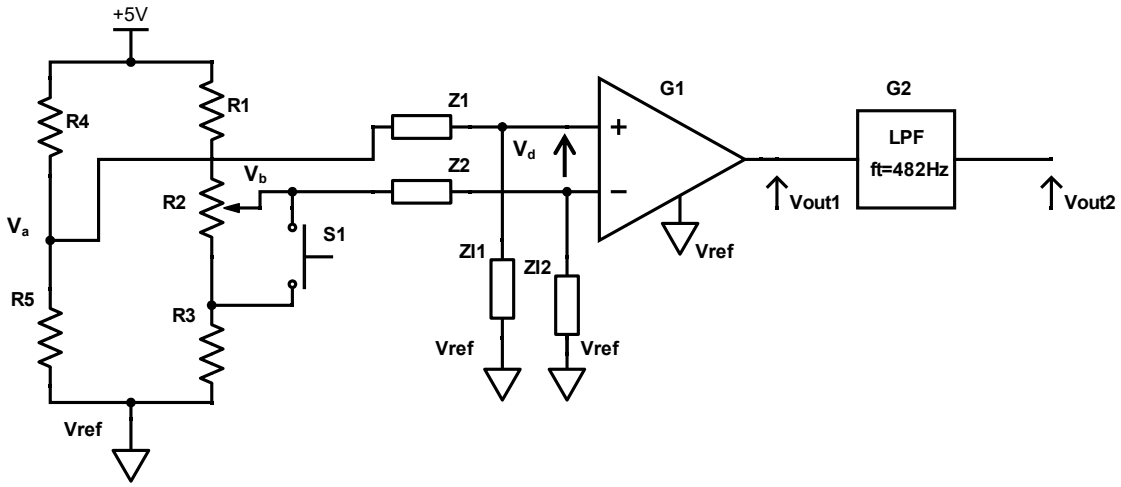

Figure 35:The electronic circuit allow to study the amplifier output with a variation of the differential-mode input voltage. R_1, R_2(trimmer), R_3, R_4 and R_5 are the resistors of the Wheatstone bridge described in paragraph 3.1.3. It creates a variable differential-mode voltage V_a-V_b at the input of the front-end simulating differential variations of the half-cell potential. The push button S_1 rapidly changes the differential input voltage V_a-V_b. Z_1 and Z_2 represent the impedance of the exploring electrodes. Z_{I1} and Z_{I2} are the input impedances of the instrumentation amplifier (INA333). G_1 is the gain of the instrumentation amplifier INA333. G_2 is the gain of the Sallen-Key low-pass filter.

TEST 1 The impedances of the exploring electrodes were the same simulating balanced exploring electrodes (without impedance unbalance). The differential input voltage V_a-V_b changed by means of the push button S_1. The amplitude of the variations of the differential voltage V_a-V_b resulted of 1mV pressing the push button.

The recorded output signals are showed in Figure 36: the red line is the unfiltered signal at the output of the INA333 amplifier, while the blue line is the low-pass filtered signal at the output of the front-end. Both signals are referred to the input. As expected, the output signals show negative and positive baseline-shifts corresponding to the push of the button S_1. The amplitude of the shift is 1mV identical to the amplitude of the input variation.

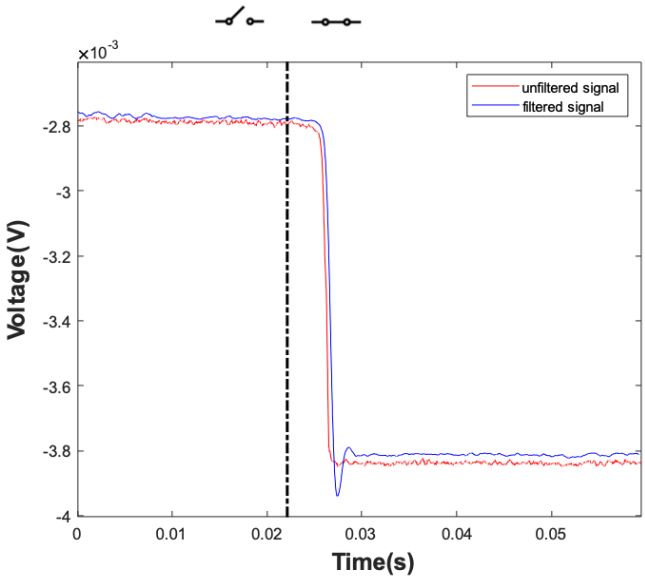

a)

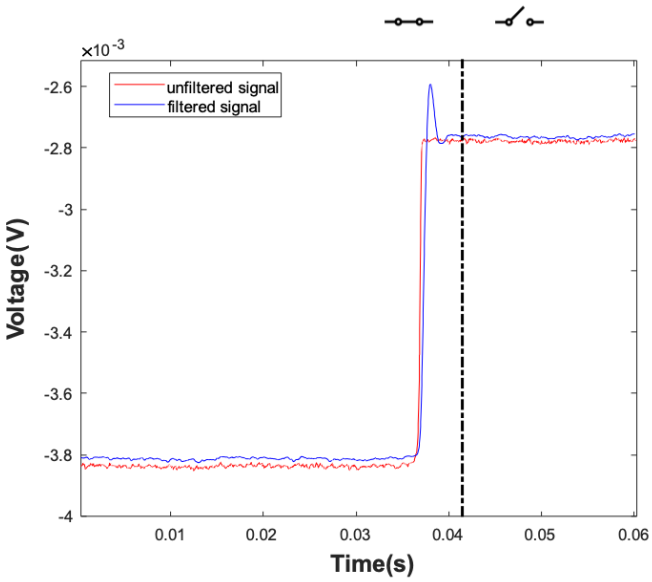

b)

Figure 36: Input-referred signals of the experiment : the red line is the unfiltered signal at the output of the amplifier INA333, while the blue line is the low-pass filtered signal at the output of the front-end. As expected, the output signals show the negative (a) and positive (b) baseline-shifts corresponding to the push of the button S_1. The amplitude of the shift is 1mV identical to the amplitude of the input variation. The filtered output signal (line blue) shows one spike corresponding to the falling and rising edge of the baseline. It is the effect of the analogic low-pass filter of Sallen-Key.

The filtered output signal (line blue) V_{out2} shows one spike corresponding to the falling and rising edge of the baseline. It is the effect of the analogic low-pass filter of Sallen-Key. For a given filter order, a steeper slope after the cut-off frequency can be achieved by allowing more pass-band ripple.

CONCLUSIONS Variations of the differential-mode input voltage cause artefact on the output signal. During a movement between the electrodes and the skin the properties of the interface change varying the half-cell potential. These variations usually are different between the exploring electrodes causing AC differential-mode voltage at the input of the sEMG front-end. As expected, the test showed the appearance of baseline-shifts on the output signals, caused by a differential variation of the input signal. If the excitation is rapid the shift of the baseline became a spike-like artefact amplified by the front-end. This differential signal cannot be rejected by the front-end, so it is always amplified.

The test had showed the appearance of additional spikes corresponding to the falling and rising edge of the low-pass filtered signal at the output of the front-end. These are caused by the analogic front-end, but they can be avoid varying the filter window. The Sallen-Key low-pass filter used within the front-end is a Chebyshev filter characterized by ripple in band-pass. Alternatively, the Butterworth filter can be used, because it has maximally-flat-magnitude response. However, the slope after the cutoff frequency is lower than the in the Chebyshev filter removing less noise components.

Chapter 4

Experimental characterization of motion-artefact sources

4.1 Introduction

The theoretical considerations (paragraph 2.2) and the analysis of the recorded signals (paragraph 3.2) showed that variations of the common-mode voltage (experiment 2, paragraph 3.2.2) cause the appearance of spike-like artifacts due to both the impedance unbalance and the input capacitance of the front-end amplifier. Usually, the sEMG front-end has low input capacitance (3-5pF), so its effect could be negligible. As expected, changes of differential mode voltage (experiment 3, paragraph 3.2.4) induce baseline-shifts of the signal, and changes of the impedance unbalance (experiment 1, paragraph3.2.2) causes baseline-shifts and modulation of the powerline interference. With impulsive variations also these effects become spike-like artefacts.

In this section, two types of movement-artefact were characterized:

- Caused by controlled and impulsive variations in the properties of the electrodes-skin contact, by changing the size of the exploring and reference electrodes;

- Caused by vibration-induced changes in properties of the electrode-skin interface, with higher frequency, by inducing vibrations of the exploring and reference electrodes.

In these experiments actual electrodes were placed on the skin. Usually, the half-cell potential at the electrode-skin interface can range within 20mV-500mV. The amplification of the front-end is 202V/V and the power supply is 0-5V. The DC component was not low-pass filtered and the amplifier could saturate. The amplification G_1 of the INA333 was lowered at 11V/V to avoid the saturation, thus the amplification G of the front-end resulted 22V/V.

The value of the input capacitance of the front-end C_i was 3pF (specifications of the INA333). The theoretical analysis of the paragraph 2.2 proved that the reactive component of the input impedance of the front-end influences the coupling between the common-mode signal and the electrode-amplifier system. The attenuation of the common-mode input decreases with the increase of the input capacitance of the front-end (Figure 18). The results of the previous experiments 1 and 2 (paragraphs 3.2.2 and 3.2.3) had showed that the amplitudes of the recorded spike-like artefacts are on the order of hundreds of μV. The output signals were recorded using 8-bit digital oscilloscope connected to the Personal computer through USB. The reference voltage of the front-end is of 2,5V (mid-supply). Considering the need to acquire DC signals, the low resolution of the oscilloscope and the 2,5V reference of the single supply amplifier, recording artifacts in the order of hundreds of μV resulted impossible. To this end, it was decided to increase the input capacitance of the front-end in order to increase the detected motion artifacts as discussed in paragraph 2.2.2. One capacitance was added in parallel with the input impedance of the front-end. The chosen value was 330pF to increase the amplitude of the spike-like artefact caused by common-mode variations (Figure 18). The input capacitance of the front-end resulted 333pF.

Also, the coupling between a differential-mode signal and the electrode-amplifier system was theoretically analyzed in the paragraph 2.2.3. The analysis had demonstrated that in this case the reactive component of the input impedance of the

front-end is irrelevant. Therefore, the differential-mode excitations at the input of the front-end are amplified similarly both with C_i=3pF and with 333pF.

4.2 Effect of the different motion-artefact sources

4.2.1 Introduction

Impulsive changes in the properties of electrode-skin contact were simulated by changing the size of the exploring and reference electrodes.
Differential-mode variations of the Ehc and changes of the impedance unbalance ΔZ_e were achieved by changing the contact-surface of the exploring electrodes, while common-mode variations of the half-cell potential (neglecting changes of the electrode impedance) were obtained by varying the contact-surface of the reference electrode.

4.2.2 EXPERIMENT 4: Changes of the contact surface between the exploring electrodes and the skin

Movements of the exploring electrodes with respect to the skin cause changes of the contact surfaces between the electrode and the skin, by creating variations of the half-cell potential at the electrode-skin interfaces and of the impedance unbalance between the electrodes. The previous tests simulated and analyzed these two effects individually by means of custom-made circuit (paragraph 3.1.3). This experiment was implemented to characterize experimentally the movement artefact caused by impulsive changes of the contact-surface of the exploring electrodes. The size of one exploring electrode was halve, keeping the surface of the second exploring electrode constant. The experimental setup is illustrated in Figure 37. Two identical exploring split-electrodes are placed on the forearm and one reference electrode is placed near the elbow. The surface of one exploring electrode is halved and the corresponding signal is detected by the front-end (INA333 and low-pass filter of Sallen-Key). The output signal is acquired using digital oscilloscope (PicoScope 3203D) connected to a Personal Computer (PC) through USB. Each exploring electrodes was both made by two dry-electrodes of one 8-electrodes

array, while the reference electrode was a Kendall gel-electrode. The output signal was recorded both after the instrumentation amplifier (INA333) and after the low-pass filter (ft=482Hz).

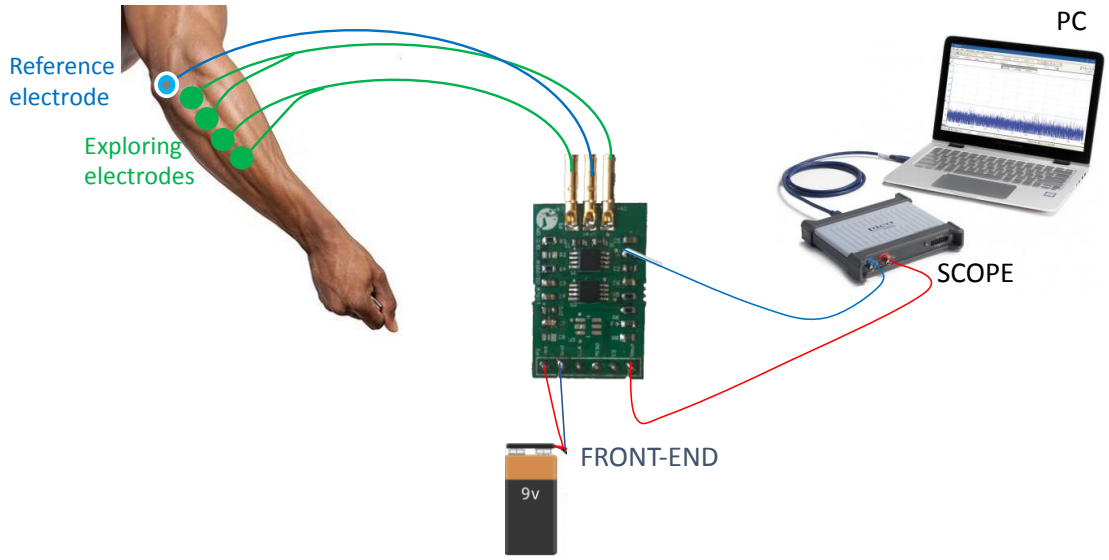

Figure 37: Experimental setup of the experiment 4. Two identical exploring split-electrodes are placed on the forearm and the reference electrode near the elbow. The surface of one exploring electrode is halve and the corresponding signal is detected by the front-end (INA333 and low-pass filter of Sallen-Key). The output signal is acquired with a digital oscilloscope (PicoScope 3203D) connected to the Personal Computer (PC) through USB.

The experimental circuit is shown in Figure 38, in which:

- Z_{e1} and E_{hc1} define the impedance and the half-cell potential of the electrode-skin interface of the exploring split-electrodes.
- Z_{e2} and E_{hc2} represent the impedance and the half-cell potential of the electrode-skin interface of half exploring split-electrode.
- S_1 is a mechanical deviator that highlights the halving-induced of one exploring electrode surface.
- Z_i is the input impedance of the instrumentation amplifier INA333, used as a front-end circuit.

- C_x is a capacitance added in parallel to Zi by reducing the reactive component of the input of the front-end.
- Zi is the input impedance of the instrumentation amplifier INA333.
- G_1 is the gain of the instrumentation amplifier INA333;
- G_2 is the gain of the Salle-Key low pass filter.

The value of the capacitance C_x was 330pF, while the Ci was 3pF (specifications of the INA333). The input capacitance of the front-end resulted $C_x \oplus C_i$, becoming 333pF. The theoretical analysis of the paragraph 2.2.3. has demonstrated that the reactive component of the input impedance of the front-end is irrelevant in the coupling between a differential-mode signal and the electrode-amplifier system; thus, with this input capacitance the attenuation of the input signals is about the same.

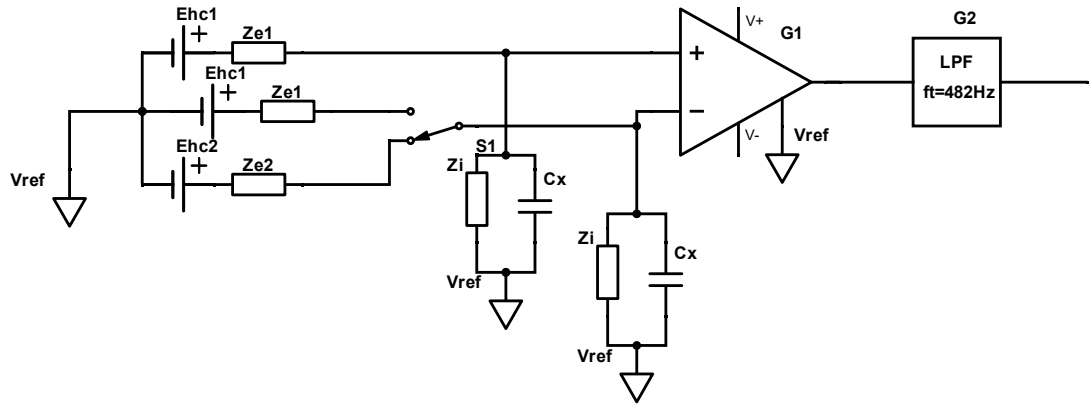

Figure 38: The electronic circuit allows to acquire the amplifier output with changes of the properties of the electrode-skin contact for one exploring electrode and the skin, halving the size of the electrode. The differential-mode voltage and the impedance unbalance at the input of the front-end change. Z_{e1} and E_{hc1}, define the electrical models of the electrode-skin interface for the exploring split-electrodes. Z_{e2} and E_{hc2} represent the electrical model of the electrode-skin interface of half exploring split-electrode. S_1 is a mechanical deviator that highlights the halving-induced of one exploring electrode surface. Z_i is the input impedance of the instrumentation amplifier INA333. C_x is a

capacitance added in parallel to Z_i by reducing the reactive component at the input of the front-end. G_1 is the gain of the instrumentation amplifier INA333. G_2 is the gain of the Sallen-Key low pass filter.

TEST 1 The contact-surface between one exploring electrode and the skin was rapidly reduced by half, halving the size of the spilt electrode. This cause changes in properties at the electrode-skin interface, creating variations of the differential-mode half-cell potential and the impedance unbalance between the exploring electrodes. The impedance Z_e 'seen' by the input of the front-end was measured in two conditions:

- The contact surface of the exploring electrodes was identical; and
- The size of one exploring electrode was halved.

The corresponding experimental setup is showed in Figure 39, and it included:

- The impedance meter;
- The DAC National Instrument;
- The PC to acquire the output signal.

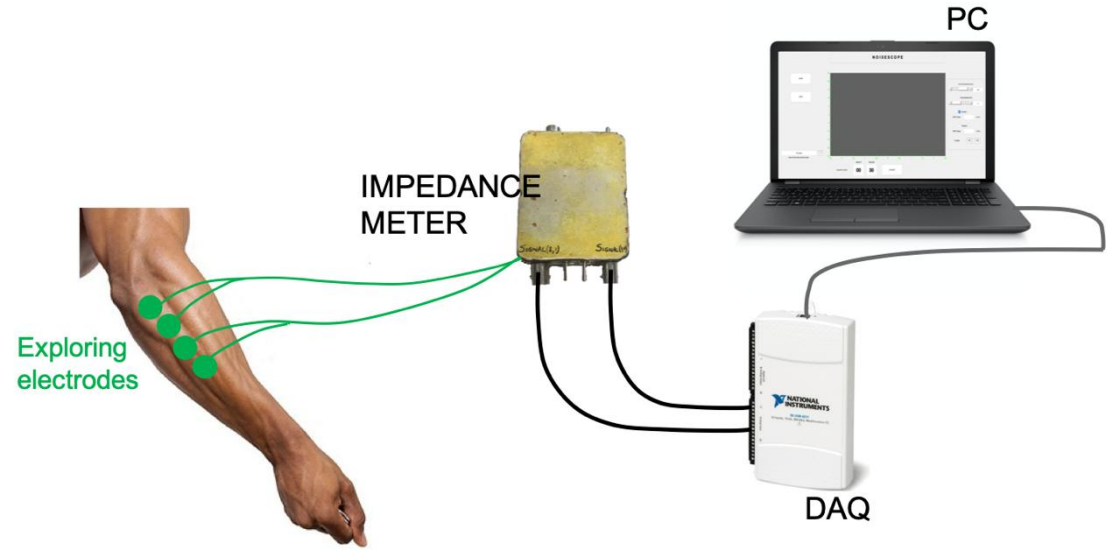

Figure 39: The experimental setup includes an impedance meter, the DAQ National instrument and the PC. It allows to measure the impedance Z_e between the exploring electrode.

TEST 1 Halving of the size of one exploring electrode. The impedance measured were:

- 3.9 MΩ when the surface of the exploring electrodes was identical.
- 6.8 MΩ halving one exploring electrode.

The impedance doubled halving the contact surface of one exploring electrode. The corresponding signals are showed in Figure 40. The red line is the unfiltered signal V_{out1} and the line blue is the low-pass filtered signal V_{out2}. Both are referred to the input of the front-end. The signals present a baseline-shift and an increasing of the powerline interference during the artefact, because of the half-cell potential at the interface changes and the impedance unbalance increases. The amplitude of the shift is of 15mV. It was on the order of magnitude of the half-cell potentials (20mV-500mV) comparable to the amplitude of the sEMG signal.

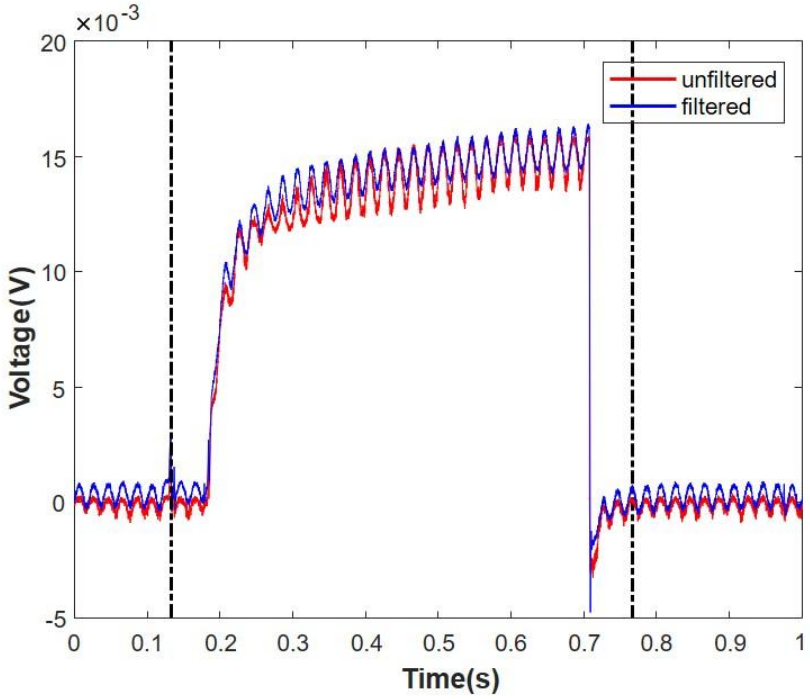

Figure 40: Output signals acquired during a rapidly change of the contact surface of one exploring electrode. The red line is the unfiltered signal V_{out1} and the line blue is the low-pass filtered signal V_{out2}. Both are referred to the input of the front-end. The signals present a baseline-shift and an increasing of the powerline interference during the artefact. The amplitude of the shift is of 15mV.

TEST 2 The same experiment was repeated by inducing a quick variation of the size of one exploring electrode. The baseline-shift should become a spike-like artefact. The impedance measured were:

- 479 kΩ when the surface of the exploring electrodes was identical.
- 736 kΩ halving one exploring electrode.

The impedance doubled halving the contact surface of one exploring electrode. The corresponding signals are showed in Figure 41. The red line is the unfiltered signal V_{out1} and the blue line is the low-pass filtered signal V_{out2}. Both are referred to the input of the front-end. The signals present a baseline-shift of 15mV and an increasing of the powerline interference during the artefact as the previous one, because of the half-cell potential at the interface changes and the impedance unbalance increases. However, in this case the variations of the contact surface of the exploring electrode is more rapid than the previous test and the baseline-shift appears as a spike-like artefact at the output.

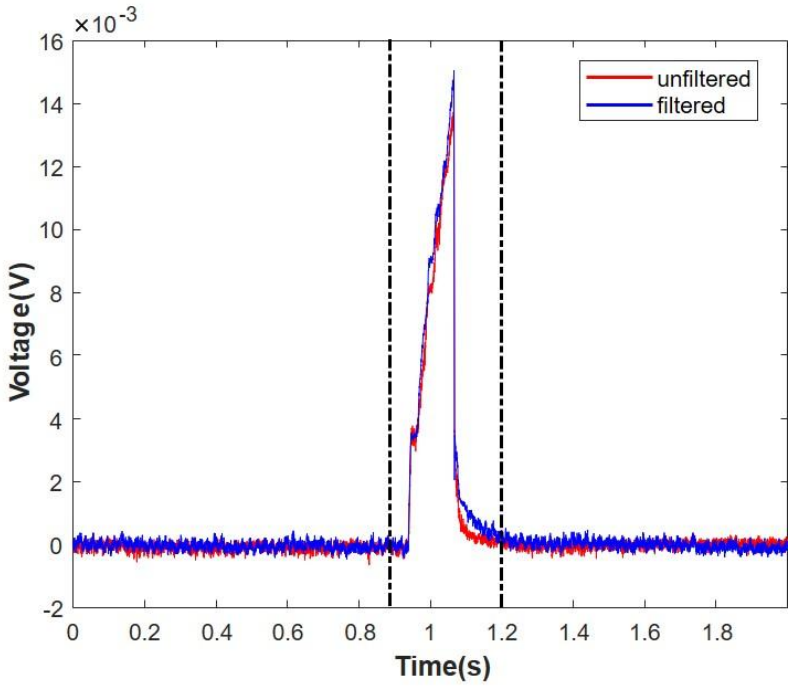

Figure 41: Output signals acquired during a rapidly change of the contact surface of one exploring electrode. The red line is the unfiltered signal V_{out1} and the blue line is

the low-pass filtered signal V_{out2}. Both are referred to the input of the front-end. The signals present a baseline-shift and an increasing of the powerline interference during the artefact. The amplitude of the shift is of 15mV.

CONCLUSION Changes of the contact surface between the exploring electrodes and the skin may cause of motion artefact. The test 1 and 2 showed that the output signals presented both baseline-shifts and powerline interference increase. It corresponds to:

- the test 3 of the experiment 1 (paragraph 3.2.2), together with
- the experiment 3 (paragraph 3.2.4).

Concluding the test explained that usually the increment of the impedance unbalance is responsible for the modulation of the powerline interference, instead the variations of the differential-mode half-cell potential are accountable for the shifts of the signal baseline. The test 1 highlights that varying in the properties of the electrode-skin interface of the exploring electrode the effect of the baseline-shift is greater than the modulations of the powerline interference. Usually, the input signals are high-pass filtered to remove the DC component and the low-frequency components. Considering the baseline-shift the rising edge of the signals remains after the high-pass filter and becomes a spike-like artefact. The test 2 (impulsive excitation) highlights that the baseline-shift can became a spike-like artefact appearing on the output signal if its frequency is within the bandwidth of the sEMG front-end. The amplitude of the shift for both the tests is resulted of 15mV at the input of the front-end. These values depend on the material of the electrode and of its half-cell potential. The design of the front-end and the material of the exploring electrodes become important to avoid the saturation the sEMG front-end. Having both low gain of the front-end and low half-cell potential of the electrode are desirable.

4.2.3 EXPERIMENT 5: Changes of the contact surface between the reference electrode and the skin

Movements of the reference electrode with respect to the skin cause changes of the contact surface, by causing variations of the E_{hc} and Z_e of the reference electrode. In the previous experiment 2 (paragraph 3.2.3) the AC common-mode signal was made by a custom-made circuit, while this experiment replaces the circuital model of the electrode-skin contact with actual electrodes on the subject. Changes of the common-mode voltage were obtained by changing the size of the reference electrode, while the influence of the impedance Z_e was neglected. The experimental setup was illustrated in Figure 42. Two identical exploring electrodes are placed on the forearm and a reference split-electrode is near the elbow. The surface of the reference electrode is halved and the corresponding signal is detected by the front-end (INA333 and low-pass filter of Sallen-Key). The output signal is acquired by means of a digital oscilloscope (PicoScope 3203D) connected to the Personal Computer (PC) through USB. The exploring electrodes were both made by one dry-electrode of an 8 electrodes array placed on the forearm. The reference split-electrode was made by:

- one Kendall AgCl gel-electrode (E^0= 0,223V);
- one Al dry-electrode (E^0= -1,663V).

Two different metal electrodes were used to obtain a variation of the half-cell potential of the reference electrode, by removing one of them.

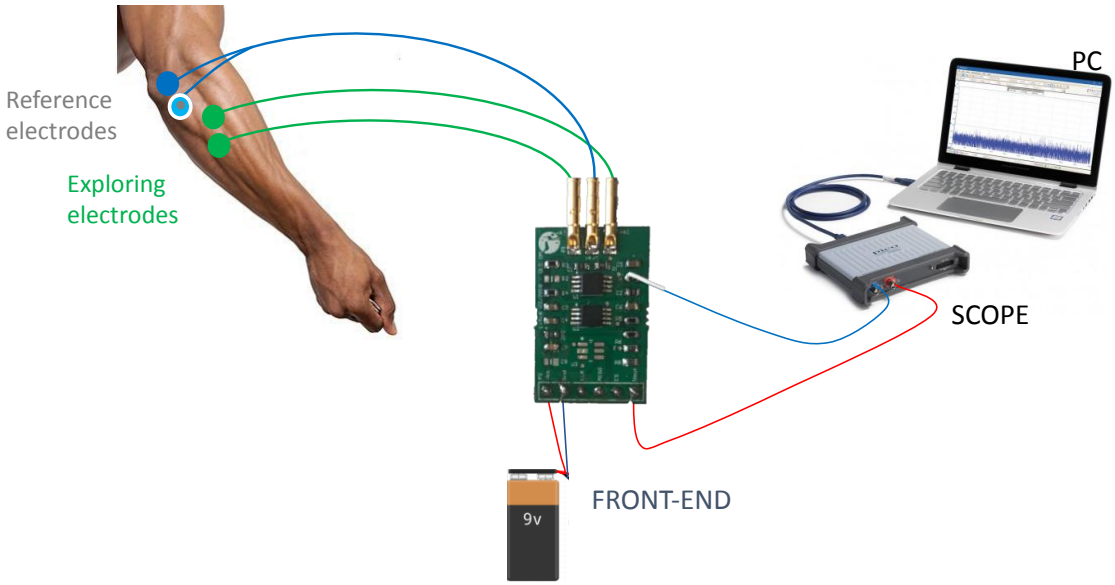

Figure 42: Experimental setup of the experiment 4. Two identical exploring electrodes are placed on the forearm and one reference split-electrodes near the elbow. The surface of the reference electrode is halved and the corresponding signal is detected by the front-end (INA333 and low-pass filter of Sallen-Key). The output signal is acquired by a digital oscilloscope (PicoScope 3203D) connected to the PC through USB.

The experimental circuit is showed in Figure 43:

- Z_{e1} and E_{hc1}, Z_{e2} and E_{hc2} are the impedances and half-cell potentials of the electrode-skin interface of the exploring electrodes;
- Z_{ref1} and V_{ref1} define the impedance and the half-cell potential of the electrode-skin interface of the reference split-electrode.
- Z_{ref2} and V_{ref2} represent the impedance and the half-cell potential of the electrode-skin interface of half reference split-electrode.
- S_1 is mechanical deviator that highlights the halving-induced of the reference electrode surface.
- Zi is the input impedance of the instrumentation amplifier INA333, used us a front-end circuit;
- C_x is a capacitance added in parallel to Z_i by reducing the reactive component of the input of the front-end;

- G_1 is the gain of the instrumentation amplifier INA333;
- G_2 is the gain of the Sallen-Key low pass filter.

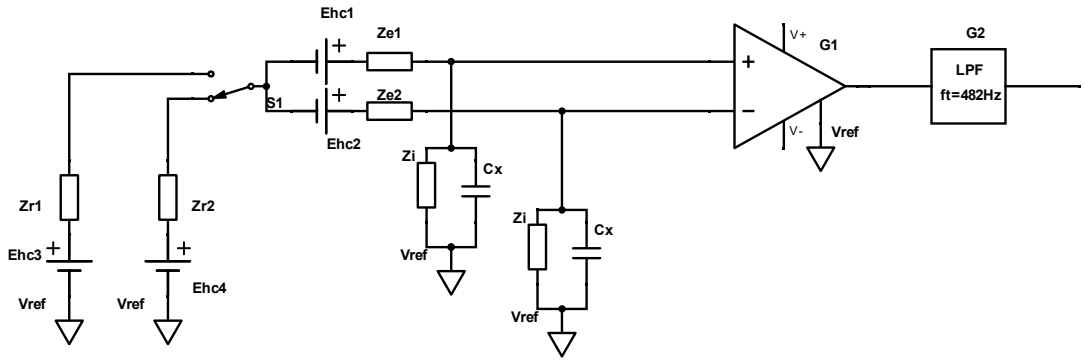

Figure 43: The electronic circuit allows to acquire the output signal with changes of the common-mode voltage obtained changing the size of the reference electrode Z_{e1} and E_{hc1}, Z_{e2} and E_{hc2} are the electrical models of the electrode-skin interface of the exploring electrodes; Z_{ref1} and V_{ref1} define the electrical model of the electrode-skin interface of the reference split-electrode. Z_{ref2} and V_{ref2} represent the electrical model of the electrode-skin interface of half split-reference electrode. S_1 is not mechanical deviator, but highlight the halving-induced of the reference electrode surface. Z_i is the input impedance of the instrumentation amplifier INA333. C_x is a capacitance added in parallel to Z_i by reducing the reactive component of the input of the front-end. G_1 is the gain of the instrumentation amplifier INA333. G_2 is the gain of the Sallen-Key low pass filter.

The theoretical analysis of the paragraph 2.2.2 proved that the capacitive component of the input impedance of the front-end influences the coupling between the common-mode signal and the electrode-amplifier system. The attenuation of the common-mode input decreases with high capacitance at the input of the front-end. The value of the capacitance C_x was 330pF and the Ci was 3pF (specifications of the INA333), so the amplifier input capacitance resulted the $C_x \oplus C_i$ becoming 333pF. This capacitance C_x was added to increase the detected using 8-bit digital oscilloscope (low resolution) with a voltage reference of 2,5V.

The surface of the reference electrode was rapidly reduced by removing the Kendall electrodes. The E_{hc} and the Z_e of the reference electrode changed and the returned signals is showed in Figure 44. It presented two spikes corresponding to the rapidly change of the reference electrode surface. The red line is the unfiltered signal at the output of the INA333, instead the blue line is the low-pass filtered signal at the output of the front-end. The two output signals are referred to the input.

The half-cell potential changes with variations of the contact surface of the reference electrode. Initially, the reference electrode was completely in contact with the skin, so the input referred signal is null, then the size of the reference electrode was reduced by half removing the gel electrode and finally the reference electrode returned to the initial condition. The output shows a positive spike when the contact-surface between the electrode and the skin is reduced, so the absolute value half-cell potential increase; while the output shows a negative spike when the contact-surface increase (returns to the initial condition), so the absolute value of half-cell potential decreases. The amplitude of the positive spike is about 10mV, while of the negative spike is above 50mV. The time period is about 50ms, so the first harmonics is 20Hz within the bandwidth of the sEMG signal. The amplitude is comparable to the previous test (paragraph 4.2.2) and with the amplitude of the sEMG signal ($\mu V - mV$).

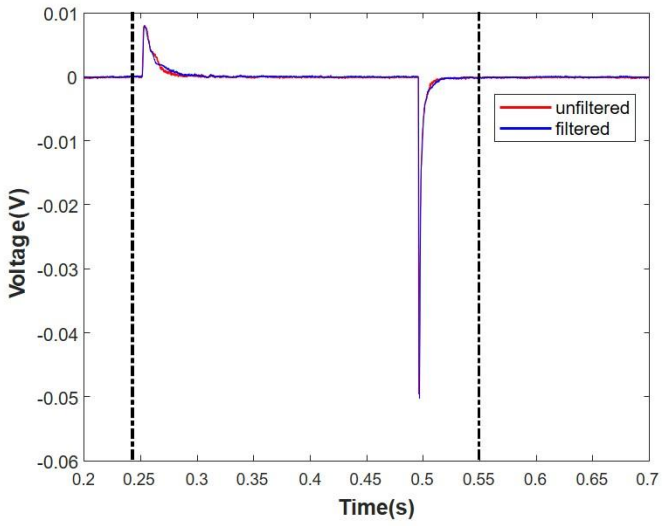

Figure 44: Output signals acquired varying the size of the reference electrode. The red line is the unfiltered signal at the output of the INA333, while the blue line is the low-pass filtered signal at the output of the front-end. The signals are referred at the input of the front-end. The amplitude of the positive spike is about 10mV, while of the negative spike is above 50mV. The time period is about 50ms, so the first harmonics of 20Hz is within the bandwidth of the sEMG signal.

CONCLUSION Changes of the contact surface between the reference electrode and the skin cause motion artefacts. The test had showed the appearance of spikes on the output signals corresponding to the experiment 2, described in paragraph 3.2.3, which create a common-mode input variation by a custom-made circuit.

The higher amplitude of the spike can be explained because of the different half-cell potentials between the two different materials (AgCl and Al) of the reference split-electrode. Moreover, the value of the input capacitance of the front-end is higher than the experiment 2 (paragraph 3.2.3) causing a lower attenuation of the common-mode input AC voltage.

Concluding, the movements of the reference electrode may cause changes of the common-mode voltage at the input of the front-end. It became a differential-mode voltage due to both the electrode-skin impedance unbalance and the input capacitance of the front-end and spike-like motion artefacts born at the output signal.

4.3 Study of vibration-induced artefact

4.3.1 Introduction

Movements artefact caused by sudden and repetitive changes in the properties of electrode-skin interface was characterized by inducing vibrations of exploring and reference electrodes. A motor-driven vibrator (Air cooled Shaker V4, Data Physics Corporation, California) was applied close to:

- the exploring electrodes;
- the reference electrode.

Considering the results of the previous experiments, vibrations of the reference and exploring electrodes should create (repetitive) spike-like artefacts at the frequency of the vibrations. The influence of the amplifier input capacitance was analyzed with the theoretical analysis of the coupling between the input excitation (common-mode and differential mode, paragraph 2.22.2.2) and the electrode-amplifier system. In the case of differential-mode input excitation (paragraph 2.2.3) the effect of the amplifier input capacitance resulted irrelevant, suggesting a constant attenuation of the expected artefact. Instead, in the case of common-mode input excitation (paragraph 2.2.2) the effect of the input capacitance of the front-end become important. Specifically, the theoretical analysis demonstrated that the attenuation of the expected artefact decreases with the increase of the input capacitance of the front-end. In order to confirm these observations, the two experiments were repeated changing the value of the amplifier input capacitance.

A new capacitance C_x parallel-connected with the input impedance of the front-end C_i was added. The equivalent input capacitance of the front-end changes, since it results $C_{eq} = C_x \oplus C_i$, where C_i is 3pF (specification of the INA333). Three tests were repeated with two different values of the capacitance C_x (330pF and 30pF), and without C_x ($C_{eq}=C_i$).

- TEST 1: C_{eq}= 333pF;
- TEST 2: C_{eq}=33 pF;

- TEST 3: C_{eq}=3pF (input capacitance of the INA333).

The motor-driven vibrator used to induce movements of the exploring and reference electrode was controlled by a sinewave. The frequency of the input sine wave was f_{sw}=15Hz, because usually the frequency of the vibro-tactile feedback used ranges from 10Hz to 20Hz.

4.3.2 EXPERIMENT 6: Vibrator near the exploring electrodes

Movements of the exploring electrodes with respect to the skin may produce variations in the properties E_{hc} and Z_e of the electrode-skin interface. In these experiments a motor-driver vibrator was placed in contact with the skin near one exploring electrode.
The Experimental setup is schematized in Figure 45. Two equal exploring electrodes were placed on the skin of the forearm and one reference electrode is placed near the elbow. A motor-driven vibrator (Air cooled Shaker V4, Data Physics Corporation, California) was placed near the distal exploring electrode. It was controlled by a sine wave generated by a Waveform Generator (Agilent 33220A). Finally, two output signals were detected by the front-end (after the INA333 and the low-pass filter of Sallen-Key), and acquired on the Personal Computer by means a digital oscilloscope (PicoScope 3203D) connected to the PC trough USB. The reference electrode was a Kendall gel-electrode. Each exploring electrode was a single electrode taken from one 8 electrodes array fixed on the forearm through Hypafix Adhesive Bandage. Two different arrays of electrodes were used. Since the presence of two different mechanical supports, the induced vibrations of each one exploring electrode resulted to be separated. The distance between the two exploring electrodes was approximately 10cm in order to vibrate the underlying skin of a single electrode.

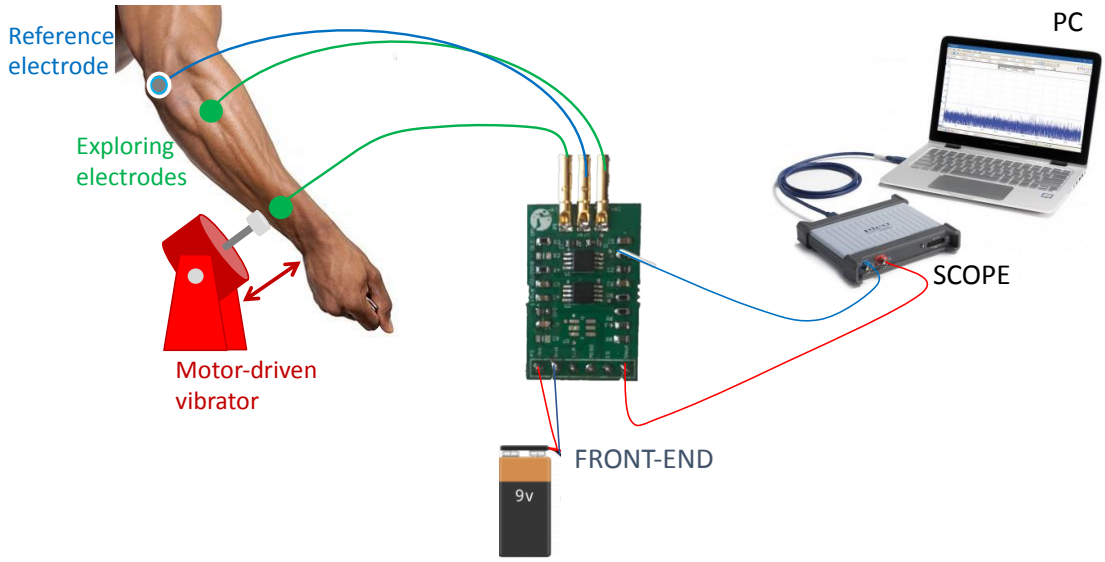

Figure 45: Experimental setup of experiment 6. Two identical exploring electrodes are placed on the forearm and one reference electrode near the elbow. A motor-driven vibrator (Air cooled Shaker V4, Data Physics Corporation, California) is placed near the distal exploring electrode. Two output signals are detected by the front-end (after the INA333 and the low-pass filter of Sallen-Key) and acquired on the PC by means of a digital oscilloscope (PicoScope 3203D) connected through USB.

The schematic is shown in Figure 46, in which:

- Z_{e1} and E_{hc1} represents the impedance and the half-cell potential of the electrode-skin interface of the exploring electrode,
- Z_{e2} and E_{hc2} are the impedance and the half-cell potential of the electrode-skin interface of the other exploring electrode, but the series-connected noise-generator ΔE_{hc2} and the variable impedance of Z_{e2} highlight the presence of a motor-driven vibrator near one exploring electrode that causes changes in properties of the electrode-skin interface.
- Zi is the input impedance of the instrumentation amplifier INA333 (C_i=3pF and R_i=100G);
- C_x is a capacitance parallel-connected with Z_i in order to reduce the reactive component of the input impedance of the front-end.

- G_1 is the gain of the instrumentation amplifier INA333;
- G_2 is the gain of the Sallen-Key low pass filter.

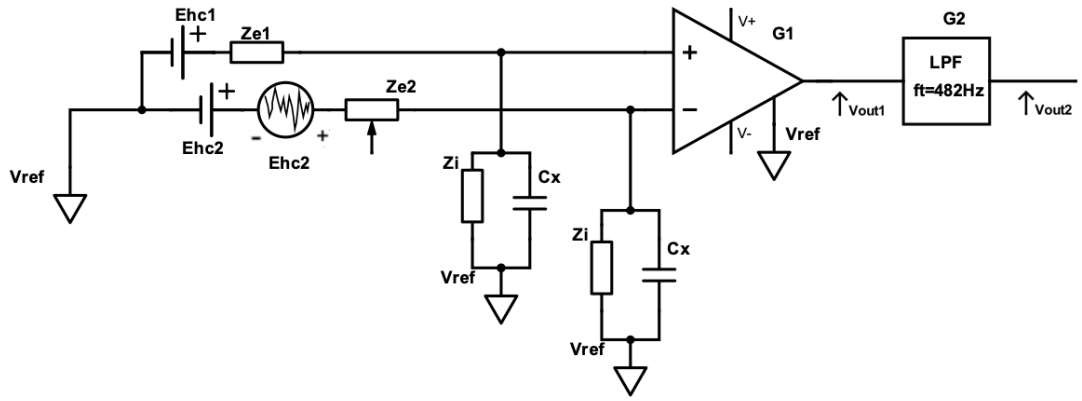

Figure 46: The electronic circuit allows to acquire the output amplified signal with vibrations-induced of one exploring electrode by a motor-driver vibrator in contact with the skin near the electrode. Z_{e1} and E_{hc1} represent the impedance and the half-cell potential of the electrode-skin interface of one exploring electrode; Z_{e2} and E_{hc2} are the impedance and the half-cell potential of the electrode-skin interface of the other exploring electrode series connected with the noise-generator ΔE_{hc2}. ΔE_{hc2} and Z_{e2} are not really implemented but highlight the presence of the motor-driven vibrator that causes changes in properties of the electrode-skin interface; Zi was the input impedance of the instrumentation amplifier INA333; C_x is a capacitance added in parallel to Zi to reduce the reactive component of the input impedance of the front-end; G_1 is the gain of the instrumentation amplifier INA333 and G_2 is the gain of the Sallen-Key low pass filter.

In the case of differential-mode input excitation (paragraph 2.2.3) the effect of this capacitance resulted irrelevant, suggesting a constant attenuation of the expected artefact. In order to confirm these observations, the two experiments were repeated changing the value of the amplifier input capacitance. The test was repeated with two different values of the capacitance C_x (330pF and 30pF), and without this capacitance.

The equivalent input capacitance of the front-end changes, since it results $C_{eq} = C_x \oplus C_i$, where C_i is the input capacitance of the INA333. Three tests were made:

- TEST 1: C_{eq}= 333pF;
- TEST 2: C_{eq}=33 pF;
- TEST 3: C_{eq}=3pF (input capacitance of the INA333).

The frequency of the input sine wave of the motor-driven vibrator was f_{sw}=15Hz, because usually the frequency of the vibro-tactile frequency ranges of 10Hz to 20Hz.

TEST 1 Vibrations of the exploring electrode with:

f_{sw}	C_{eq}
15Hz	333pF

The output signals showed the appearance of baseline-shift at the vibration-frequency both in the unfiltered (V_{out1}) and filtered (V_{out2}) signals. Only the filtered signal was analyzed in MATLAB. Considering the periodic nature of the vibro-tactile excitation, the signal was divided into 67ms long epochs. These were averaged in order to exclude random fluctuation of the signal and to extract a clear trend of the motion artefact related to the vibro-tactile excitations.

Figure 47a shows the averaged spike and the Figure 47b shows the corresponding Power Spectral Density (PSD).

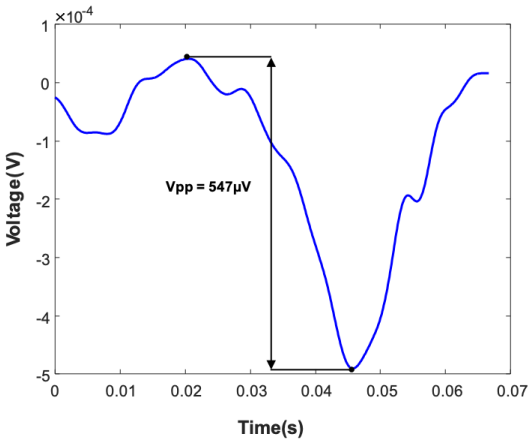

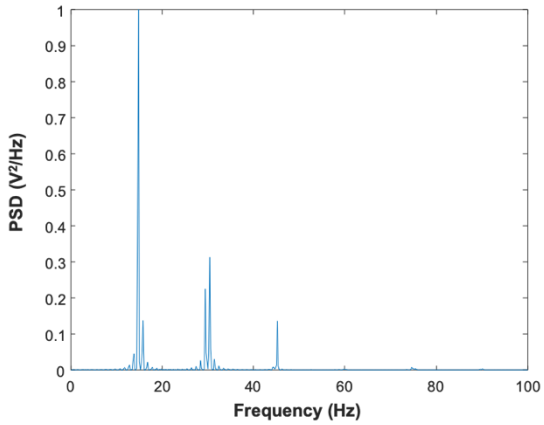

a) *b)*

Figure 47: The figures show the results of the test 1 obtained vibrating one exploring electrodes with a motor-driven vibrator. The frequency of the induced vibrations is of 15Hz and the input capacitance of the front-end is 333pF. Figure a) shows the trend of the spike-like artefact referred to the input that have a peak-to-peak amplitude of 547μV. Figure b) shows the corresponding PSD which presented a decreasing amplitude passing from the first harmonic components of 15Hz to the successive of 30 and 45Hz.

The greater frequency component is at the first harmonic of 15Hz, while at the successive harmonic the amplitude of the PSD decreases. The peak-to-peak amplitude referred to the input of the spike is 547μV (comparable with the amplitude of the sEMG signal). Moreover, the frequency components are within the bandwidth of the sEMG signal. For these reasons this type of signal is amplified by the front-end, becoming a spike-like artefacts.

TEST 2 Repetition of the Test 1, varying the value of the capacitance C_x to 30pF.

f_{sw}	C_{eq}
15Hz	33pF

A clear trend of motion artefact was found as the previous test and is showed in Figure 48a. The Power Spectral Density (PSD) is showed in Figure 48b in which the greater harmonic component is at 30Hz and lower components at 15,45 and 60Hz. The corresponding averaged-spike is at 30Hz, and its amplitude referred to the input is 995μV. The frequency of the spike-induced is within the bandwidth of sEMG front-end and also the amplitude is comparable with the sEMG amplitude ($\mu V - mV$), so it is detected with the sEMG signal.

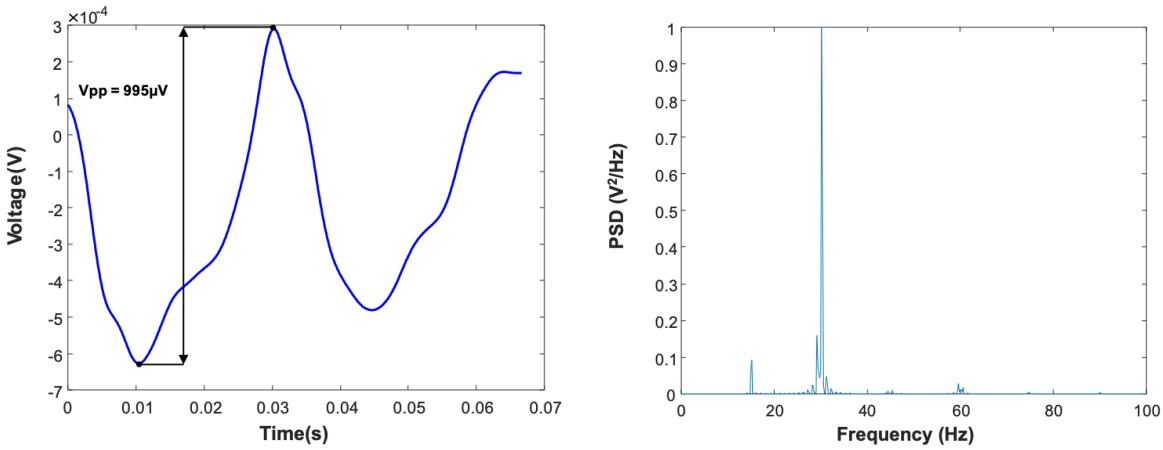

a) *b)*

Figure 48: The figures show the results of the test 2 obtained vibrating one exploring electrodes with a motor-driven vibrator. The frequency of the induced vibrations is of 15Hz and the input capacitance of the front-end is 33pF. Figure a) shows the trend of the spike-like artefact referred to the input that have a peak-to-peak amplitude of 955μV. Figure b) shows the corresponding PSD which presented the higher amplitude at the harmonic of 30Hz and lower harmonic components at 15,45 and 60Hz.

TEST 3 Vibrations of the exploring electrodes removing the parallel-connected capacitance C_x at the input of the front-end.

f_{sw}	C_{eq}
15Hz	3pF

The trend of the spike was computed as test 1 and is showed in Figure 49a. The corresponding Power Spectral Density (PSD) is showed in Figure 49b. The greater frequency component is at the first harmonic of 15Hz and at the successive harmonic components the amplitude of the PSD decreases. The referred-input amplitude of the spike-like artefacts is of 858μV. It is comparable with the sEMG signals and the frequency is within the bandwidth of sEMG front-end.

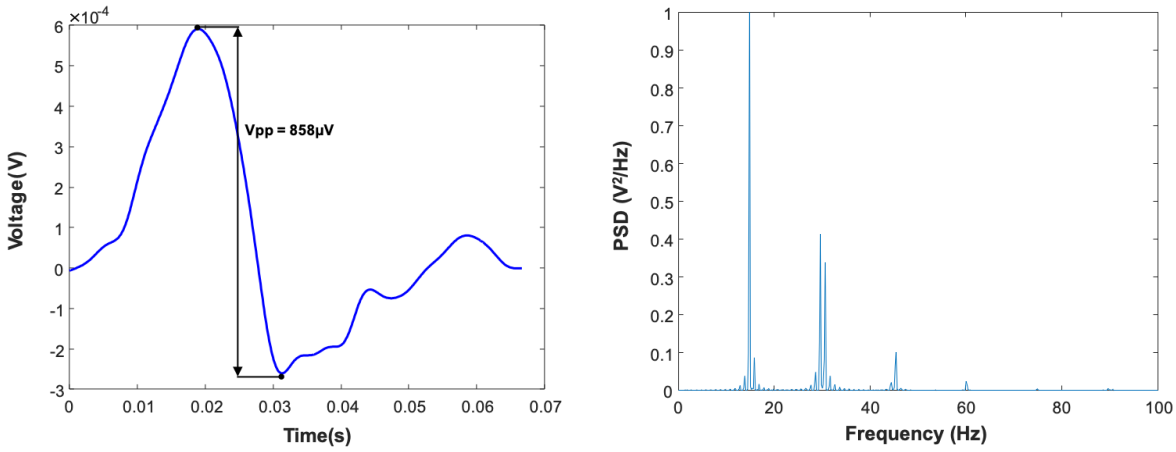

a) *b)*

Figure 49: The figures show the results of the test 3 obtained vibrating one exploring electrodes with a motor-driven vibrator. The frequency of the induced vibrations is of 15Hz and the input capacitance of the front-end is 3pF. Figure a) shows the trend of the spike-like artefact that have an input-referred peak-to-peak amplitude of 858μV. Figure b) shows the corresponding PSD which presented the decreasing of the amplitude passing from the first harmonic components of 15Hz to the successive of 30 and 45Hz.

CONCLUSION

Vibration of the exploring electrodes cause spike-like artefacts on the sEMG signals. The recorded signals of these three tests correspond to the effects observed in the previous experiments 1, 3 and 4 (paragraphs3.2.2, 3.2.4 and 4.2.2), which showed baseline-shift or modulation of the powerline interference that becomes a spike-like artefact with impulsive variations. Vibrations-induced changes of the electrode-skin contact between the electrode and the skin may cause changes of the impedance unbalance between the exploring electrodes and differential variations of the half-cell potential. For all the tests the modulation of the powerline interference is negligible, therefore the changes of the impedance unbalance resulted limited. The electrodes were fixed by the Hypafix adhesive garbage maintaining a stable contact between electrodes and the underlying skin. The results of this experiment show rapidly shifts of the

baseline, which appears as a spike-like artefact. Considering the result of the previous experiments these artefacts are caused by changes of the half-cell potential at the electrode-skin interface.

The amplitude of the averaged spike is about the same for all three tests with different input capacitance of the front-end. The theoretical analysis of the coupling between a differential-mode signal and an electrode-amplifier system (described in paragraph 2.2.3) had showed that the input capacitance of the front-end not cause distortion or attenuation of the differential input voltage. This observation was confirmed by this experiment, because the amplitude of the recorded spike-like artefacts is of hundreds μV for each test (with the three value of amplifier input capacitance tested: 333pF, 33pF, and 3pF).

Concluding this experiment confirmed the results obtained with the experiment 3 and 4, which showed spike-like artefact with impulsive input variations. The amplitude of the recorded artefacts (hundreds of μV) in these tests are comparable with the amplitude of the sEMG signal. The frequency components are within the bandwidth of the sEMG signals. Therefore, the vibration of the exploring electrodes causes vibration-induced artefacts.

4.3.3 EXPERIMENT 7: Vibrator near the reference electrode

Movements of the reference electrode with respect to the skin may cause variations in the properties of the electrode-skin interface (E_{hc} and Z_e). In this experiment a motor-driven vibrator was placed in contact with the skin near the reference electrode.

The experimental setup is schematized in Figure 50. Two equal exploring electrodes and one reference electrode were placed on the skin of the forearm. The reference electrode was placed on the distal part of the forearm close to the motor-driven vibrator (Air cooled Shaker V4, Data Physics Corporation, California) controlled by a sine wave generated by a Waveform Generator (Agilent 33220A). Finally, two output signals were detected by the front-end (after the INA333 and after the low-pass filter of Sallen-Key), and acquired by means of a digital oscilloscope (PicoScope 3203D) on the Personal

Computer (PC) through USB. Both exploring and the reference electrodes were a single electrode of 8 electrodes array fixed on the forearm through Hypafix Adhesive Bandage. Two different arrays of electrodes were used. Since the presence of two different mechanical supports, the induced vibrations of the exploring and reference electrode resulted to be separated. The distance between the exploring and electrodes was approximately 10cm in order to vibrate the underlying skin of the reference electrode.

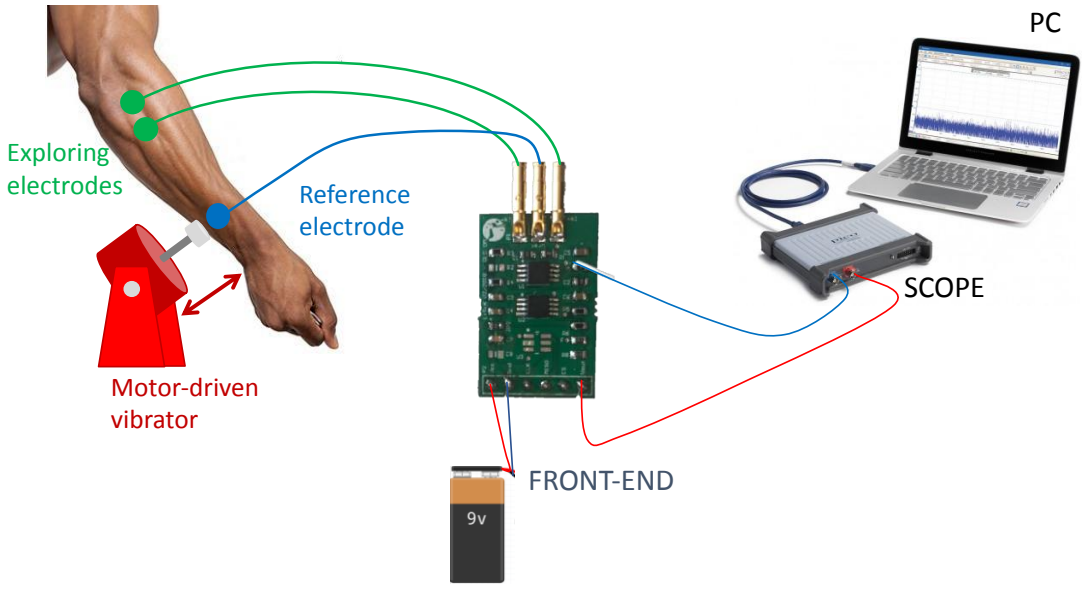

Figure 50: Experimental setup of the experiment 7. The exploring and reference electrodes are placed on the forearm. A motor-driven vibrator (Air cooled Shaker V4, Data Physics Corporation, California) is placed near reference electrode. Two output signals are detected by the front-end (after the INA333 and after the low-pass filter of Sallen-Key), acquired by means of a digital oscilloscope (PicoScope 3203D) on the Personal Computer (PC) through USB.

The schematic is showed in Figure 51:

- Z_{e1} and E_{hc2}, Z_{e2} and E_{hc2} are the impedance and half-cell potential of the electrode-skin interface of the exploring electrodes.

- Z_r and E_{hc3} define the impedance and half-cell potential of the electrode-skin interface of the reference electrode. The noise generator ΔE_{hc3} and the variable value of the impedance Z_r highlight the vibration-induced changes in the properties of the electrode-skin interface caused by the motor-driven vibrator.
- Z_i is the input impedance of the instrumentation amplifier INA333 (C_i=3pF and R_i=100GΩ);
- C_x is a capacitance parallel-connected with Z_i to reduce the reactive component of the amplifier input impedance.
- G_1 is the gain of the instrumentation amplifier INA333;
- G_2 is the gain of the Sallen-Key low pass filter.

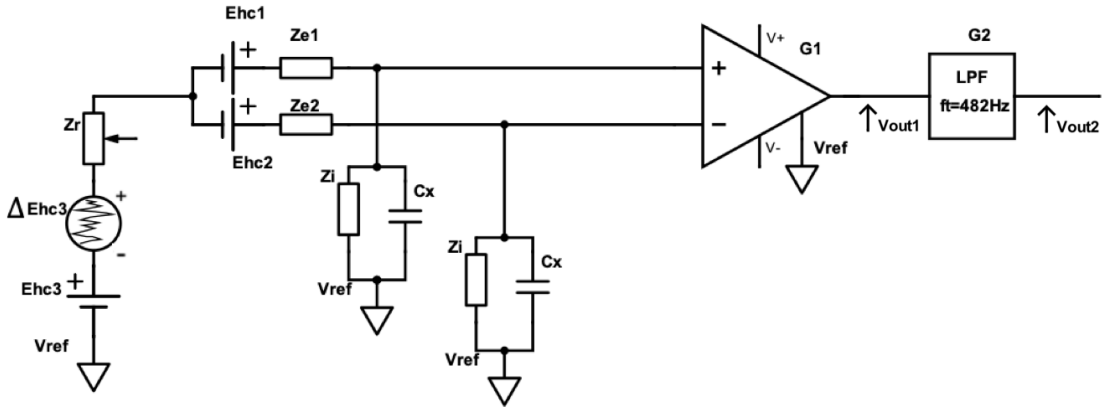

Figure 51: The electronic circuit allows to record the detected signal while a motor-driver vibrator is placed in contact with the skin near the reference electrode. Z_{e1} and E_{hc2}, Z_{e2} and E_{hc2} are the electrical models of the electrode-skin interface of the exploring electrodes. Z_r and E_{hc3} define the electric model of the electrode-skin interface of the reference electrode. In this case the noise generator ΔE_{hc3} and the variable value of the impedance Z_r highlight the vibration-induced changes in the properties of the electrode-skin interface caused by the motor-driven vibrator. Z_i is the input impedance of the instrumentation amplifier INA333. C_x is a capacitance parallel-connected with Z_i to reduce the reactive component of the input impedance of the front-

end. G_1 is the gain of the instrumentation amplifier INA333. G_2 is the gain of the Sallen-Key low pass filter.

The theoretical analysis of the paragraph 2.2.2 had proved that the amplifier input capacitance influences the coupling between the common-mode signal and the electrode-amplifier system. Higher capacitances at the input of the front-end cause lesser attenuation of than input common-mode signal (Figure 18). The test was made with two different values of the capacitance C_x (330pF and 30pF) to evaluate this observation experimentally. Three tests with different values of the equivalent capacitance C_{eq} at the input of the front-end were implemented:

- TEST 1: C_{eq}= 333pF;
- TEST 2: C_{eq}=33 pF;
- TEST 3: C_{eq}=3pF (input capacitance of the INA333).

Each test was replaced setting the sine wave frequency of the motor-driven vibrator at f_{sw}=15Hz, because the frequency of the vibro-tactile feedback usually ranges from 10Hz to 20Hz.

TEST 1 Vibration of the reference electrodes with:

f_{sw}	C_{eq}
15Hz	333pF

The output signals showed the appearance of spikes at the vibration-frequency both in the unfiltered (V_{out1}) and filtered (V_{out2}) signals. Only the filtered signal was analyzed in MATLAB. Considering the periodic nature of the vibro-tactile excitation, the signal was divided into 67ms long epochs. These were averaged in order to exclude random fluctuation of the signal and to extract a clear trend of the motion artefact related to the vibro-tactile excitations.

Figure 52a shows the trend of the spike and the Figure 52b shows the corresponding Power Spectral Density (PSD).

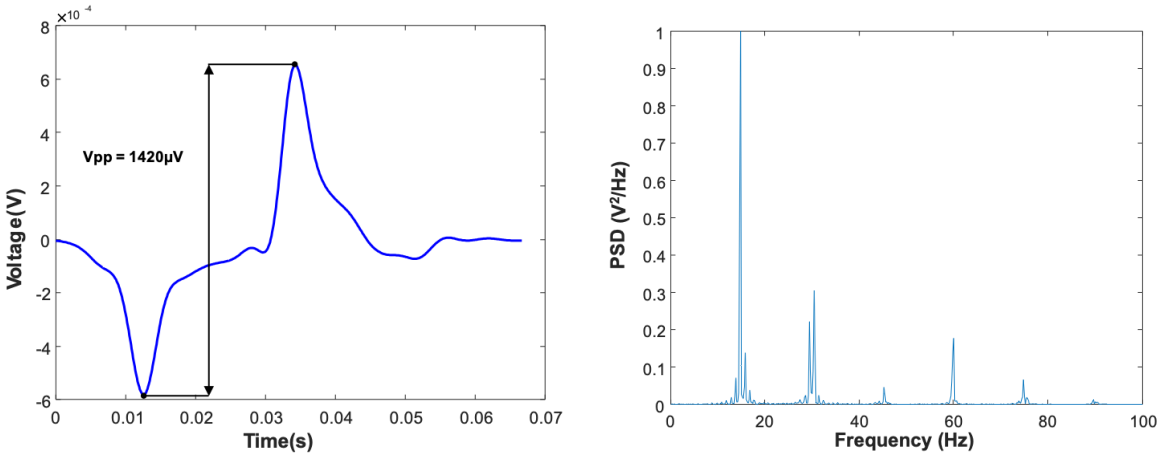

a) *b)*

Figure 52: The figures show the results of the test 1 obtained vibrating the reference electrode with a motor-driven vibrator. The frequency of the induced vibrations is 15Hz and the input capacitance of the front-end C_{eq} is 333pF. Figure a) shows the trend of the averaged spike-like artefact that have an input-referred peak-to-peak amplitude of 1,42mV. Figure b) shows the corresponding PSD which presented a decreasing amplitude passing from the first harmonic components of 15Hz to the successive of 30, 45, 60 and 75Hz.

One positive and negative spikes appear at the signals. The input-referred peak-to-peak amplitude of the averaged spike is 1,42mV like showed in figure a. The frequency components showed in the PSD decrease passing from the first harmonics to the successive. The spike amplitude is comparable with respect to the sEMG signal ($\mu V - mV$). Also, the frequency components are within the bandwidth of the sEMG becoming as a vibration-induced spike-like artefact.

TEST 2 Repetition of the test 1, changing the capacitance C_x to 30pF.

f_{sw}	C_{eq}
15Hz	33pF

The trend of the artefact was obtained as in the previous test. It is showed in Figure 53a and presents one positive and negative spikes. The input-referred peak-to-peak amplitude is $366\mu V$ similar to the amplitude of the sEMG signal ($\mu V - mV$). The Power Spectral Density (PSD) of the signal is showed in Figure 53b in which the highest frequency component corresponds to the excitation-frequency of 15Hz.

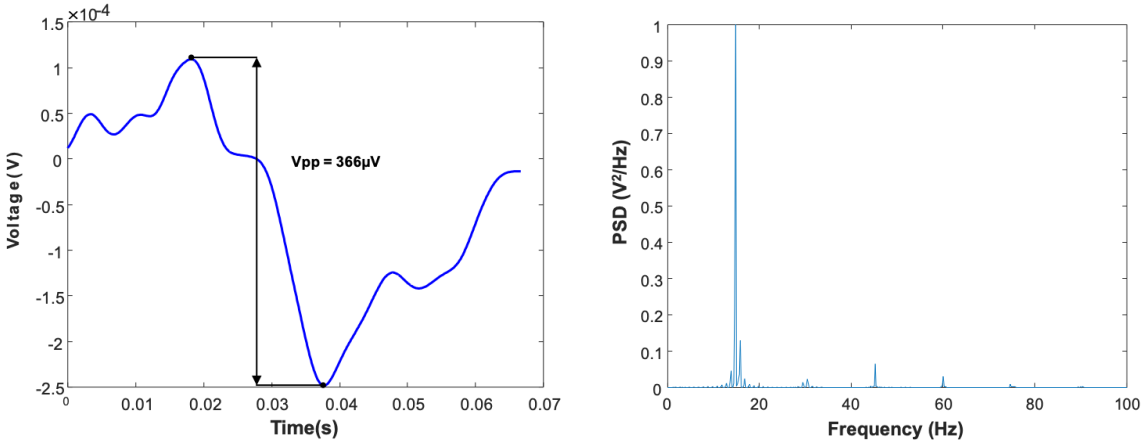

Figure 53: The figures show the result of the test 2 recorded when a motor-drive vibrator was placed near the reference electrode changing the properties of the electrode-skin interface. The figure a) shows the trend of the spike observed at the output of the front-end. The peak-to-peak amplitude referred to the input is 366µV and the frequency is the same of the vibration induced. The figure b) shows the Power Spectral Density of the signal, that has the greatest frequency component at the vibration-frequency.

The amplitude and the frequency of the averaged spike is comparable to the sEMG signal, so it appears as a spike-like artefacts on the sEMG signal.

TEST 3 Vibration of the reference electrode without the capacitance C_x at the input of the front-end.

f_{sw}	C_{eq}
15Hz	3pF

The trend of the artefact (obtained as in the test1) is showed in Figure 54a and displays the two spikes, instead the corresponding PSD (Power Spectral Density) is in Figure 54b. The signal is characterized by two spikes at the vibration frequency; hence the PSD shows the greatest component at this frequency. The input-referred peak-to-peak amplitude of $96\mu V$ is comparable with the amplitude of the sEMG signal. The frequency components are included in the bandwidth of the sEMG front-end so the signal is detected, becoming a vibration-induced artefact.

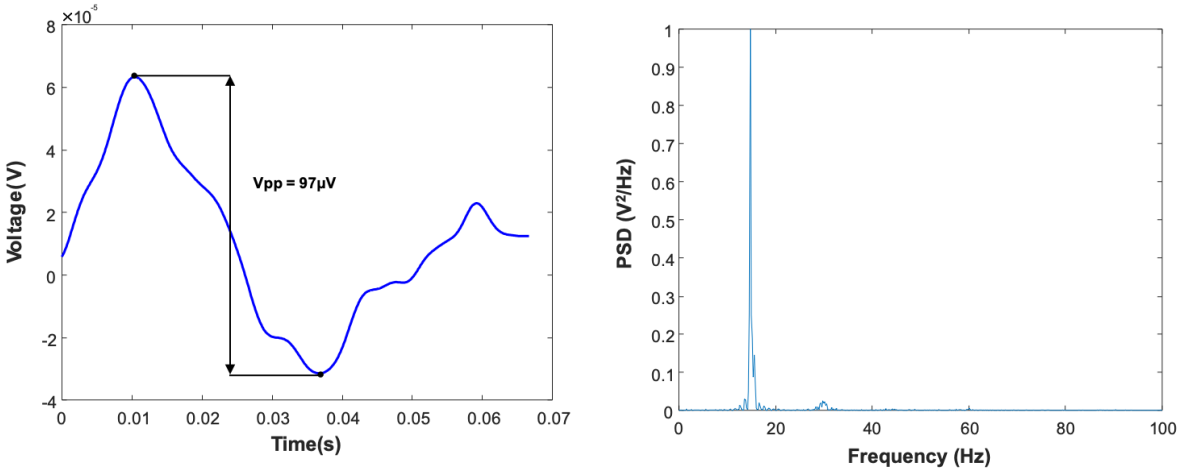

a) *b)*

Figure 54: The figures show the output signal of the test 3 acquired when the reference electrode vibrates because of a motor-driven vibrator placed close by. The figure a) show the averaged artefact within a time-width of 1s of the output signal. The input-referred peak-to-peak amplitude is 97μV and its frequency is identical to the vibration-frequency. The figure b) shows the corresponding Power Spectral Density of the recorded signal, that have the greatest frequency component at the first harmonic 15Hz.

CONCLUSION

Vibrations of the reference electrodes cause spike-like artefacts on the sEMG signal. The recorded signals in these tests correspond to the results obtained with the previous experiments 2 (paragraph 3.2.3) and 5 (paragraph 4.2.3), which showed the appearance of spike-like artefact whit an impulsive common-mode voltage variation. Moreover,

decreasing the value of the amplifier input capacitance the amplitude of the output artefacts reduced. The theoretical analysis of the coupling between the common-mode input signal and the electrode-amplifier system (described in paragraph 2.2.2) showed that the attenuation of the common mode input (i.e. at 10Hz) decreases with the increase of the capacitive components at the input of the front-end. This observation was confirmed by the results of this experiment in which the amplitude passes from 1,42mV in the test 1 (Ceq=333pF) to 366μV in the test 2 (Ceq=33pF) and 96μV in the test 3 (Ceq=3pF). A non-linear decrease was obtained experimentally. In this case, also the the capacitive component Ce of the exploring electrodes, and the frequency components of the spike-like artefact are relevant with the amplifier input capacitance C_i.

Despite the decreasing of the artefact-amplitude with lower amplifier input-capacitance, the artefact appears at the output of the front-end because its amplitude results comparable to the sEMG signal.

Concluding, this experiment confirms the results of the experiments 2 and 5 (showed the appearance of spike-like artefact whit an impulsive common-mode voltage variation) and the theoretical analysis about the effect of the amplifier input capacitance. Considering the lowest value of the input capacitance (usually designed at the input of the front-end) the amplitude of the spike-like artefacts is of tens μV. This amplitude is comparable with the sEMG signal and the frequency components of the artefact may be within the bandwidth of the signal. Therefore, vibrations-induced changes in the properties of the electrode-skin interface for the reference electrode causes vibration spike-like artefacts on the sEMG signal.

Chapter 5

Conclusions

In recent years, the manufactures of myoelectric-controlled prosthesis started to include in their devices the possibility to provide the subject with sensory feedback with the aim of improving the usability of the prosthetic device. A possible approach to reach this goal is the use of vibro-tactile devices positioned on the prosthetic socket.

In the case of myoelectric-controlled prosthesis, EMG electrodes are also placed on the socket covering the stump residual muscles and for constructive reasons, vibrating devices and EMG electrodes are usually placed in close proximity. The presence of a vibro-tactile device can represent a source of motion artefacts overlapping with the EMG signal and can compromise the possibility to actively control the protheses. The characterization of this problem requires to understand the causes underlying the appearance of motion artefacts in analogy to the classical methodological analysis made to understand the problems related to the power line interference.

The aim of this work was the characterization of the vibration artefact on the EMG signal related to the vibro-tactile feedback used to control hand prosthesis.

The effects of three possible causes of motion artefacts were investigated:

1. Sudden changes of the impedance unbalance (ΔZ_e) between the exploring electrodes;
2. Variations of the half-cell potential (E_{hc}) due to e.g. shocks on the electrodes;
3. Design characteristics of the analog front-end amplifier.

The study of the above-mentioned factors was performed by means of theoretical analysis, bench experiments and experimental tests.

Bench experiments consisted in the simulations of the three possible sources of motion artefacts through a custom-made circuit allowing to:

- Induce sudden changes of the electrode impedance unbalance in the case of common mode excitation;
- Study the effect of the differential and common variations of the half-cell potential at the electrode-skin interface;
- Study the effect of the input capacitance of the analog front-end.

Experimental tests were conducted by applying to subject forearm a vibro-tactile stimulus varying the electrode-skin interface properties in terms of electrode-skin impedance unbalance and half-cell potential variation. Tests were repeated for different values of the input capacitance of the analog front-end.

As expected, both bench and experimental tests confirmed the occurrence of two types of motion artefact that are frequently observed during EMG signals recordings, especially during dynamic tasks: Spike-like artefacts and Baseline shifts.

Vibrations of either exploring or reference electrodes placed on the skin showed spike-like artefacts, whose amplitude was comparable with the amplitude of the sEMG signal. The artefact caused by vibrations applied near to the reference electrode results lower

than that observed applying the vibration near the exploring electrodes. Therefore, by positioning both the reference electrode and the vibro-tactile feedback source distant with respect to the exploring electrodes, the vibration-induced artefacts on the sEMG signal decrease.
Despite the lower amplitude of the vibration-artefact caused by the reference electrode, our findings suggest the potential usefulness of the two-electrodes biopotential amplifiers to remove one source of motion artefact. In this case, the vibrator can be placed distant with respect to the exploring electrodes.

More generally, the results suggest the importance of proper skin preparation to achieve stable properties of the electrode-skin interface (Z_e and E_{hc}). This study also suggests that the reduction of motion artefacts caused by a vibro-tactile feedback sources used in active hand prosthesis is influenced by all the components of the electrode-amplifier system: i) the electrode-skin interface that should allow both good contact (low electrode-skin impedance) and low half-cell potential at the electrode-skin interface; ii) design of the analog front-end amplifier; iii) positioning of the reference and exploring electrodes with respect to the vibro-tactile feedback source.
This study contributed to the identification and characterization of the main causes of motion artefacts in the EMG signal, a fundamental step for the identification of experimental settings and front-end design solutions to obtain high quality recordings.

Bibliography

[1] M. Atzori and H. Müller, “Control Capabilities of Myoelectric Robotic Prostheses by Hand Amputees: A Scientific Research and Market Overview,” *Front. Syst. Neurosci.*, vol. 9, no. November, pp. 1–7, 2015.

[2] M. A. Lebedev and M. A. L. Nicolelis, “Brain-machine interfaces: past, present and future,” *Trends Neurosci.*, vol. 29, no. 9, pp. 536–546, 2006.

[3] N. Lago, P. Dario, S. Micera, T. Stieglitz, X. Navarro, and T. B. Krueger, “A critical review of interfaces with the peripheral nervous system for the control of neuroprostheses and hybrid bionic systems,” *J. Peripher. Nerv. Syst.*, vol. 10, no. 3, pp. 229–258, 2005.

[4] C. Cipriani *et al.*, “Online myoelectric control of a dexterous hand prosthesis by transradial amputees,” *IEEE Trans. Neural Syst. Rehabil. Eng.*, vol. 19, no. 3, pp. 260–270, 2011.

[5] C. Castellini, E. Gruppioni, A. Davalli, and G. Sandini, “Fine detection of grasp force and posture by amputees via surface electromyography,” *J. Physiol. Paris*, vol. 103, no. 3–5, pp. 255–265, 2009.

[6] M. S. Peerdeman B, Boere D, Witteveen H, Huis in `t Veld R, Hermens H, Stramigioli S, Rietman H, Veltink P, “Myoelectric forearm prostheses: state of the art from a user-centered perspective.,” *J. Rehabil. Res. Dev.*, vol. 46, no. 6, pp. 719–737, 2011.

[7] A. Fougner, O. Stavdahl, P. J. Kyberd, Y. G. Losier, and P. A. Parker, “Control

of upper limb prostheses: Terminology and proportional myoelectric control-a review," *IEEE Trans. Neural Syst. Rehabil. Eng.*, vol. 20, no. 5, pp. 663–677, 2012.

[8] D. Farina *et al.*, "The extraction of neural information from the surface EMG for the control of upper-limb prostheses: Emerging avenues and challenges," *IEEE Trans. Neural Syst. Rehabil. Eng.*, vol. 22, no. 4, pp. 797–809, 2014.

[9] J. T. Belter, J. L. Segil, A. M. Dollar, and R. F. Weir, "Mechanical design and performance specifications of anthropomorphic prosthetic hands: A review," *J. Rehabil. Res. Dev.*, vol. 50, no. 5, p. 599, 2013.

[10] J. Basmajian and C. J. De Luca, "Description and Analysis of the EMG Signal," in *Muscles alive : their functions revealed by electromyography*, 1985, pp. 65–100.

[11] M. Knaflitz, *Bioingegneria elettronica e sicurezza*. 2015.

[12] J. G. Webster, *MEDICAL INSTRUMENTATION Application and design*. 1997.

[13] Richard Normann, *Principles of Bioinstrumentation*. 1988.

[14] M. Knaflitz, "Dispense Bioingegneria elettronica e sicurezza." 2018.

[15] B. S. Day, "Important Factors in Surface EMG Measurement," pp. 1–17, 2004.

[16] J. Duchene and F. Goubel, "Surface electromyogram during voluntary contraction: Processing tools and relation to physiological events," *Crit. Rev. Biomed. Eng.*, vol. 21, no. 4, pp. 313–397, 1993.

[17] H. J. Hermens, B. Freriks, C. Disselhorst-Klug, and G. Rau, "Development of recommendations for SEMG sensors and sensor placement procedures," *J. Electromyogr. Kinesiol.*, vol. 10, no. 5, pp. 361–374, 2000.

[18] R. Merletti, *Electromyography : Physiology, Engineering, and Non-Invasive Applications*, vol. 11. 2004.

[19] K. Farry, J. Fernandez, R. Abramczyk, M. Novy, and D. Atkins, "Applying Genetic Programming To Control Of An Artificial Arm," *Proc. 1997 MyoElectric Control. Prosthetics Symp. MEC 97*, pp. 50–55, 1997.

[20] T. Flash and N. Hogan, "The coordination of arm movements: An experimentally confirmed mathematical model," *J. Neurosci.*, vol. 5, no. 7, pp. 1688–1703,

1985.

[21] B. Gerdle, S. Karlsson, S. Day, and M. Djupsjöbacka, “Acquisition, Processing and Analysis of the Surface Electromyogram,” in *Modern Techniques in Neuroscience Research*, 1999, pp. 705–755.

[22] CHILDRESS D.S., “A myoelectric three-state controller using rate sensitivity,” *Med. Biol. Eng. Comput.*, vol. 8th Int., no. Session 5-4, 1969.

[23] A. Y. J. Szeto and F. A. Saunders, “Electrocutaneous Stimulation for Sensory Communication in Rehabilitation Engineering,” *IEEE Trans. Biomed. Eng.*, vol. 29, no. 4, pp. 300–308, 1982.

[24] Martin and James Ingram and San Diego Biomedical Symposium, *Proceedings of the San Diego Biochemical Symposium*. New York, Academic Press, 1976.

[25] Webster JG., “Reducing Motion Artifacts and Interference in Bipotential Recording,” *IEEE Trans Biomed Eng.*, vol. BME-31, no. 12, pp. 823–826, 1984.

[26] H. W. Tam and J. G. Webster, “Minimizing Electrode Motion Artifact by Skin Abrasion,” *IEEE Trans. Biomed. Eng.*, vol. BME-24, no. 2, pp. 134–139, 1977.

[27] Andrey B Simakov and John Webster, “Motion artifact from electrodes and cables,” *Iran. J. Electr. Comput. Eng.*, pp. 139–143.

[28] M. A. Rossetto and D. H. Vandercar, “Lightweight FET circuit for differential or single-ended recording in free-moving animals,” *Physiol. Behav.*, vol. 9, no. 1, pp. 105–106, 1972.

[29] A. G. Ratz, “Triboelectric noise,” *ISA Trans., vol 9*. pp. 154–158, 1970.

[30] J. A. J. Klijn and M. J. G. M. Kloprogge, “Cable artefact suppressor for electrophysiological recording,” *Electromyogr. Clin. Neurophysiol.*, vol. 13, no. 1, pp. 87–92, 1973.

[31] A. R. Kahn, “Motion artifacts and streaming potentials in relation to biological electrodes,” in *Dig. 6th Int. Conf. Med. Electr. Biol. Eng.*, 1965, pp. 562–563.

[32] R. D. Gatzke, “Electrode: Measurement System Viewpoint.,” 1974.

[33] J. L. Day, “Review of NASA-MSC electroencephalogram and electrocardiogram electrode systems including application techniques. NASA TN D-4398.,” *Tech. Note. U. S. Natl. Aeronaut. Space Adm.*, 1968.

[34] Texas Instruments, “INA333 INA333 Micro-Power (50μA), Zerø-Drift, Rail-to-Rail Out Instrumentation Amplifier,” 2008.

Ringraziamenti

Ringrazio il direttore del LISiN, il professore Marco Gazzoni e tutti i suoi collaboratori per avermi permesso di svolgere la tesi all'interno del laboratorio fornendomi i mezzi per farlo nel migliore dei modi.
In modo particolare vorrei ringraziare il mio relatore, l'ingegnere Alberto Botter per avermi seguita con costanza e dedizione in tutti questi mesi; lo ringrazio per la sua attenzione ad ogni mio stato d'animo, per i consigli datimi in tutti questi mesi e per la sua infinita simpatia. Mi ha insegnato ad amare il nostro lavoro e ad affrontare i momenti più critici.
Vorrei ringraziare anche l'ingegnere Giacinto Luigi Cerore, per me Gigi, mio correlatore, perché con la sua stravaganza e infinita voglia di conoscere mi ha insegnato che non si è mai preparati abbastanza. Grazie anche alle sue battute ciniche che mi hanno insegnato a non abbattersi mai.
Vorrei ringraziare la BionIT LABs di Lecce per avermi dato il privilegio di affrontare questo lavoro di tesi. Con particolare attenzione ringrazio l'ingegnere Matteo Aventaggiato che nonostante non mi conosca personalmente si è sempre mostrato disponibile ad ogni mia richiesta o dubbio.

Ringrazio le mie due compagne di avventura di questi mesi Alessandra ed Enrica, con cui ho condiviso tutti i momenti più o meno difficili che questo lavoro ha comportato. Ringrazio il nostro amico Marco, che ci ha accolte nel suo ufficio trasformandolo nella

nostra sala relax e che ci ha sopportato e supportato ogni giorno in questi mesi. Accomunati dalla cura per l'igiene orale so di aver trovato tre amici veri.

Ringrazio Daniela, il mio angelo custode, che mi ha protetto e sostenuta da lassù in tutti questi mesi, che mi ha insegnato a lottare per la nostra stessa vita e ad essere grati di tutto.
Ringrazio Dorotea che da quindici anni mi sostiene in ogni momento, che con il suo essere a volte anche un po' lunatica, mi riempie le giornate di sorprese; Due caratteri molto diversi che insieme formano un connubio perfetto.
Ringrazio la mia omonima Daria, mi ha insegnato ad essere determinata e a puntare sempre in alto, non ci diciamo mai ti voglio bene noi due, ma entrambe sappiamo che legame indissolubile ci lega.

Ringrazio Claudia per aver creduto in me dall'inizio di questo percorso, anche quando neanche io riuscivo a crederci. È un punto fisso nella mia vita e una spalla su cui sorreggermi quando ne ho avuto il bisogno.
Ringrazio Emanuela che esattamente da ventitré anni mi sta a fianco senza mai stancarsi; la mia compagna di banco dall'asilo al liceo e adesso la mia compagna di vita.

Ringrazio Laura mia amica, collega e coinquilina. Abbiamo condiviso il giorno e la notte, le gioie e i dolori, salute e malattie, praticamente è diventata mia moglie!
Ringrazio Giovanni il mio migliore amico, in grado di parlare pure con i sassi. I suoi monologhi mi hanno sempre aiutato a riflettere e a prendere la scelta giusta.
Ringrazio Salvatore, per me Toto, dotato di un super potere: la pazienza. Mi ha sopportato anche quando lo rimproveravo senza alcun motivo.
Ringrazio Karina, la mia coinquilina brasiliana che questi anni mi ha insegnato a ballare e a cucinare piatti brasiliani. Ho solo una cosa da rimproverarle: non mi ha presentato neanche un bel brasileiro!!
Ringrazio Giada, il mio minion, che con il suo fare così silenzioso è riuscita sempre a starmi accanto. C'è voluto un po' per scioglierla, ma ovviamente ci sono riuscita.

Ringrazio Federico e Lorenzo, due “pulcini” che in questi anni nonostante la distanza sono riusciti a starmi sempre vicina con videochiamate, foto e racconti molto dettagliati.
Ringrazio mio nonno, che con le sue preghiere e i lumini accesi ha contribuito in modo fondamentale al conseguimento di questo traguardo. Lo ringrazio per avermi amato fin da subito più degli altri nipoti, nonostante lo neghi.
Ringrazio mamma e papà perché se sono arrivata fin qui è soprattutto grazie a loro. Mamma perché mi ha sempre trasmesso forza e determinazione e papà per la fiducia che ha sempre posto in me lasciandomi sempre carta bianca. Entrambi mi hanno insegnato che tutto accade per un motivo e che bisogna sempre dare tempo al tempo non perdendo mai di vista l’obiettivo. Mi hanno insegnato a credere che prima o poi la vita ti sorride e come sempre avevano ragione.
Infine ringrazio mia sorella Sarah, per i nostri litigi e per i nostri momenti di amore spassionato. La ringrazio per i suoi consigli sinceri e maturi e per il suo sostegno fisico e morale. La ringrazio per il suo essere buffa e distratta in ogni cosa che dica o faccia, questa è stata sempre la sua parte più bella. Lei è la mia anima gemella.